CRANFIELD UNIVERSITY

Jun Wei Tan

Multi-Disciplinary Investigation of a Flap Blown Turboelectric Distributed Propulsion Blended Wing Body Aircraft

School of Aerospace, Transport and Manufacturing

PhD
Academic Year: 2013 – 2017

Supervisors: Prof. R. Singh & Dr. P. Laskaridis
April 2017

CRANFIELD UNIVERSITY

School of Aerospace, Transport and Manufacturing

PhD

Academic Year 2013 – 2017

Jun Wei Tan

Multi-Disciplinary Investigation of a Flap Blown Turboelectric Distributed Propulsion Blended Wing Body Aircraft

Supervisors: Prof. R. Singh & Dr. P. Laskaridis

April 2017

© Cranfield University 2017. All rights reserved. No part of this publication may be reproduced without the written permission of the copyright owner.

ABSTRACT

Growing concerns about the rising costs of fuel as well as environmental issues have led to multiple innovative and futuristic aircraft concepts to tackle these issues. Turboelectric Distributed Propulsion (TeDP) and boundary layer ingestion are two such concepts. When applied to a conceptual aircraft such as the N3-X, it results in a blended wing body (BWB) aircraft with an array of fan propulsors mounted near the rear of the aircraft body and driven by superconducting motors powered by superconducting generators in the wing tip mounted turbogenerators. The elevator flaps of such a BWB aircraft are located at the trailing edge of the aircraft body. Coupled with the exhaust mass flow from the propulsor fan nozzles, it presents a chance to utilize flap blowing and/or thrust vectoring to further improve on the aircraft performance. By utilizing boundary layer ingestion, there can be expected 5-6% total fuel savings while flap blowing can further enhance the fuel savings to a total of 8-9%. However, integration issues such as intake pressure losses, deficiency in fan propulsor efficiency tends to mitigate the benefits derived. Furthermore, it is difficult to separate various design disciplines such as aerodynamics and propulsion in such a high integrated aircraft. Flap blowing further correlates to both disciplines.

This dissertation addresses a broad overall design methodology that is both multi-disciplinary and multi-fidelity, addressing the above mentioned issues. Flap blowing can be seen to be a linkage between the often separate aerodynamics and propulsion design disciplines in an aircraft. The strip method code, designed to incorporate flap blowing into the preliminary design and analysis is presented in this study, showing its impact on aerodynamic performance, flight dynamic response and propulsion system design. Furthermore, other disciplines such as boundary layer ingestion, weight, and flight dynamics are considered and incorporated into the methodology. The main figure of merit used is the total fuel consumption of the aircraft and in addition, take-off distances are also studied and analysed. Take-off distances incorporating flap blowing and thrust vectoring demonstrated a reduction in distances between 25-30%.

The reduction in take-off distance also led to the study on the potential of re-sizing the BWB outer wings to further reduce total fuel consumption and has shown great promise.

Keywords:

BLI, TeDP, N3-X, Strip method, Multi-disciplinary, Aerodynamics, Flight dynamics, Take-off

ACKNOWLEDGEMENTS

First and foremost, I would like to thank my family, especially my dear wife, who has made tremendous sacrifice in forsaking her own career and years of her life to accompany me on this journey. Our two well taken care of and happy children in a foreign land is testament to her dedication and sacrifice.

I would like to thank my family in Singapore who has had to endure our time away from them and the constant help they have provided throughout this time.

I would like to express my gratitude to my supervisor Dr. Panagiotis Laskaridis for his thoughtful discussions, advice and guidance he provided during this journey. Our discussions have led me to develop my research capabilities as well as presented me with numerous chances to showcase the work.

Mention must be given to Prof. Riti Singh, who has contributed to the work with his mass experience and thoughtful insights which have directly led to the development of the ideas presented here.

I would like to thank Dr. Nalianda Devaiah, who provided great help in guidance to form the ideas presented here as well as providing help in procuring much needed data and software.

I would also like to give mention to all the people and new friends I have made in Cranfield to make this journey here much more enjoyable. Friends that I have known for many years have also shown great support when they have visited.

Last but not least, I would like to thank my company, DSO National Laboratories Singapore, who have kindly sponsored my research here, without it, none of these would have been possible.

TABLE OF CONTENTS

LIST OF FIGURES

LIST OF TABLES

LIST OF ABBREVIATIONS

Acronyms

A	Area
ac	Aerodynamic centre
AoA	Angle of Attach
ADP	Aerodynamic Design Point
BLI	Boundary Layer Ingestion
BWB	Blended Wing Body
C	Aerodynamic coefficient
cBPR	Core Bypass ratio
cFPR	Core Fan pressure ratio
CG	Centre of gravity
CMF	Corrected mass flow rate
D	Diameter
DM	Discretised Miller
Eff	Efficiency
F	Force
FDM	Flight dynamic model
FPR	Fan pressure ratio
g	Gravitational constant
h	Height
H_CS	Capture sheet height
H_BL	Boundary layer height
HTS	High temperature superconducting
L	Length
M	Mach number
MTOW	Maximum Take Off weight
N	Yawing moment
NDP	Non-dimensional power
NF	Number of propulsors
OD	Off design

P	Pressure
PW	Power
q	Dynamic pressure
r	Radius
Re	Reynolds number
S	Wing/Reference area
T	Temperature
TQ	Torque
TS/TSR	Thrust split/Thrust split ratio
TSFC/SFC	Thrust specific fuel consumption/Specific fuel consumption
TV	Thrust vectoring
t	Thickness
TeDP	Turboelectric Distributed Propulsion
TO	Take-off
TS	Thrust split
USB	Upper surface blowing
V	Velocity
W	Weight

Symbols

α	Angle of Attack
β	Sideslip
δ	Deflection angle
∞	Freestrream
ρ	Density
σ	Blade solidity
ω	Rotating speed
θ	Rotation angle
η	Efficiency

Subscripts

D	Drag
EM	Electric motor
f	Flap

jet	Jet
L	Lift
N	Net
m	Pitching moment
OB	Obstacle
S	Static
SLS	Sea level static
t	Thrust
T	Total
u	Blowing

Chapter 1

INTRODUCTION

1.1 Aims and Objectives

The aim of this thesis is to develop an adequately accurate and flexible multi-disciplinary and multi-fidelity methodology incorporating new and existing tools to investigate the synergy between various aspects of advanced Turboelectric Distributed Propulsion (TeDP) architecture for civil aviation on a thrust vectored & flap blown blended wing body aircraft. These aspects include aerodynamic performance, flight dynamics, propulsion architecture, weight and boundary layer ingestion. The benefits and drawbacks of different variables in regards to these aspects would be investigated with the developed methodology.

The architecture of a TeDP aircraft is such that there is an array of distributed fan propulsors driven electrically by a system of core engines. These core engines provide either entirely electrical power or a combination of electrical power as well as thrust whereas the fan propulsors provide entirely thrust force. The usage of distributed fan propulsors each “decoupled” from the core engine shaft through electrical transmissions allows a possible efficient means of controlling the fans and core engines at their optimal operating state. The placement of the fan propulsors would possibly impact upon the aerodynamics of the aircraft when in operation. Meanwhile, the weight of different configurations would impact upon the thrust, control and stability requirements for various flight segments. Consequently, the usage of thrust vectoring and flap blowing would have an impact upon the aerodynamics of the aircraft, thrust requirements for control and stability and overall weight. Such examples describe the closely knitted influence of each of these aspects in such an aircraft. Thus, the ability and methodology to model the synergy of these aspects between aerodynamic performance, flight

dynamics, propulsion architecture, weight and boundary layer ingestion becomes a highly sought after tool.

The approach to this involves developing methodologies to model each of the stated aspect before synergizing each of them together to obtain the overall methodology for a complete study. In this way, the potential benefits and drawbacks of each aspect can be clearly identified, providing an overall methodology to obtain an optimised solution incorporating all the individual aspects.

The aims and objectives of the individual aspects are explained below.

1.1.1 Aerodynamic performance

1. Develop a methodology that is able to adequately predict the overall aerodynamic coefficients of the defined aircraft and its control surfaces including the lift, drag, moment coefficients.
2. Develop a flexible methodology to model the impact of flap blowing on the aerodynamic coefficients. The model allows for the flexible placement of the flaps for blowing as well as changeable size of flaps.

1.1.2 Flight Dynamics Modelling (FDM)

1. Develop a methodology to assess the trim conditions of the aircraft at a given flight condition using aerodynamic coefficients with flap blowing considerations, weight, propulsion architecture as inputs.
2. Develop a methodology to model the take-off segment of the aircraft with the same inputs.

1.1.3 Propulsion architecture

1. Develop a methodology for the design and performance assessment of the fan propulsors for distributed propulsion under clean conditions.
2. Develop a methodology for the assessment of core engine performance to power the distributed fan propulsors including the possibility of Thrust Split (TS).

3. Identify or develop a methodology to account for the losses associated with the electrical components.

1.1.4 Boundary Layer Ingestion (BLI)

1. Develop a methodology to adequately predict the profile of the boundary layer over a defined body surface.
2. Identify or develop a methodology to account for the intake pressure losses due to BLI.
3. Develop a methodology to model the impact on the fan propulsor performance due to the distortion arising from BLI.

1.1.5 Weight

1. Develop a methodology to adequately identify and predict the weight of the various components of the blended wing aircraft.

Overall, the main objective of the research is to be able to synergize all the above various aspects to have a complete methodology to optimise the aircraft's propulsion architecture configuration for a stated figure of merit. The benefits of flap blowing, thrust vectoring, BLI, and their individual impact on the overall performance of the aircraft can be identified in the process.

1.2 Motivating Influence

The demand on air transport is always on an increasing curve. The continuously increasing demand in air transport places a strong emphasis on developing more sustainable modes of air transport which is made ever more relevant with the ever increasing hikes in fuel prices as these become depleted in the world.

Studies forecast that demand on air travel would double to quadruple that of current one by 2025 [1]. Coupled with the premium on fuel prices and the lack of airport space, new revolutionary concepts of air travel that provides a reduction in fuel consumption and smaller airports would prove to be of vital importance in the next step of the air travel revolution.

Furthermore, there is the persistent concern that air travel places a huge strain on environmental concerns, and with that, stricter regulations regarding air travel are forecasted with respect to environmental concerns [2].

These factors have led and are leading to the development of the next generation of fuel-efficient, low emissions, highly controllable aircrafts that can make use of shorter runways and with it, smaller airports.

NASA set three specific timeline objectives for future air transport research and development which allowed the industry as a whole to have a defined set of objectives to work consistently towards. These objectives are catered to bring air travel to a new level of efficiency with various limiting factors in mind. These include goals that would limit fuel burn, noise, emissions and field length. These timeline objectives are named N+1, N+2, N+3 programmes to with a timeframe of 2015, 2020 and 2030 respectively. Table 1 shows the respective objectives.

Table 1: NASA N+3 target

	N+1	N+2	N+3
Noise	-32 dB	-42 dB	55 dBa loudness index
LTO NOx Emissions	-60%	-75%	Better than -75%
Fuel Burn	-33%	-40%	Better than -70%
Field Length	-33%	-40%	Suitable for short runways (<900m)

Blended wing distributed propulsion has received greater attention in recent years as a possible answer to these issues. Research in this has been and is currently ongoing as different aspects of it are investigated. The use of array propulsor fans making use of boundary layer ingestion and powered by separate core engines tackles the fuel and emissions issues.

The array of propulsor fans also puts forth an interesting prospect. By allowing the propulsors to have the ability of vectoring or flap blowing, would they then be able to provide sufficient control power to the aircraft and hence, allow the removal or reduction of the control surfaces on the aircraft? Presumably, the

weight reduction due to the removal of the control surfaces would allow a lighter aircraft and hence, reduced fuel consumption. Also, without the deflection of the control surfaces, trim drag is reduced in cruise and this could lead to substantial fuel savings.

Can the thrust vectoring be managed to allow a shorter take-off distance for a smaller airport? How does flap blowing affect the aerodynamic characteristics of the aircraft or the propulsion design requirements?

These possibilities and questions preclude the work for this research and provide the motivating factors for the work being done in this thesis.

1.3 Novelty of Research & Contribution

The novelty of the research is the methodology and application of flap blowing and thrust vectoring on a TeDP aircraft. The synergy of the various aspects especially aerodynamics and propulsion design is described and a methodology using the blowing coefficient as the design criteria that allows for preliminary design of both aerodynamics and propulsion aspects of the aircraft.

The main contributions of the research is the methodology presented to synergize the various aspects or modules in preliminary design phase of a TeDP aircraft incorporating flap blowing and thrust vectoring as well as the application of this on the NASA developed N3-X aircraft

Traditional aircraft design methodology involves aerodynamics design and propulsion design being separate entities. As has been described, the architecture of a TeDP aircraft involves a complicated relation between various different design aspects of the aircraft. The methodology developed would allow a synergy of all the described aspects of aircraft design in the early stage of aircraft development, providing an early aircraft design tool that co-relates all the various aspects.

Furthermore, the methodology developed includes a component for flap blowing and thrust vectoring on a TeDP aircraft. The methodology described would allow for a detailed design phase whereby flap blowing can be used as the ‘linkage’ or

reference point between the aerodynamics design and propulsion design for such an aircraft. A quick view on the various aspects is shown in Figure 1. Core to all the modules is thrust vectoring and flap blowing. It can be perceived that this acts as a linkage between the important aspects of propulsion and aerodynamics in such a highly integrated aircraft and it helps to synergize these two important components.

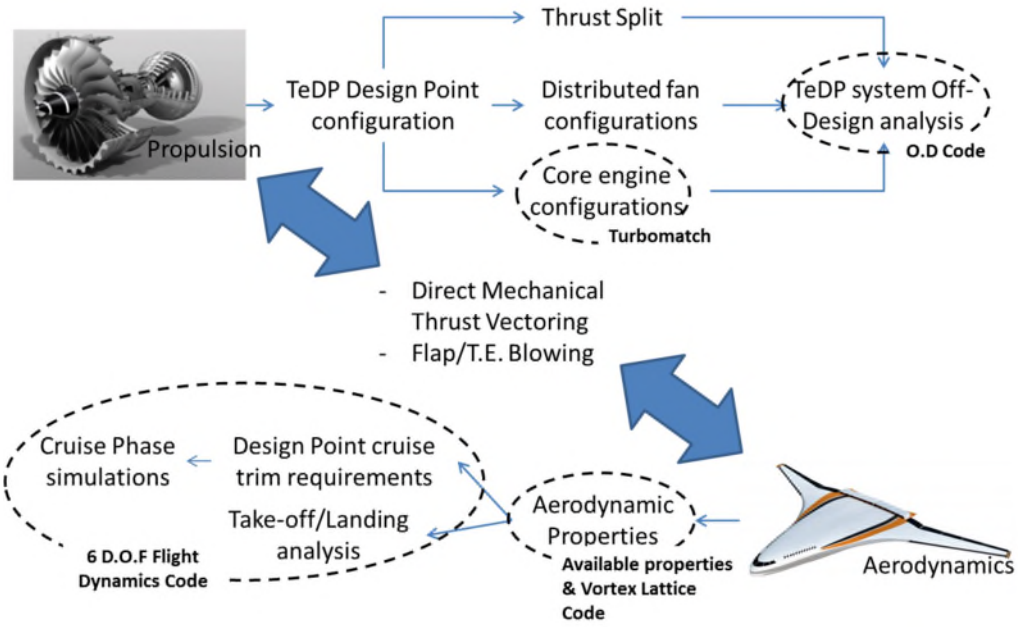

Figure 1 Summary overview of design aspects

The benefits and disadvantages of various inputs such as blown flaps, BLI, weight changes and thrust split on the N3-X are presented mainly in terms of fuel consumption and take-off distance. Various trends are identified that would aid future studies.

1.4 Thesis Organization

The literature research performed during the research is first described in Chapter 2. These include the history of distributed propulsion and how it has been developed or used in the past, recent advances in the development of distributed propulsion and an overview of some of the initial aircraft designs that have developed from such advances, the fundamental aspects of thrust vectoring and

flap blowing, flight dynamics characteristics of a Blended Wing Body (BWB) aircraft, the N3-X aircraft and the various approaches of modelling BLI.

Following that, the thesis is organized in a way to describe how each individual aspect is initially developed before they are integrated and synergized together.

Chapter 3 describes the aerodynamics modelling undertaken to obtain the aerodynamic properties of the aircraft. This chapter focuses on the strip method code developed and how it incorporates flap blowing into the aerodynamics modelling. Chapter 4 describes how the flight dynamics aspects of the aircraft are modelled to obtain both cruise control requirements as well as take-off simulations. Chapter 5 focuses on the propulsion architecture design including distributed fans, core engines, Thrust Split (TS), and various electrical components. Chapter 6 describes the Boundary Layer Ingestion (BLI) module. The methodology involved in obtaining the boundary layer profile is described as well as how the distortion in the profile impacts on the fan performance. Chapter 7 describes the various weight models developed and adopted to adequately determine the weight of various aircraft components. Chapter 8 describes how all the afore-mentioned modules are integrated and synergised together on the N3-X aircraft. Chapter 9 further applies this overall methodology on the off design take-off condition. Chapter 10 explores additional potential benefits that can be derived consequently from flap blowing, describing how flap blowing can aid in reducing the wing area. Lastly, Chapter 11 will conclude the thesis and future potential work.

Chapter 2

LITERATURE RESEARCH

2.1 History of Distributed Propulsion

Distributed propulsion on aircrafts in general is the idea whereby propulsion forces to drive the plane is provided in a distributed manner spread out around the aircraft. Instances of different forms of distributed propulsion have been seen since the inception of the jet engine for aircraft propulsions in the 1900s. In 1954, Griffith [3] proposed the concept of an aircraft with a master combustion engine unit working together with a number of gas turbines that were spread out along the span the wings as shown in Figure 2.

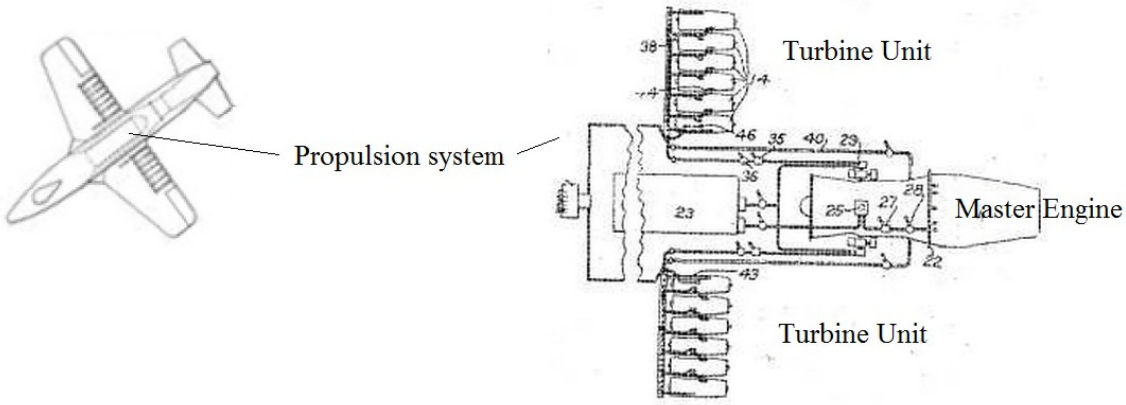

Figure 2: Griffith [3] proposed concept

In 1964, Reyle's [4] suggested an aircraft that could use gas turbine technology for the distributed engines placed between the ducting surfaces powered by nuclear engines positioned in the nacelles. Reyle proposed that such a concept would enhance the power-weight ratio.

From 1970s to 1990s, NASA proposed a number of distributed propulsion concepts and detailed studies on airframe and propulsion system [5] [6]. One early concept is shown in Figure 3. The aircraft was based on a 'tube-and-wing' configuration with tip-driven fans spread along the top surface near the wing trailing edge. The tip-driven fans were powered by high-pressure discharge air from the low pressure compressor stages and mounted on a hinged flap to achieve high lift through flap blowing. The suction across the wing surface fore of the inlets created additional lift on the airframe and delayed flow separation on the wing upper surface [5].

Figure 3: Early distributed propulsion concept

2.2 Turboelectric Distributed Propulsion (TeDP)

TeDP is a concept whereby superconducting power generators provide electrical power to individual superconducting fans which in turn provide the thrust for the aircraft. The usage of electrical transmission provides a platform whereby the fans and generators can be positioned individually to maximize their potential. The large core engine generators are able to retain the high efficiency as expected of large engines. The utilization of many small distributed fans meanwhile allows a very high effective bypass ratio. Furthermore, being electrically linked, both generators and fans are able to operate in their own optimal design points for maximum efficiencies.

The usage of superconductors however, presents a problem itself on its own as the technology is not mature enough to provide minimal losses in the electrical

system to make the system viable. However, this is expected to be overcome in the near future as continued efforts are made in this aspect. The development of advanced cryocoolers is essential in this aspect.

TeDP was determined as a possible way for future N+3 aircrafts with various other transmission methodologies being assessed. A study was done comparing three most possible transmission modes: mechanically driven fans, tip turbine driven fans and electrically driven fans [7]. The main drawbacks and inhibiting factors of mechanically driven and tip turbine driven fans are the space and weight requirements of such a system. The study revealed that combined efficiency of transmission and motors to be increased to 96% with superconductivity and the total weight of electric motors for the studied configuration is only approximately the weight of one single conventional core generator. Reliability is increased as the incorporation of intelligent redundant system would allow the loss of one fan propulsor to be negated by the large presence of the other fans. Furthermore, the usage of the small fan propulsors would allow maximum benefit from boundary layer ingestion when mounted on top of the body along the span. The propulsors would also make possible the use of thrust vectoring for flight control, reducing the weight by reduction of flight control surfaces as well as improving manoeuvrability with the vectoring.

NASA conducted a system study on integration of advanced cryogenic electric propulsion system onto a 150-passager STOL airliner as Figure 4 shows. The airplane integrates superconducting-electric-motor-driven fans completely embedded within the wing. This reduces the wing weight and it's bending moment as the distributed fans have a common nacelle along the wing rib structure providing stress relief to the wing structure. Furthermore, the presence of low temperature exhaust nozzles allow the possibility of flap blowing and thrust vectoring, thereby increasing the lift coefficients of the plane. The vehicle uses liquid hydrogen both as the fuel and cooling fluid. Liquid hydrogen has a boiling point of 23 K at 2 atm, making it a viable option in cooling the electric system. NASA predicted such a configuration would result in a large reduction in fuel consumption.

Figure 4: NASA advanced cryogenic electric propulsion system

The usage of TeDP also provides an added incentive for alternative fuels. The superconducting materials require a medium for cooling and the most common studies done on these mediums have been hydrogen and methane, both of which can be termed as alternative fuels for future aircrafts. Both fuels provide their own set of advantages and disadvantages as a cooling medium and fuel.

2.3 Advances in Distributed Propulsion

Various advances in distributed propulsion in various areas have been recorded to fulfil the various NASA targets.

2.3.1 Aircraft Concepts

First off, different aircraft concepts and configurations have been proposed. Designs proposed for N+1 target focused on design modifications to existing aircraft structures. An example is a conventional aircraft architecture that is powered by two ultra-high bypass ratio engines incorporating various noise reduction methods [8] as shown in Figure 5. N+2 proposed configurations generally make use of the blended body aircraft concept. Figure 6 shows an example whereby two podded engines are installed above the body of the aircraft close to the trailing edge. Figure 7 shows the SAX-40 aircraft proposed via the "Silent Aircraft Initiative" from the Cambridge-MIT Institute [9]. This aircraft makes used of the concept of boundary layer ingestion by embedding three gas turbine core engines each driving three mechanically driven fans adjacent to the core engine. This results in nine boundary layer ingesting mechanically-driven fans providing the thrust. The CESTOL (Cruise-Efficient Short Take-Off and Landing)

shown in Figure 8 is a blended wing body aircraft with twelve conventional turbofan engines embedded in the body to utilize the benefits of boundary layer ingestion. The most recent configuration is catered towards the N+3 targets. The aircraft N3-X shown in Figure 9 and makes use of turboelectric distributed propulsion concept (TeDP). The aircraft has two engines at the tip of the wings providing necessary power for an array of propulsor fans along the trailing edge of the body.

Figure 5: N+1 configuration [8]

Figure 6: N+2 configuration [10]

Figure 7: SAX-40 aircraft [9]

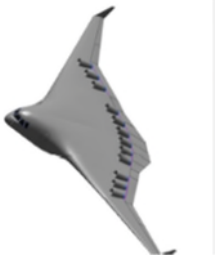

Figure 8: CESTOL aircraft [9]

Figure 9: N3-X aircraft [9]

Cranfield University has also worked upon a concept of thrust split whereby the core engines provide a certain amount of thrust and the propulsor fans provide the balance thrust required. Lodesani [11] coined the term thrust split (TS) and is defined as follows

$$TS = \frac{F_{propulsors}}{F_{total}} \quad \textbf{(2-1)}$$

It is basically the fraction of thrust force provided by the propulsors with respect to the total thrust force required by the aircraft. The work also described the optimal thrust split level which corresponds to the lowest SFC would be that in the region of approximately 60% for a specific set of conditions.

2.3.2 Superconductivity

The electrical system involved in a TeDP platform is essential for the success of such a concept due to the specific power requirements of the fan propulsors. Conventional electrical motors have a specific power of 0.5 kW/kg while a turbofan engine requires a specific power in the region of 3.8 kW/kg [12]. Conventional motors increase the torque density by increasing the current density in the copper windings. This in turns lead to significant increase in losses and a decrease in efficiency. High temperature superconducting(HTS) machines, on the other hand, can be designed to allow both high torque and high power density and makes it a viable means of efficient transmission [13]. The HTS system comprises superconducting motors, generators, cables and power electronics. There is also a high expectation that transmission efficiencies of above 99% can be achieved [14].

Superconductivity also requires operational cryogenic temperature. In the last 40 years, this temperature has increased steadily from 0K to 92K [15]. There are various ways to achieve such temperatures including cryocoolers and cryogen storage.

Cryocoolers directly cool the system but are presently, too heavy for TeDP applications. They have a mass to power ratio of about 3kg/kW input without the associated compressors and ancillaries external to the cold head portion which can weigh up to 5 times the weight [16] [14]. However, in the N3-X timeframe, crycoolers are expected to achieve a 3kg/kW input for the complete system [13].

Cryogen storage is the form of storing cryogenic fluids in thermally isolated tanks and using the liquid to cool the system. The benefit of this is the usage of cryogenic fluids that also function as fuel for the aircraft. These include liquid hydrogen and natural gas [17] [12] [18] [19].

2.3.3 Alternative Fuels

A study on the potential of hydrogen as a fuel for long range aircraft [20] showed that the main advantages compared to jet fuel includes reduced fuel weight by a 2.8 factor due to its high heat of combustion and as a result, a lower structural and overall mass of the aircraft. This studied focused on conventional aircraft. Hydrogen, however, has much lower density and would require approximately 4.15 times the amount of volume as required by jet fuel. This would result in bulky and heavy fuel tanks. Take-off weight reduced between 13% - 25% depending on the number of passengers the aircraft can take.

A study done by MIT [21] which resulted in an aircraft design named H3.2 also included studies on the application of Liquefied Natural Gas (LNG) which consists of approximately 90% methane as a fuel. Its main promises are a 16% lower carbon emissions as well as a 16% higher specific energy resulting in a lower mass from fuel as per that of hydrogen, albeit on a smaller scale. It has a 33% lower energy density compared to jet fuel, resulting, similarly to hydrogen, a larger amount of volume requirement for storage, although once again, at a smaller scale as that of hydrogen.

A comparison between the two alternative fuels would therefore show that LNG or methane to have better promise in terms of volume requirements while hydrogen would provide a greater reduction in fuel weight. They, however, both have cryogenic benefits.

An assessment of propulsion system configuration on hybrid wing body fuel efficiency [22] showed the possibility of using LNG as a cryogenic fuel for TeDP and at the same time enabling laminar flow on the bottom of the outer wing by using wall cooling with integral fuel tanks to increase the critical Reynolds number and delay Tollmien-Schlichting wave instability dominated transition. The boiling

point of LNG at 110K at 1 atm would allow the fuel to be stored as a boiling liquid and using the enthalpy of vaporization to cool the wall pressure side and hence allowing modest pressure gradients for flow laminarization. Aircraft performance was deemed to have increased by 4% mainly due to flow laminarization and a 57% fuel burn reduction as compared to conventional aircrafts.

Liquid hydrogen was analysed as a coolant and fuel for TeDP [23]. In TeDP, the superconducting materials have to be constantly cooled between 30K and 60K depending on the type of material of the electrical components. The study showed that the design of a cryocooler would add substantial power requirements and weight to the aircraft. Liquid hydrogen has a boiling point of 20.4K which is well below the cooling requirements of the TeDP. Hence, by using liquid hydrogen as a cooling medium, it replaces the requirements of housing cryocoolers on board the aircraft, hence lowering power requirements and losses as well as reducing the weight. Furthermore, the heated hydrogen can then be used as fuel for the core engines which is further beneficial as it replaces approximately 2.8 times the mass of jet fuel. A similar analogy can be used with LNG or methane as a coolant and fuel. However, the higher boiling point of approximately 110K would mean additional heat sinks are required to eject the heat to that below the required temperatures of 30-60K. This would be the main drawback of LNG as a cryogenic coolant.

2.4 NASA N3-X Aircraft Concept

This TeDP aircraft concept, as previously mentioned is a conceptual aircraft developed to fulfil the N+3 goals. In its infancy stage, it is a blended wing body with two turbogenerators at the tip of the wings to provide electrical power. This electrical power drives an array of propulsor fans mounted along the trailing edge of the main body. It makes use of high temperature superconducting (HTS) technology [24] to transmit the required megawatts of power from the turboshafts to the propulsors. The possible main benefits of such a concept are

- High effective bypass ratios achieved without excessive engine size or other installation issues as the fan propulsor array is spread out along the trailing edge.

- De-coupling of the propulsor shaft with the core engine shaft, allowing for optimal operating points for both.
- Redundancy, ease of maintenance and cost efficiency as there are numerous fan propulsors providing the thrust.
- Possible reduction of noise as the propulsors are embedded.
- Possible reduction of fuel consumption through various means such as boundary layer ingestion, thrust vectoring, flap blowing, weight reductions.

Drawbacks for such a concept might include

- Highly integrated system which would make design a challenge as every design shift on any component would inadvertently have an impact on the other component designs.
- Boundary layer ingestion would probably mean an impact on the designed performance of the propulsor fan due to the distorted flows.
- The design of the intake ducts would be a challenge to reduce the losses and distortion of the boundary layer flow as mentioned.
- The lack of existing superconducting technology that would minimize the losses in the electrical system to make the benefits feasible.

The main concepts explored in this thesis are design of a TeDP aircraft comprising various concepts such as boundary layer ingestion, flap blowing, thrust vectoring and the synergy between these systems. The presence of a blended wing body with a fan array mounted on the trailing edge would allow the flaps to be positioned aft of the propulsors' exhaust. Furthermore, the availability of the preliminary design data of the aircraft such as geometry and design conditions from NASA makes this a viable aircraft for the study. As such, the N3-X was selected to be used as the demonstrative aircraft to apply the various concepts and methodologies developed.

The following flight requirements [24] were defined for the N3-X. It should be noted the values here have taken into account an estimation of the benefit derived from boundary layer ingestion.

Table 2: N3-X Thrust specifications

Flight Condition	Minimum Thrust Required
Aerodynamic Design Point (ADP) (30,000 ft / MN 0.84 / ISA)	26,750 lbf (119 kN)
Rolling Take-Off (RTO) (SL / MN 0.25 / ISA+27 R)	65,000 lbf (289 kN)
Sea Level Static Take-off (T/O) (SL / MN 0.0 / ISA)	90,000 lbf (400 kN)

Other defined parameters include

- Payload: 118,100 lbm (53569 kg)
- Range: 7500 nm (13890 km)

To conduct a meaningful study on the aircraft in the various aspects, other parameters undefined as at the beginning of the study would have be assumed or derived in the latter stages of the thesis.

Figure 10 shows the N3-X. Some features of the geometry and structure [16] of the N3-X are as follows

- Single box nacelle
- High aspect ratio 2D ‘mail-slot’ inlet with vertical splitters just behind inlet lip to segment incoming flow into diffusion sections for each fan.
- 2D box nozzles for each fan with small dividers similar to the inlet.
- No vertical fins. [25]
- Continuous nacelle span of 780 inches (19.82m). This is hence also the total span width of the propulsor fans as well as the elevator flaps aft of the exhaust.
- Number of propulsor fans differ depending on FPR and thrust requirements.

Figure 10: Conceptual N3-X aircraft

2.5 Flap Blowing and Thrust Vectoring

Thrust vectoring is basically defined as the ability to point the thrust produced in a specific direction to enable the aircraft to perform a turning manoeuvre. It has been studied and used since 1950s albeit primarily on military aircrafts. It can broadly be classified into external thrust vectoring and internal thrust vectoring.

External thrust vectoring turns the flow after it has exited the engine nozzle. It makes use of vanes or paddles aft of the nozzle to turn the flow. Its main advantage is the non-complexity of the nozzle making it a simple design and cheap to manufacture.

Internal thrust vectoring makes use of variable geometry designed into the nozzle to allow the flow to exit the nozzle at the required direction. It can further be differentiated into mechanical thrust vectoring and fluidic thrust vectoring.

Flap blowing can be considered another type of thrust vectoring as jets of air are blown across the flap. Jets blown across a wing and flap are sometimes also known as upper surface blowing. These jets of air can be blown at the trailing edge to form a fluid flap in the required direction which is also known as jet flaps. The presence of blowing over an existing flap at the trailing edge of the wing is also known as flap blowing.

Lugo [26] showed that the direct thrust provided by a deflected jet is small compared to the lift of the airfoil and direct thrust vectoring would require a very high jet nozzle pressure ratio or a very high mass flow rate. The deflected jet from flap blowing or jet flaps would however, influence the aerodynamics of the aerofoil and increase the lift of the aerofoil.

2.5.1 Mechanical Thrust Vectoring

Mechanical thrust vectoring is achieved by manipulating the nozzle geometry to turn the thrust in the required direction. Traditionally, in single engine aircrafts, a rectangular nozzle can only control the pitch angle while additionally vanes are added to control the yaw angle of the aircraft. The basic design of a pitch only rectangular nozzle is simple and provides good performance and efficiency. It

can also provide thrust reversal control. Multi-directional thrust vectoring control can only be achieved by an axisymmetric nozzle with a large number of small movable parts, however resulting in a high level of complexity. Inherently, with the deflection of the flow, there are bound to be at least minimal losses.

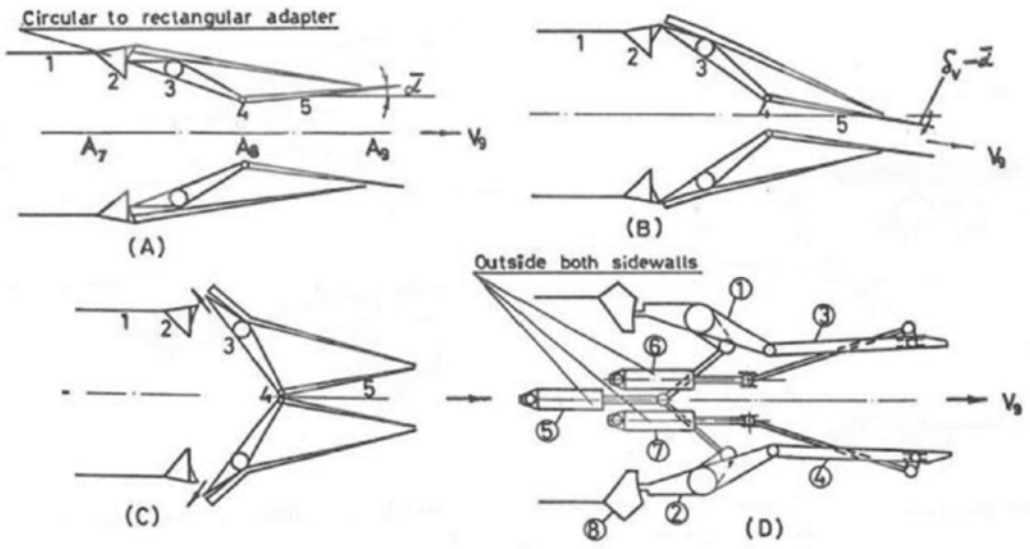

Figure 11: Mechanical thrust vectoring with rectangular nozzle in pitch direction only [27]

2.5.2 Fluidic Thrust Vectoring

Fluidic thrust vectoring is achieved by turning the flow at the nozzle exit without the use of mechanical moving parts. Its basic concept is to attain flow turning through flow interactions based on fluid dynamics principles. Without the moving mechanical parts, overall weight of the system is reduced and fewer losses are expected. Fluidic throat shifting, shock vector control, and counterflow method are various fluidic thrust vectoring control methods that have been studied [28] through CFD or experimentally.

Throat shifting method makes use of an injection of a secondary flow to create a new aerodynamic minimum area or throat in the nozzle. The shifting of the throat creates an asymmetric pressure distribution and thus, turning the flow direction to produce the vectoring.

Shock vector control inherently requires supersonic exit flow to be present for shock induction. It is achieved by an injection of flow to create an oblique shock in the divergent section of the nozzle and hence, turning the flow in the required direction. Flow injection is made after the throat to produce a low pressure region and hence, creation of a shock due to the sudden pressure changes. This method inherently produces large losses due to the shock formation.

The counterflow method is achieved by introducing a low pressure zone such that the flow is suctioned through a slot between the suction collar and the primary nozzle zone. The asymmetric pressure distribution created thus produces a deflection of the thrust.

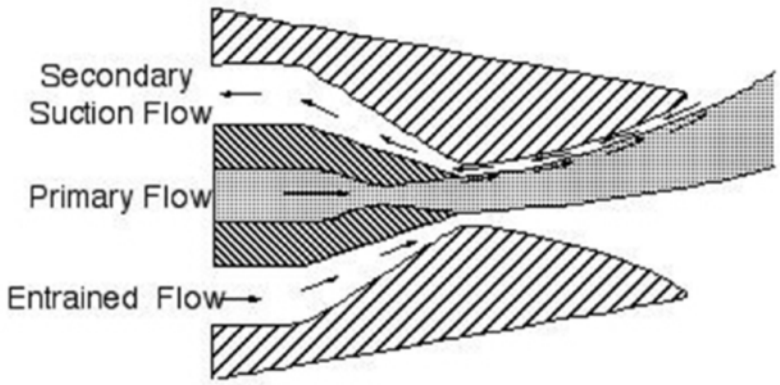

Figure 12: Counterflow thrust vectoring method [28]

2.5.3 Flap Blowing and Jet Flaps

There are two main methods to change the lift coefficient of an airfoil. They are (i) to adjust the angle of attack the aerofoil is facing in the face of the airflow or (ii) changing the geometry of the wing by deflecting the end of the trailing edge such as by that of a flap. Both would effectively result in a higher lift coefficient. Excessive deflection of both methods though, would result in flow separation and loss of lift as the frictional losses in the boundary layer results in the flow losing much of its kinetic energy and increasing pressure gradient, would result in flow separation.

This can be overcome by re-energizing the boundary layer using circulation control. Circulation control makes use of the well-known Coanda-effect whereby

a high velocity, tangentially blown air jet remains attached to a convex surface due to the balance between centrifugal force and the pressure differential produced by the jet velocity. Flap blowing or jet flap is one way of utilizing this.

Spence [29] derived an expression for lift coefficient as a function of angle of attack, flap deflection and blowing momentum coefficient for pure jet flaps. This was based largely around a parameter known as the blowing coefficient defined as

$$C_u = \left(\frac{\dot{m}V_{jet}}{\bar{q} \cdot \mathrm{S}}\right) \quad \textbf{(2-2)}$$

Further work was then conducted by Williams [30] theoretically as well as experimentally to develop the original work. The work enabled the use of relations involving the blowing coefficient to be applied on pure jet flaps as well as flap blowing to determine the change in lift on a 2D aerofoil. On a pure jet flap, the increase in zero AoA lift coefficient due to blowing is

$$\Delta C_{L,\alpha=0} = \left[4\pi C_u \left(1 + 0.151 C_u^{\frac{1}{2}} + 0.139 C_u\right)\right]^{\frac{1}{2}} \times \delta_f \quad \textbf{(2-3)}$$

The change in the lift curve slope is a product of the original lift curve slope with a factor K defined as

$$\mathrm{K} = (1.0 + 0.151 C_u^{\frac{1}{2}} + 0.219 C_u) \quad \textbf{(2-4)}$$

Studies [6] on super-critical airfoil applied to a distributed propulsion platform have shown an increase in lift with jet deflection.

Naveed [31] investigated flaps jet-blowing on a blended wing body aircraft and showed that the coupling of jet blowing with control surfaces provided a vast improvement in control authority and reduction in take-off distance for a blended wing body. The original blended wing body had issues of handling and flying deficiencies due to the lack of a tail plane and hence low moment arms. The drawback though was the bleed required from the engines for the blowing,

resulting in more engine transients and also degradation of the engine performance.

2.6 Blended Wing Body Flight Dynamics

Blended wing body aircrafts inherent does not have a tail plane and is commonly termed as a tailless aircraft. While the flight dynamics principles of a conventional aircraft and that of a blended wing body are governed by the same sets of rules and principles, the effect of a missing tail creates variations in the longitudinal and lateral stability of the aircraft that has to be addressed by other control means to provide flight stability and control power.

2.6.1 Blended Wing Body Static Longitudinal Stability

It can be found in basic flight dynamics literature [32] that static pitch stability can only occur if

$$C_{m\alpha} < 0 \quad \textbf{(2-5)}$$

$$C_{m0} > 0 \quad \textbf{(2-6)}$$

It is interpreted that change of pitching moment with respect to angle of attack must be negative while the pitching moment at zero angle of attack must be positive. Hence, the aircraft can only be trimmed at a positive angle of attack. An increase in angle of attack would cause a negative pitching moment which would cause the aircraft to nose down back to its trim angle of attack and vice versa. Furthermore, the pitching moment about the CG must be positive at zero angle of attack. Blended wing body aircrafts' flight dynamics differ from that of conventional aircraft.

Naveed [33] provided a detailed explanation of these differences.

The forces and moments diagram as shown in Figure 13 is that of a conventional aircraft whereby there is a tail component.

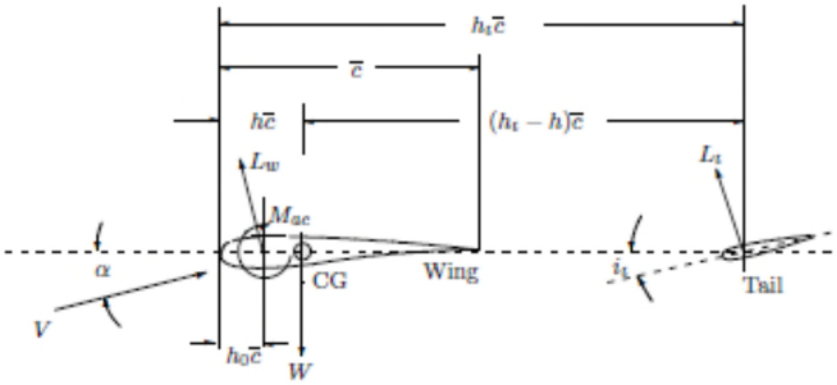

Figure 13: Conventional aircraft forces and moments [33]

Total pitching moment is a sum of the moments due to lift of the wing, lift of the tail and moment about the aerodynamic centre. It is assumed that no propulsion force and tail drag are present. Angle of attack is also assumed to be small such that $\cos\alpha \approx 1$. Hence, the total pitch moment about the CG is

$$M_{CG} = M_{ac} + (h - h_0)\bar{c}L_w - (h_t - h)\bar{c}L_t \quad \textbf{(2-7)}$$

Dividing throughout by $qS\bar{c}$, the non dimensionalised form is

$$C_{mcg} = C_{mac} + (h - h_0)C_{Lw} - (h_t - h)\frac{S_t}{S}C_{Lt} \quad \textbf{(2-8)}$$

Both wing and tail coefficients can be given a linear definition whereby

$$C_{Lw} = a_w\alpha \quad \textbf{(2-9)}$$

$$C_{Lt} = a_t\left[\alpha\left(1 - \frac{d\epsilon}{d\alpha}\right) - i_t\right] \quad \textbf{(2-10)}$$

n which a_w, a_t, i_t are the lift curve slopes of the wing and tail, and tail incidence angle respectively. $\frac{d\epsilon}{d\alpha}$ is the effective angle of attack as seen by the tail. Therefore, by defining

$$C_{m0} = C_{mac} + (h_t - h)\frac{S_t}{S}a_t i_t \quad \textbf{(2-11)}$$

$$C_{m\alpha} = (h - h_0)a_w - (h_t - h)\frac{S_t}{S}a_t\left(1 - \frac{d\epsilon}{d\alpha}\right)C_{Lt} = a_t\left[\alpha\left(1 - \frac{d\epsilon}{d\alpha}\right) - i_t\right] \quad \textbf{(2-12)}$$

The total pitching moment about the CG can now be rewritten in the simple form of

$$C_{mcg} = C_{m0} + C_{m\alpha} \quad \textbf{(2-13)}$$

We have seen that C_{m0} should be positive and from equation (2-11), it consists of a wing component, C_{mac}, and a tail component. C_{mac} which is inherently negative and unaffected by the angle of attack. Hence, it is the tail component that allows C_{m0} to be positive.

For blended wing body aircrafts,

$$C_{m0} = C_{mac} \quad \textbf{(2-14)}$$

A reflex in incorporated at the trailing edge of the wing to allow C_{m0} to be positive at the expense of a deficiency in the lift coefficient. This can also be achieved by the usage of control surfaces at the trailing edge or a force applied in the correct direction at the trailing edge.

A similar analogy is done on the $C_{m\alpha}$ moment component. It is known that $C_{m\alpha}$ must be negative for stability. The tail component of equation (2-12) provides the negative component whereas the wing component provides the positive component. For a blended wing body, equation (2-12) reduces to

$$C_{m\alpha} = (h - h_0)a_w \quad \textbf{(2-15)}$$

This means that for $C_{m\alpha}$ to be negative, $h < h_0$. This would mean that the CG would have to be located fore of the aerodynamic centre which is contrary to conventional aircrafts and severely limits the CG range of the blended wing body aircraft.

The static margin of an aircraft is defined as the non-dimensional distance between the aerodynamic centre and the centre of gravity. It is defined positive when CG is fore of the aerodynamic centre. Castro [34] deduced that the positive

static margin for a blended wing body has to be lower than that of conventional aircrafts due to the lack of control power whereas there are also assumptions that a negative static margin augmented with fly by wire digital flight control systems would result in a blended wing body aircraft with adequate control power and stability.

It can be summarized that for basic static longitudinal stability of a blended wing body, the CG must be fore of the aerodynamic centre and adequate forces must be applied at the trailing edge of the wing contrary to conventional aircrafts to allow the aircraft to trim longitudinally. Alternatively, it has also been proposed that the ideal way for a blended wing body aircraft would be for an inherently unstable longitudinal configuration whereby the CG is aft of the aerodynamic centre and controlled by a fly-by-wire system to provide adequate control to stabilize the plane.

2.6.2 Blended Wing Body Lateral-Directional Stability

As per longitudinal stability, lateral-directional stability for blended wing bodies has differences as compared to that for conventional aircrafts. Directional stability refers to the response of the aircraft to yawing moments whereas lateral stability refers to the response of the aircraft to rolling moments. They are generally termed together as there are usually roll-yaw coupling effects.

Naveed [33] once again provided a very good explanation for directional stability for blended wing body aircrafts. Figure 14 shows a sample blended wing body experiencing positive sideslip.

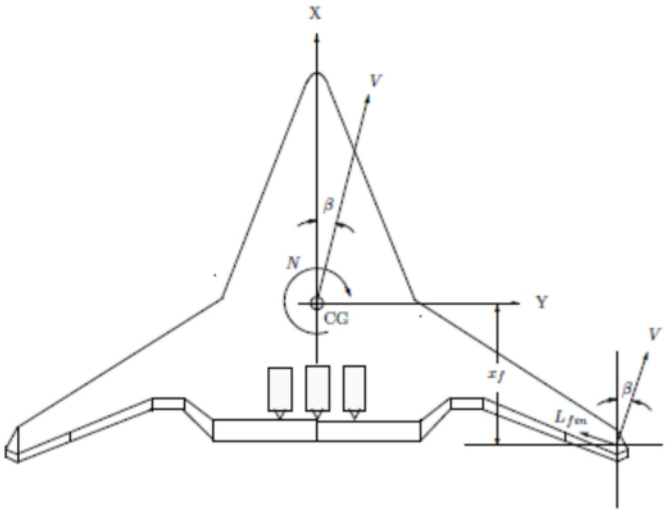

Figure 14: Blended wing body with positive sideslip [33]

There is hence a velocity component in the Y-axis. A yawing moment, N, is created by the fuselage and the vertical fin. Standard flight dynamics define that positive directional stability is present if

$$\frac{dN}{d\beta} = N_\beta > 0 \tag{2-16}$$

Hence, a positive sideslip, β, results in a positive yawing moment and turns the aircraft nose into the flight direction and hence, minimizes sideslip. The yawing moment due to the fuselage is usually destabilizing while the vertical fin provides stabilizing yawing moment. It can be derived that

$$N_f = \frac{1}{2}\rho {V_t}^2 S_f a_f x_f \left(1 - \frac{d\epsilon}{d\beta}\right)\beta \tag{2-17}$$

whereby a_f and $\frac{d\epsilon}{d\beta}$ are the vertical fin lift cure slope and downwash factor of the fuselage and wing on the vertical fin. Non-dimensionalising with $\bar{q}Sb$ and partial derivative with β results in

$$C_{n\beta fin} = \frac{S_f}{S}\frac{x_f}{b} a_f \left(1 - \frac{d\epsilon}{d\beta}\right) \tag{2-18}$$

Hence, it can be inferred that directional stability depends on the vertical fin area, S_f, and the moment arm, x_f. Generally, vertical fins are positioned at wingtip

locations for blended wing body aircrafts. Structurally issues would dictate that these fins have limited area, limiting the effect of these vertical fins. It can then be suggested that alternative means of directional stability augmentation must be provided.

Lateral stability is more straightforward for blended wing body aircrafts. Conventional aircrafts almost always have dihedral wings and the dihedral effect due to the weight component in the y-axis when the aircraft is in a roll inducing a sideslip velocity and hence a restoring roll moment would bring the wings level again. Blended wing body aircrafts should display similar attributes.

2.7 Boundary Layer Ingestion

Boundary layer ingestion is a common feature in ships and torpedoes. For aircraft purposes, its idea is for the engine to ingest the boundary layer flow created over the aircraft fuselage to result in fuel savings. This benefit is derived through re-energizing the aircraft wake, resulting in a far less energy waste as that of common aircraft/engine setup. This can be illustrated as shown in Figure 15.

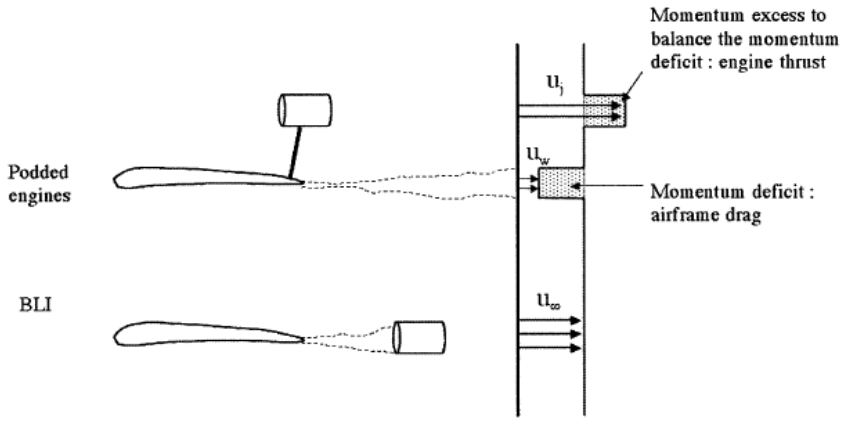

Figure 15: Podded engines vs Boundary layer ingestion [35]

The two cases shows a conventional podded engine on top of an aircraft and away from the boundary layer region and a100% boundary layer ingesting scenario whereby the engine is directly aft of the aircraft and ingesting the aircraft wake. The podded engines are ingesting freestream velocity, u_∞ and the engine

is exhausting an accelerated flow, u_j. In an ideally expanded nozzle, the momentum excess created by the engine or the engine thrust is equals to the momentum deficit or the airframe drag, D_a. u_w is the average velocity in the aircraft wake. Thus,

$$F_{engine} = \dot{m}(u_j - u_\infty) = \dot{m}(u_\infty - u_w) = D_a \quad \textbf{(2-19)}$$

The power required from the engine to the flow is

$$P_{podded} = \frac{\dot{m}}{2}({u_j}^2 - {u_\infty}^2) = \frac{F_{engine}}{2}(u_j + u_\infty) \quad \textbf{(2-20)}$$

The actual power required for flight or useful power is

$$P_{useful} = D_a u_\infty = \frac{\dot{m}}{2}(u_j - u_\infty)u_\infty \quad \textbf{(2-21)}$$

Hence, it can be deduced that the useful power is less than that of the power provided by the podded engine. Propulsive efficiency is the ratio of useful power to power provided.

Considering the 100% boundary layer ingested situation, the propulsive force or force provided by the engine is the same as that of the podded case since the engine accelerates the flow to the freestream velocity. The power required from the BLI engine is however

$$P_{BLI} = \frac{\dot{m}}{2}({u_j}^2 - {u_w}^2) = \frac{\dot{m}}{2}({u_\infty}^2 - {u_w}^2) = \frac{F_{engine}}{2}(u_w + u_\infty) \quad \textbf{(2-22)}$$

Comparing equation (2-20) and equation (2-22) and as can be seen from Figure 15, and noting that jet velocity, u_j, is more than wake velocity, u_w, it can thus be concluded that the power required from the non-boundary layer ingesting engine is higher than that of a boundary layer ingesting engine. This is due to the fact that less power needs to be added to an incoming flow into the engine with lower velocity to produce the same thrust force compared to a high velocity incoming flow.

The force created by the engine with incoming flow velocity u_1 and exit velocity u_2 is

$$F = \dot{m}(u_2 - u_1) = \dot{m}\Delta u \quad \textbf{(2-23)}$$

The power required would then be

$$P = \frac{\dot{m}}{2}({u_2}^2 - {u_1}^2) = \frac{F}{2}(u_1 + u_2) = F\left(u_1 + \frac{\Delta u}{2}\right) \quad \textbf{(2-24)}$$

When the mass flow and propulsive force is constant, the resulting change in velocity would also be constant and hence, the power required would be dependent on the inlet velocity into the engine. Therefore, a lower inlet velocity would equate to a lower power requirement.

Early work on boundary layer ingestion was conducted by Smith [36]. The most important concept was the definition of the power saving coefficient (PSC). It is defined as

$$\frac{P_{no\ BLI} - P_{BLI}}{P_{no\ BLI}} \quad \textbf{(2-25)}$$

Whereby $P_{no\ BLI}$ is the propulsive power for non-boundary layer ingesting engine and P_{BLI} is that for boundary layer ingesting engine. The study was based upon an axisymmetric unducted propeller ingesting a wake modelled as an actuator disk. The power saving coefficient was found to be a function of boundary layer displacement thickness to boundary layer thickness, shape factor, energy factor, wake recovery, airframe drag coefficient, and ratio of ingested airframe drag to total airframe drag. Important point to note was that the studies shows savings of up to 7% can be achieved.

2.7.1 Modelling of Performance of Boundary Layer Ingesting Fan

Conventional fans and compressors are designed for uniform inlet flow conditions. With boundary layer ingestion, there exists anomalies in the flow patterns and hence flow distortions appear.

Plas [37] did a comprehensive review of modelling methods of fan response to flow distortions from boundary layer ingestion which included one-dimensional parallel compressor approach, integral boundary layer type analysis and a full

three-dimensional body force model of non-uniform flow into the fan. The body force model method providing a result which was capable of capturing the fan response to both circumferential and radial flow distortions seen in boundary layer ingesting flows. Despite differences in PSC ranging from 10-40% from the results of the different methods, all show qualitatively similar results, which suggests the most important features are the inviscid response of the non-uniform flow through the fan and the resulting distortion transfer through the fan.

NASA proposed a 1D modelling method [38] for boundary layer ingestion modelling. Figure 16 shows the control volume of one engine with the proposed method.

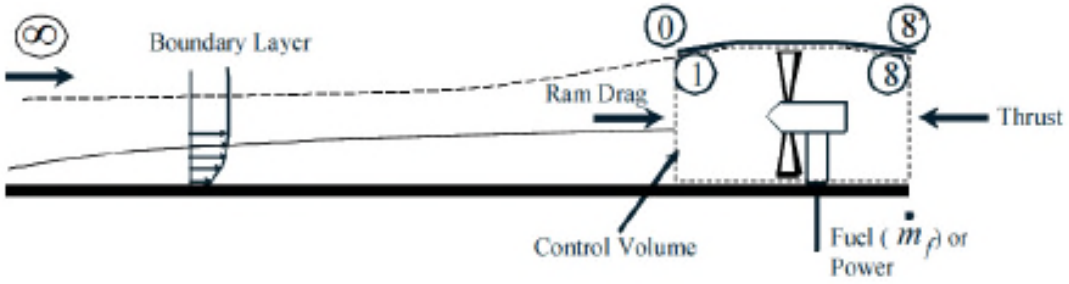

Figure 16: NASA proposed control volume

The net thrust is given by

$$Thrust_{net} = \left(\dot{m_1} + \dot{m}_f\right)U_8 - \dot{m}_1 U_1 + \left(P_{S,8} - P_{S,8'}\right)A_8 - (P_{S,1} - P_{S,0})A_1 \quad \textbf{(2-26)}$$

The inlet average total pressure and Mach number can be calculated by

$$\mathrm{P}_{T,1} = P_{T,0} \times R_{P_T} = \sum_0^i (\dot{m}_\iota P_{T,i}) \,/ \sum_0^i \dot{m}_\iota \quad \textbf{(2-27)}$$

$$\mathrm{M}_1 = M_0 \times R_{MN} = \sum_0^i (m_i M_i) / \sum_0^i m_i \quad \textbf{(2-28)}$$

The mass average total pressure and Mach number in each *i*-segment of the profile was calculated with the equations. Based on NASA's existing CFD data of a similar aircraft boundary layer profile, the mass averaged total pressure and Mach number profile at different centreline chord percentage is calculated.

Another important assumption is that the boundary layer thickness for different design propulsor pressure ratios are the same and the height of the stream tube or capture sheet height entering the propulsor inlet at design point is the same as the inlet height. The calculation is then iterated to obtain the values of R_{P_T} and R_{MN} to ensure mass flow convergence. Figure 17 shows the boundary layer velocity profile along the centreline at various percentage chord length. In this way, the mass averaged values are used to design the fan propulsor with no regards to the impact of the distortion on the fan performance.

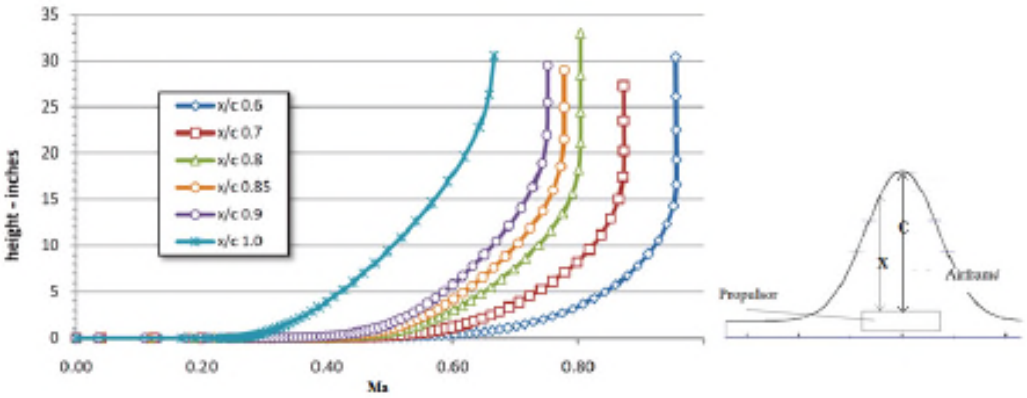

Figure 17: NASA existing CFD velocity profile

Another methodology to model BLI and its impact on fan performance is the 2D parallel stream method developed by Longley and Greitzer [39]. They modelled the non-uniform inlet velocity profile by 2 uniform, same height streams of different stagnation pressure and velocity, while assuming no mixing losses between the streams. The static pressure after the fan for both streams is assumed to be the same.

With the known velocity profile, the profile is divided into two equal height streams and the velocity of each stream is obtained as follows

$$V = \frac{\int_0^h \rho V dh}{\int_0^h \rho dh}, h = height\ of\ stream \quad \textbf{(2-29)}$$

The overall velocity is assumed constant across the stream as it passes through the fan stage. The ratio of the flow velocity between the two streams is assumed

to be constant before and after the fan stage. The total pressure at the inlet for each stream is obtained from the boundary layer profile and mass-averaging across the stream. There is assumed to have no temperature distortion and is the same as that of the freestream conditions. Finally, the static pressure after the fan stage is assumed to be constant across both streams. With these assumptions, an initial guess of the FPR across one stream is utilised to obtain the static pressure after the fan stage, the fan pressure ratio for the other stream is then iterated to obtain the same static pressure as calculated after the fan stage. The overall performance of fan stage for the two streams is mass-averaged across the two streams. While this method is easy to apply, there is a major drawback due to the assumptions made as they imply both streams operate on the same fan operating line as there is no temperature distortion This in reality, however, would not necessary be true.

A more recent study by Liu [40] presented a method to estimate the impact of boundary layer ingesting flow on the design point of the engine. The main benefits of this method is its independence of the blade shape or design which would be useful for preliminary overall system design or modelling without the need for an existing fan design. It makes use of existing generic fan performance maps. It provides a way to calculate the change in thrust generated due to the inlet flow distortion as well as presenting the possible benefits of BLI. .

Another method, Discretised Miller Method, developed by Valencia [41] made use of traditional mean-line compressor design relations to model the performance of a designed compressor under distorted inlet flow conditions. The entire inlet face is discretised in both radial and circumferential directions as seen in Figure 18 and various relations applied to predict the performance of each discretised region.

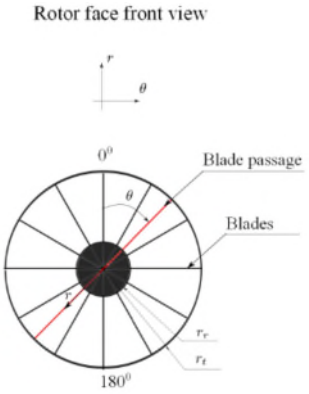

Figure 18: Fan rotor inlet discretised area [41]

The main benefits of this methodology is its ability to model both radial and circumferential performance of the compressor as well as the ability to predict the compressor under distorted inlet flow off-design conditions.

This method shows great promise as it has shown to be able to predict adequately the performance and trends of the fan in normal inlet conditions as seen in Figure 19 as well as under distorted conditions using CFD analysis [41].

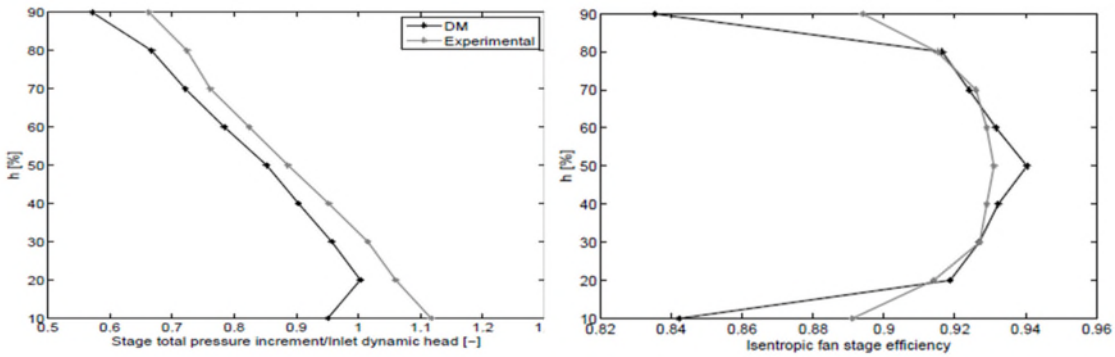

Figure 19: Comparison of D.M method and experimental results [41]

Chapter 3

AERODYNAMICS MODELLING

3.1 Introduction

On a TeDP aircraft which incorporates flap blowing, flap blowing can be seen as a possible applicable benefit from the thrust force produced by propulsor fans since the fans are mounted near the trailing edge. This then inherently changes the aerodynamic properties of the aircraft, which would in turn affect the propulsion requirements for the aircraft to fulfil the flight mission. These two traditionally separate design aspects then become highly integrated and it is important to be able to have a methodology or tool at an early design stage whereby flexibility in investigating the impact of different propulsion and structural architecture and variables have on flap blowing as well as the aerodynamic properties. This chapter would explain the strip methodology developed to fulfil these criteria.

Figure 20 shows the general flowchart of the aerodynamic module modelling. Various tools used include open source software such as Javafoil and Tornado. Javafoil [42] is a design and analysis tool for aerofoils. It allows calculation of the pressure distribution to the aerofoil and hence is able to obtain lift and drag characteristics as well as aerodynamic geometry properties such as centre of pressure and centre of lift. Tornado [43] is a vortex lattice method for linear aerodynamic wing design applications in conceptual aircraft design. It models the lifting surfaces as thin plates and solves the aerodynamic derivatives for the design.

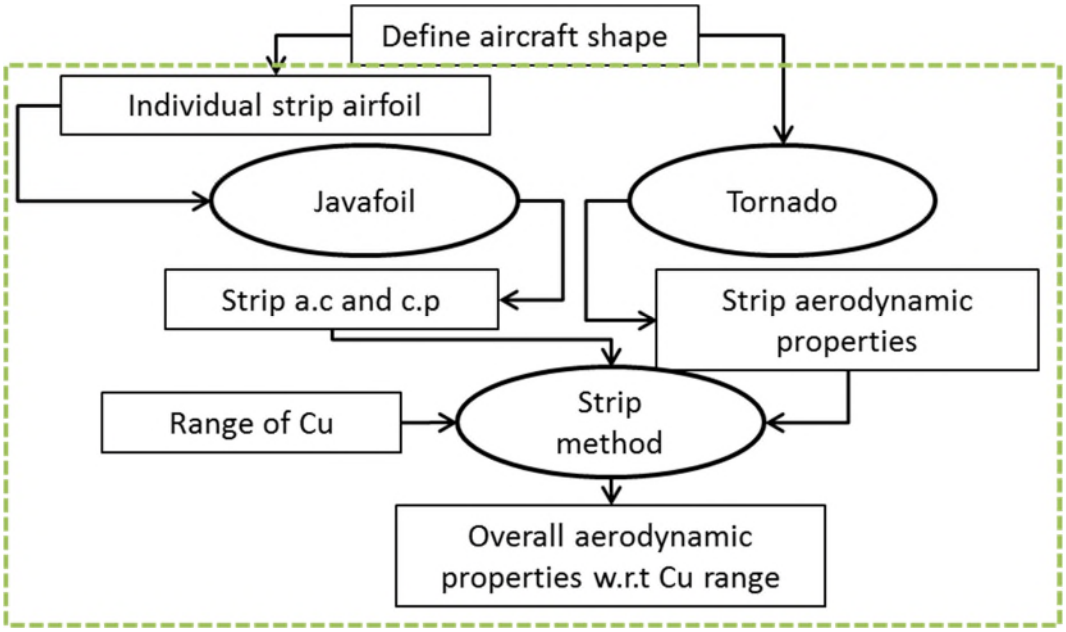

Figure 20: Aerodynamics analysis flow chart

3.2 Strip Method Code

To model the effects of flap blowing on the aircraft as well as providing a platform for parametric study of flap position and size and their impact on the propulsion system design, a strip model methodology was developed. In the model, the preliminary designed aircraft geometry is divided into multiple spanwise 2D strips of a selected width.

Each individual strip has its own lift characteristics such as baseline lift coefficient, lift curve slope, pitching moment coefficient, aerodynamic centre and centre of pressure. Furthermore, geometrical properties of the design as well as of the individual strips such as aerofoil shape, thickness, span, tip to chord ratio, taper, sweep, twist, dihedral angles at individual span locations are known. These act as inputs into Tornado. Tornado is able to output overall aerodynamic properties for the complete aircraft design at required flight conditions. These include the lift, drag, moment coefficients. Furthermore, Tornado is also able to output the spanwise local lift coefficient distribution. This would allow the local lift coefficient of each individual strip to be derived. The aerofoil shape and geometry of each individual strip is used as an input into Javafoil to calculate the pressure

distributions around the strip aerofoil. The aerodynamic centre and centre of pressure data is derived from the Javafoil analysis.

3.2.1 Strip Method Lift Force

The lift coefficient of each zero flap deflection individual strip at a specified AoA can be expressed as a function of the lift coefficient at zero AoA and the product of the lift-curve slope and AoA.

$$C_{L,strip} = C_{L0,strip} + C_{L,\alpha,strip} \times \alpha \qquad \textbf{(3-1)}$$

A sample spanwise local lift coefficient generated from Tornado of the N3-X aircraft is seen in Figure 21.

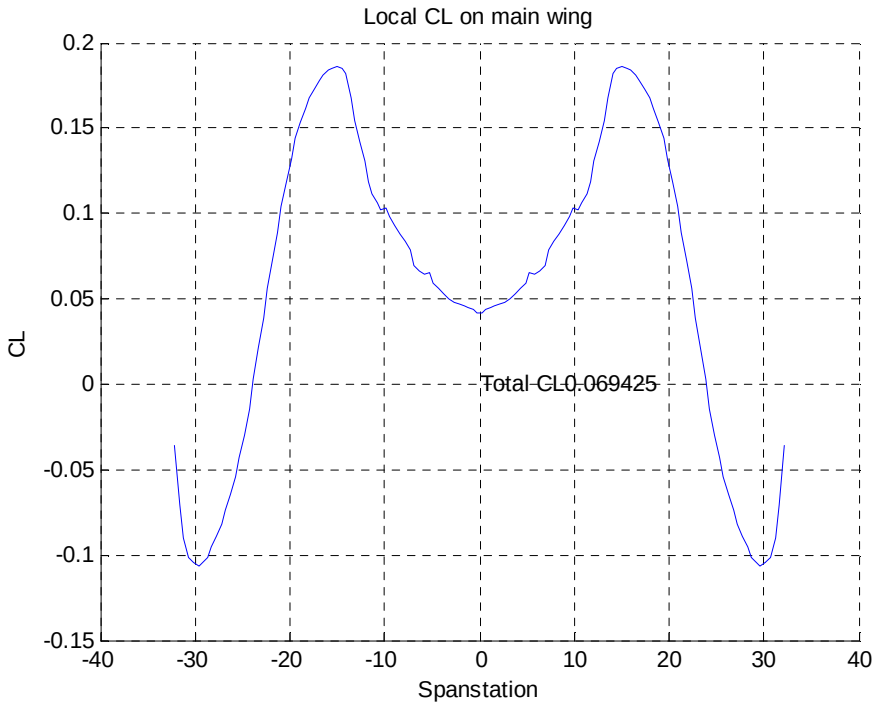

Figure 21: Local CL from Tornado

The lift generated along each defined strip of length *y* [m] is as follows

$$L_{strip} = \frac{C_{L,span=x} \times \bar{q} \times chord_{span=x} + C_{L,span=x+\mathrm{y}} \times \bar{q} \times chord_{span=x+\mathrm{y}}}{2} \qquad \textbf{(3-2)}$$

The lift coefficient generated along each strip is then

$$C_{L,strip} = \frac{L_{strip}}{\bar{q}\frac{(chord_{span=x} + chord_{span=x+y}) \cdot y}{2}} \quad \textbf{(3-3)}$$

The lift coefficient at zero AoA for each strip can be obtained from Tornado while the lift curve slope $\frac{\partial C_{L,strip}}{\partial \alpha}$ can be obtained by varying the AoA input in Tornado to obtain a series of strip lift coefficient. The impact of 3D properties such as effective AoA, sidewash, dihedral, wing sweep and wing twist on the strip lift coefficient has been catered for in the Tornado output.

The next logical step would be to determine the change in lift coefficient due to the presence of a flap deflection at the trailing edge of the individual strip. This would allow a systematic approach to allow a flexible variation in flap size and location to be studied and its impact upon the aerodynamic properties.

3.2.1.1 Change in Lift Coefficient Due to Flap Deflection

The presence of a flap and its deflection would affect the centre of pressure location of the strip as well as changing the pressure distributions around the strip aerofoil, thereby changing the lift created by the strip.

The change in the local lift coefficient at zero angle of attack for an aerofoil due to plain trailing edge flaps is documented in ESDU 94028 [44]. The increment in lift coefficient at zero angle of attack due to a plain trailing edge flap is

$$\Delta C_{L0} = 2J_P\delta_t \left\{ \pi - \cos^{-1}\left(\frac{2c_t}{c'} - 1\right) + \left[1 - \left(\frac{2c_t}{c'} - 1\right)^2\right]^{\frac{1}{2}} \right\} \quad \textbf{(3-4)}$$

whereby $c_t = flap\ chord, c' = chord\ after\ flap\ deployment, \delta_t = deflection\ angle,$ and J_P is a constant dependent on the deflection angle

Hence, at any selected strip, the deflection of any selected size flap chord can be incorporated to determine the change in lift produced by the individual strip.

3.2.1.2 Change in Lift Coefficient Due to Flap Blowing

Blown flaps on a strip with defined flaps would result in a change in the pressure distributions around the flap region as well as the presence of super circulation resulting in a change in amount of lift generated by the strip.

An important function in the description as well as the determination of the aerodynamic properties of an aerofoil with a blown flap is the dimensionless blowing coefficient as described in equation (3-5).

For the strip method, the blowing coefficient of each individual strip is defined as

$$C_{u,strip} = \left(\frac{\dot{m} V_{jet}}{\bar{q} \cdot \frac{(chord_{span=x} + chord_{span=x+y}) \cdot y}{2}} \right)_{strip} \quad \textbf{(3-5)}$$

The thin jet-flap theory by Spence [29] and Williams [30] made available 2D relations that can be applied to existing aerofoil lift relations to determine the new lift characteristics when a blown flap is applied. Studies [45] have shown that this thin jet-flap theory is inadequate for configurations with a thick jet such as upper surface blowing (USB) whereby the whole exhaust engine is situated at the fore of the wing with blowing across the whole wing or when it is blown as a jet flap. However, presence of the distributed propulsion greatly reduces the jet exhaust to a thin enough jet whereby this theory can be applied without the modifications as per mentioned in [45]

The lift coefficient of each individual strip is defined accordingly in (3-6). There is a change in the zero AoA lift coefficient when there is a pure jet flap deflected by an angle δ_f.

$$\Delta C_{L0,C_u,strip} = \left[4\pi C_{u,strip} \left(1 + 0.151 C_{u,strip}^{\frac{1}{2}} + 0.139 C_{u,strip} \right) \right]^{\frac{1}{2}} \times \delta_f \quad \textbf{(3-6)}$$

This interpolation formulae fits the graph in Figure 22 when $\frac{c_f}{c} = 0$ which is the case of a pure jet flap. The change in zero AoA lift coefficient due to flap blowing for various flap chord ratio can be derived from the graph.

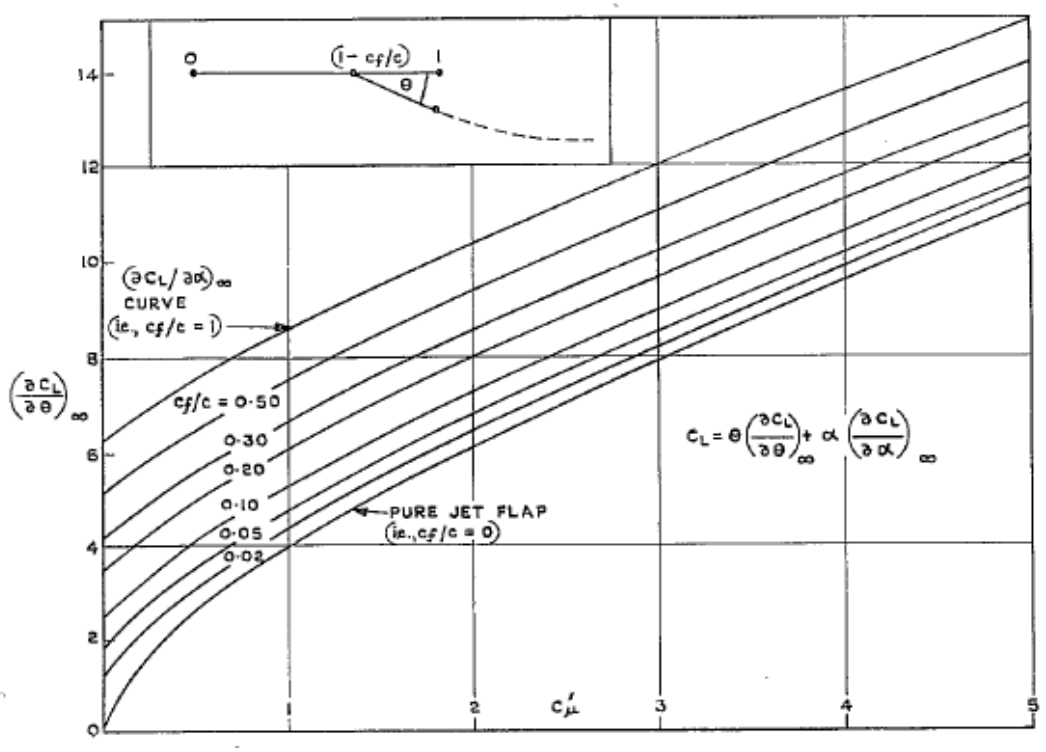

Figure 22: Change in zero AoA lift coefficient

.The lift curve slope of the aerofoil, $C_{L,\alpha,strip}$, is also changed when blowing is applied onto the flap. This is changed by a factor K_{Cu} defined as

$$K_{Cu} = (1.0 + 0.151C_{u,strip}^{\frac{1}{2}} + 0.219C_{u,strip}) \quad \textbf{(3-7)}$$

3.2.1.3 Overall Lift Coefficient

The strip lift coefficient and the strip lift force taking into account the flap deflection and flap blowing effects at any AoA is thus

$$C'_{L,strip} = C_{L0,strip+}\Delta C_{L0,strip} + \Delta C_{L0,C_u,strip} + K_{Cu} \cdot C_{L,\alpha,strip} \times \alpha \quad \textbf{(3-8)}$$

$$L'_{strip} = C'_{L,strip} \times \bar{q}_{strip} \times chord_{strip} \quad \textbf{(3-9)}$$

The overall total lift is then a summation of all the individual strip lift while the overall total lift coefficient is

$$C'_L = \frac{\sum_{i=1}^{n} L'_i}{\bar{q}S_{ref}} \; ; n = total\ number\ of\ strips \quad \textbf{(3-10)}$$

3.2.2 Strip Method Drag Force

The drag coefficient of the aircraft before flap deflection and blowing is applied can be expressed in the form of its drag polar as a function of the overall lift coefficient.

$$\mathrm{C}_D = \mathrm{C}_{D0} + K_D \cdot {C_L}^2 \quad \textbf{(3-11)}$$

These parameters can be obtained from the strip aerodynamics data obtained from Tornado.

3.2.2.1 Change in Drag Coefficient due to Flap Deflection

With flap deflection, induced drag due to the lift component will be changed and this is accounted for in the drag polar. Additionally, there is an incremental in the drag in the form of additional profile drag. The formulation in obtaining this additional profile drag is based on ESDU 87024 [46] for full span flap with modifications using ESDU Aero F.02.01.07 [47] to apply it on a part-span flap.

$$\Delta C_{D,flap} = \mu \Delta C_{Du} \cos \Lambda_{1/4} \quad \textbf{(3-12)}$$

whereby ΔC_{Du} is the change in profile drag coefficient for an unswept wing with full span flap deflection and $\Lambda_{1/4}$ is the quarter chord sweep angle for the strip.

ΔC_{Du} is dependent on whether the flap is positive or negative and both are functions of the flap deflection, δ_f, angle between chord line of aerofoil section and line joining mid-thickness point at hinge location to trailing edge of undeflected flap, γ, and the flap chord to strip chord ratio, $\frac{c_f}{c}$.

$$F\left(\delta_f, \gamma; \frac{c_f}{c}\right) = \frac{c_f}{c} \sin^2\left(\left|\delta_f + \gamma\right|\right) \cos\left(\left|\delta_f + \gamma\right|\right) \quad \textbf{(3-13)}$$

For positive flap deflections,

$$\Delta C_{Du} = F\left(\delta_f, \gamma; \frac{c_f}{c}\right) - F\left(\delta_f, 0; \frac{c_f}{c}\right) \quad \textbf{(3-14)}$$

For negative flap deflections,

$$\Delta C_{Du} = k(y)F\left(\delta_f, \gamma; \frac{c_f}{c}\right) - F\left(\delta_f, 0; \frac{c_f}{c}\right) \quad \textbf{(3-15)}$$

Whereby

$$k(y) = 1.0 - 0.005\gamma^2 \qquad \delta_f < -\gamma$$

$$k(y) = 1.0 \qquad \delta_f \geq \gamma$$

μ is a correction factor applied to the calculations to correct for part span flap instead of a full span wing flap. This factor is depicted in ESDU Aero F.02.01.07.

The factor is a function of the span of the strip and span of the whole wing and which differs depending on the taper ratio of the strip.

3.2.2.2 Change in Drag Coefficient due to Flap Blowing

Flap blowing essentially makes use of circulation control to alter the flow field around the flap region, enabling better attached flows as well creating a change in the lift properties. It can be imagined that a thick jet being blown would therefore alter the induced drag appreciably across the neighbouring lifting surfaces while a thin jet less so. This is explained in [48]. Studies have shown that the Coanda effect works best when the jet height is about 1-5% of the trailing edge radius and also within 0.1-0.2% of the chord length [49]. CFD studies [50] have shown that with USB jet heights of 3-4% of the chord length, drag increase at cruise can be between 10-20% whereas blown flaps with jet heights of 0.1-0.2% can result in no drag penalty at cruise

The changes in drag coefficient due to flap blowing is modelled in a pessimistic way whereby the drag polar is applied on the overall lift coefficient which includes the lift changes due to flap blowing to obtain the drag coefficient. The drag penalty due to flap blowing would probably be over-estimated in this method.

The overall drag coefficient would thus be

$$C'_D = C_{D0} + K_D \cdot C'^2_L + \Delta C_{D,flap} \quad \textbf{(3-16)}$$

3.2.3 Strip Method Pitching Moment

Each individual strip would have its own pitching moment about a specific point. The strip lift force is applied at the strip centre of pressure whereby there would be no resultant pitching moment around that point. The strip centre of pressure changes with changing AoA. The aerodynamic centre of the strip is a point whereby the pitching moment around that point does not change with AoA. This would hence imply that

$$\frac{dC_m}{dC_L} = 0 \tag{3-17}$$

For a symmetrical aerofoil, this is 25% chord length aft of the leading edge. For any other aerofoil, this location has to be determined.

Javafoil ouputs the moment data about a point 25% chord length aft of the leading edge. By inputting minute changes in the AoA, $\frac{dC_m}{dC_L}$ can be calculated for the strip.

The aerodynamic centre of the strip, $c_{a.c,strip}$, would thus be

$$c_{a.c,strip} = 0.25 - \frac{dC_m}{dC_L} \tag{3-18}$$

The pressure distribution on the upper surface of the aerofoil and lower surface of the aerofoil are also outputs from Javfoil.

To calculate the centre of pressure at a specified angle of attack, the force at each upper location along the aerofoil is calculated while the moment is a product of the distance of the location from the leading edge and the force. Similarly, the calculation is done for the lower surface of the aerofoil. The total force and moments acting on the aerofoil is the summation of the upper and lower surfaces' values. The centre of pressure location from the leading edge is then the overall moment divided by the overall force.

The pitching moment of the strip about its aerodynamic centre at a specified AoA is therefore

$$m_{strip,a.c} = L_{strip} \times \left(h_{a.c,strip} - h_{c.p\ strip}\right) \tag{3-19}$$

whereby h is the distance from the leading edge of the strip to the specified point of the strip.

The pitching moment generated by the strip about its aerodynamic centre at any angle of attack remains constant.

3.2.3.1 Change in Pitching Moment with Flap Deflection

ESDU 98017 [51] describes the change in aerofoil and wing pitching moment about the quarter chord position at zero angle of attack due to the deployment of trailing-edge plain flaps.

For a strip that has flap deflection, it is being modelled with the relations that describe a wing with full span flap deflection.

$$\Delta C_{m\alpha 0,{}^{1}/_{4}c,\text{strip}} = -K_f(K_o - K_i)\Delta C_{L0} h_2 \tag{3-20}$$

Whereby K_o and K_i are functions of the strip taper ratio and inboard and outboard limits of the strip flap, $K_f = \left(\frac{a_1}{2\pi}\right)^{0.46}$ and a_1 is the strip lift slope. h_2 is the increment of the centre of pressure at zero angle of attack, expressed as a fraction of the chord and measured positive aft from the quarter chord point and is defined as

$$h_2 = h_{2T} + 0.012\left(44 - \delta_t{}^{\circ}\right) z_{um}/c + 0.011\left(\frac{c_t}{c}\right)^3 \delta_t{}^{\circ} \tag{3-21}$$

$$h_{2T} = 0.25\left[1 - \left(2\frac{c_t}{c} - 1\right)^2\right]^{\frac{1}{2}}\left[1 - \left(2\frac{c_t}{c} - 1\right)\right] \Bigg/ \left\{\pi - \cos^{-1}\left(2\frac{c_t}{c} - 1\right) + \left[1 - \left(2\frac{c_t}{c} - 1\right)^2\right]^{\frac{1}{2}}\right\} \tag{3-22}$$

whereby $\frac{c_t}{c}$ is the ratio of flap chord to aerofoil chord, z_{um}/c is the ratio of maximum upper-surface coordinate to the aerofoil chord.

The change in strip moment coefficient at zero AoA due to flap blowing around the aerodynamic centre is then

$$\Delta C_{m\alpha 0,\text{a.c,strip}} = \Delta C_{m\alpha 0,{}^{1}/_{4}c,\text{strip}} \times (c_{a.c,strip} - 0.25) \times chord_{strip} \tag{3-23}$$

Due to the change in the centre of pressure location, there is also a change in the moment produced around the aerodynamic centre from the original strip lift.

$$\Delta C_{m,\text{a.c,strip}} = \left(C_{L,\text{strip}} + \Delta C_{L0,\text{strip}}\right) \times \left(c_{a.c,strip} - (0.25 + h_2)\right) \times chord_{strip} - C_{L,\text{strip}} \times \left(c_{a.c,strip} - 0.25\right) \times chord_{strip} \quad \textbf{(3-24)}$$

3.2.3.2 Change in Pitching Moment due to Flap Blowing

There is a change in the overall pitching moment around the aerodynamic centre due to the change in the lift produced from flap blowing as well as the change in the centre of pressure location.

$$\Delta C_{m_{Cu},\text{a.c,strip}} = \left[\Delta C_{L0,C_u,strip} + (K_{Cu} - 1) \cdot C_{L,\alpha,strip} \times \alpha\right] \times h_2 \times chord_{strip} \quad \textbf{(3-25)}$$

3.2.3.3 Overall Pitching Moment

The strip pitching moment around the aerodynamic centre is the sum of the original pitching moment and the various changes due to flap blowing and deflection.

The complete aircraft pitching moment around a specific point, x should be a summation of the individual strip pitching moment around the point.

$$C'_{m,x} = \frac{\sum_i^n \left[m_{strip,a.c} + (\Delta m_{\alpha 0,\text{a.c,strip}} + \Delta m_{\text{a.c,strip}} + \Delta m_{Cu,\text{a.c,strip}}) \times \frac{(h_x - h_{a.c})}{(h_{a.c} - h_{c.\text{p}})}\right.}{\bar{q} S_{ref} \bar{c}} \quad \textbf{(3-26)}$$

3.3 Application of Strip Method Code on N3-X

The strip method code is first validated on the N3-X aircraft by comparing the aerodynamic coefficients obtained from the code with that obtained from Tornado. A parametric study is then conducted to observe the impact of flap blowing for both positive and negative flap deflection on the aerodynamic properties.

3.3.1 N3-X Geometry

The complete N3-X aircraft geometry is obtained from OpenVSP [52] which is made available by NASA. This is shown in Figure 23.

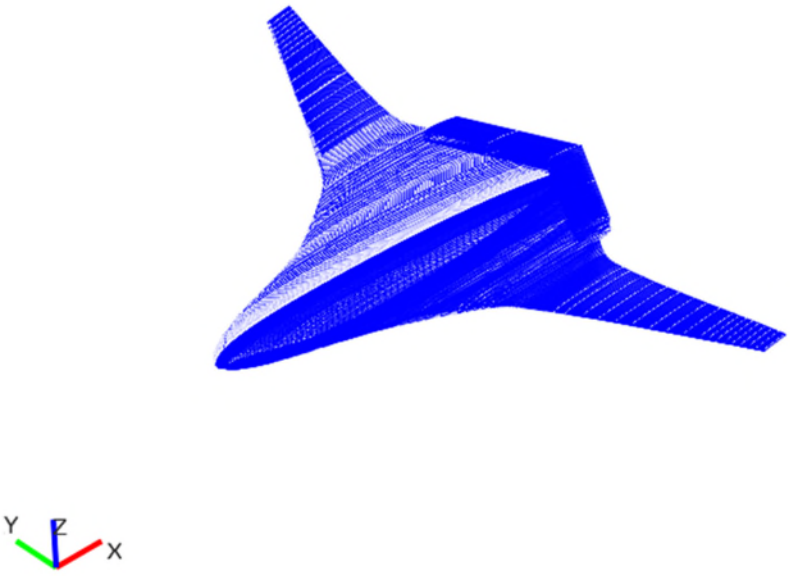

Figure 23: NASA N+3 OpenVSP aircraft geometry

This geometry is then divided into multiple strips and can also be built up in Tornado. The geometry in Tornado is shown in Figure 24.

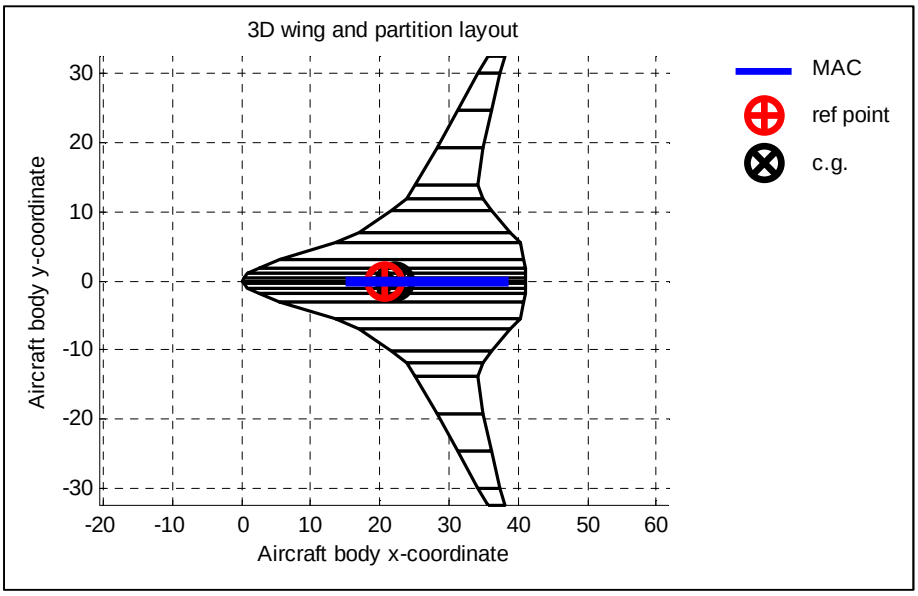

Figure 24: N3-X Tornado geometry

The reference point in Tornado is the coordinate whereby the moment coefficients are computed. The baseline N3-X aerodynamic properties can be found in Appendix A.

3.3.2 Application and Comparison of Strip Method Code

The strip method code is applied on the obtained geometry and the outputs obtained from both Tornado and the results are compared to confirm application of the code. Figure 25 shows the lift and pitching moment coefficient with differing AoA and no flap deflections as well as differing flap deflection angles at a selected 4 deg AoA. The flap for the N3-X in this instance is assumed to be a fixed 20% chord length across the span of the whole aircraft. The lift coefficient from the code when there is no flap deflection is the exact output from Tornado and this implies the number of strips whereby the aircraft is dissected into is sufficient for convergence of the code. The pitching moment thus calculated from the code also matches well with that of the Tornado output. Both lift coefficient and pitching moment coefficient from the code when flap deflection is varied also matched well from the direct output from Tornado.

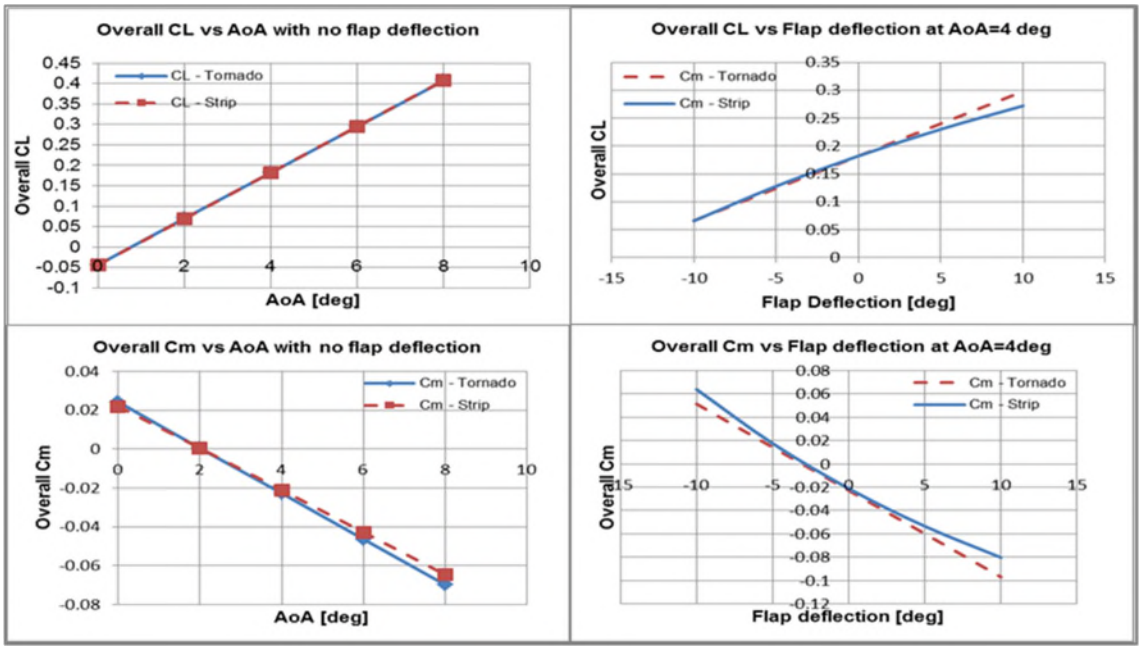

Figure 25: Comparison of results for strip method code

Figure 26 shows the corresponding drag coefficient output with varying flap deflections at a AoA of 4 deg from the code. There exists the possibility that the aerodynamic properties would differ when methodology is applied for different flight conditions as seen in [53]. However, it is assumed in this study that the aerodynamic properties are constant across the various flight regimes and conditions.

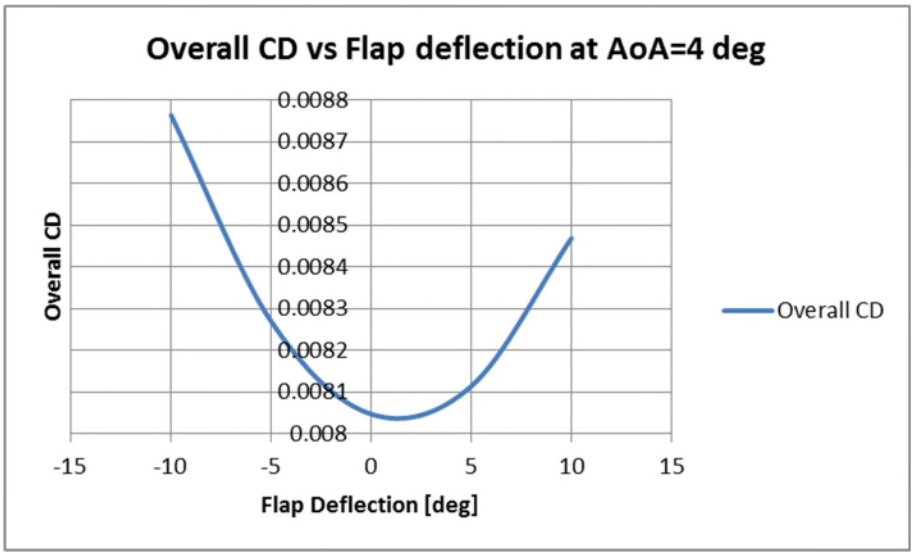

Figure 26: Drag coefficient output from strip method code

3.3.3 Parametric application of flap blowing on N3-X

The application of flap blowing is expected to change the aerodynamic properties of the aircraft. The impact of blown flaps on each individual strip can be observed when 20% chord length blown flaps is applied across the entire span of the aircraft with different flap deflection angles. Figure 27 shows the local lift and local pitching moment comparison along the half span of the N3-X when 0 and -2 deg deflections and flap blowing is applied at an AoA of 4 deg.

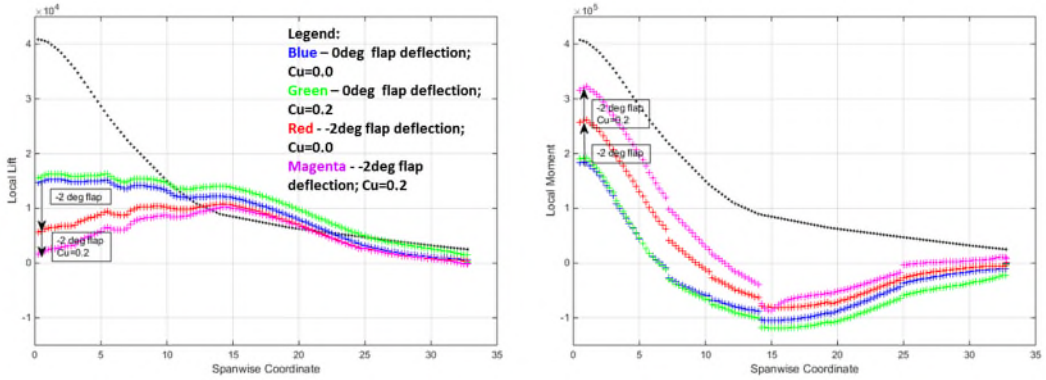

Figure 27: N3-X local lift and pitching moment with varying blowing coefficient

Negative flap deflections decrease the local lift generated by the aircraft. This is further amplified when flap blowing with a reasonable Cu=0.2 is applied. This is detrimental to the aircraft in various flight conditions as it would mean a higher AoA would be required to achieve the same amount of lift, thereby generating more drag as well as longer take-off distances. On the other hand, the amount of pitching moment generated is significantly increased when flap blowing is applied. This would then imply a lower AoA to trim as well as increased rotation rate during take-off which would reduce take-off distances. At positive AoA, the reverse would be expected. The decrease in lift and the increase in pitching moment contribute opposing effects and hence detailed studies would need to be undertaken to be certain if flap blowing is beneficial.

Another interesting point to note is that the impact of flap blowing differs along the span of the aircraft despite a constant 20% flap chord. This suggests a study into the location and span of the flaps for flap blowing in the overall scheme would be beneficial.

3.4 Conclusion

In this chapter, the strip method code that calculates the lift, pitching moment and drag while incorporating flap deflection and flap blowing is formulated. This allows for a flexible approach in locating the flaps as well as the size of the flaps. The impact of flap blowing on the aerodynamic properties is captured in the code using theoretically and experimentally derived equations.

The code was applied on the N3-X The geometry was obtained from OpenVSP and allowed for detailed study with the code. A validation was done on the code with the N3-X for the aerodynamic properties generated at various flap deflection angles as well as AoA.

Flap blowing was applied on the N3-X across the complete span of the aircraft for a 20% chord length flap and it was shown that flap blowing decreases the local lift generated by the aircraft for a negative flap deflection while it significantly increases the pitching moment generated. The degree of impact on the aerodynamic properties also differs across the span, implying that consideration should be given for location and span of the blown flap.

Chapter 4

FLIGHT DYNAMICS MODELLING

4.1 Introduction

Flight dynamics modelling (FDM) makes use of the six degree of freedom equations to model the static and dynamic response of the aircraft in motion. These include the lift, drag, side forces and the pitching, yawing, rolling moments. The aerodynamic properties from the previous chapters act as inputs for the FDM. The methodology flow for the FDM module is shown in Figure 28.

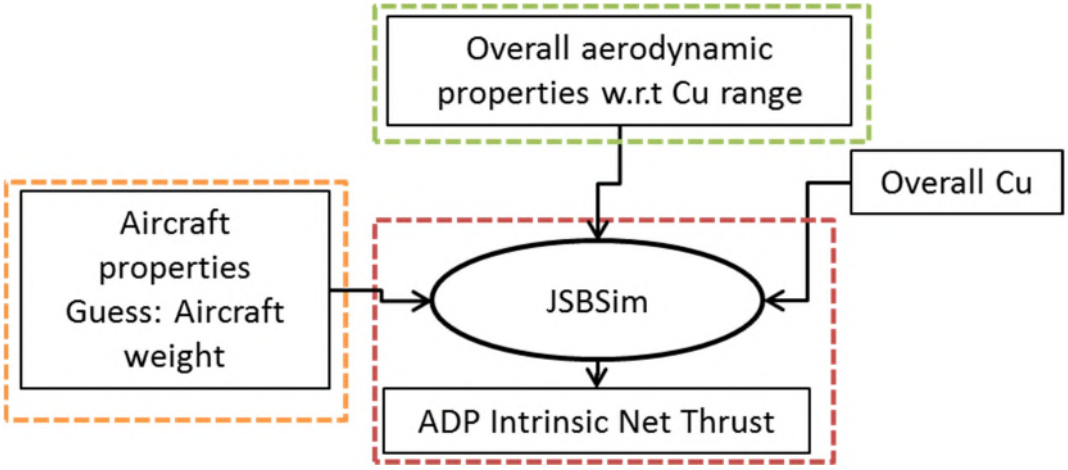

Figure 28: Flight Dynamics Modelling flowchart

The methodology incorporates blowing coefficient, aerodynamic properties, aircraft properties as well as the aircraft weight as inputs into JSBSim [54] to calculate the intrinsic net thrust requirements for a specific trim flight condition. A dynamic flight response phase such as take-off simulations can also be performed in JSBSim.

JSBSim is an open-source FDM code which allows modelling of flight dynamic related aircraft characteristics. These include mass and inertia properties, engines, thrusters, landing gears, control surfaces, ground effects. The forces

and moments of the aircraft due to each individual aircraft component can be modelled through mathematical formulations into the code. These essentially form the six degree of freedom (6 D.O.F) equations that govern the flight dynamics of an aircraft.

Using the code, the Blended Wing Body (BWB) aircraft selected for the study can be modelled through its individual components and their effect on the flight dynamics of the plane can be observed. Thus, the study can investigate the effect of removing the control surfaces in controlling the plane and replacing them with thrust vectoring control inputs as well as the impact of flap blowing.

The code can also be used to assess longitudinal and lateral trim requirements of the aircraft at various flight conditions using its control surfaces or thrust vectoring inputs. This would form a flight dynamics static analysis of the aircraft. The response of the aircraft to longitudinal and lateral requirements commands can also be assessed through dynamic analysis using the code. This also allows an investigation into the take-off requirements of the distributed propulsion blended wing aircraft using thrust vectoring and flap blowing.

4.2 Thrust Definition & Book-keeping

At this point, it is useful and pertinent to properly define the various thrust definitions used in the thesis. This would minimize confusion on how the relations are developed and modelled in the various modules and allows for consistency.

The control volume defined for the study affects how the thrust requirements on the propulsion system are defined as well as the inputs required to calculate the thrust. Plas [37] considered the control volume for study of podded engine as shown in Figure 29.

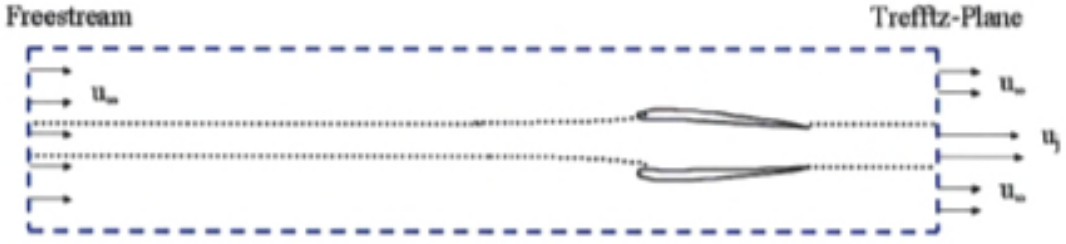

Figure 29: Plas [37] proposed Control Volume

The propulsive force provided by the engine is thus defined as

$$T = W(u_j - u_\infty) \tag{4-1}$$

Neglecting the drag of the nacelle, and for trim flight whereby there are no resultant forces, this propulsive force would have to balance the bare airframe drag defined as

$$D_A = \int \rho(u_\infty - u_w)u_w dA \tag{4-2}$$

However, in the case of the embedded engine, the control volume as applied and seen in Figure 30 would have to take into consideration from the start of the pre-compression zone to the Treffz-Plane. Hence, the control volume analysis would require information regarding the non-freestream air entering the engine as well as the pressure forces acting on the airframe.

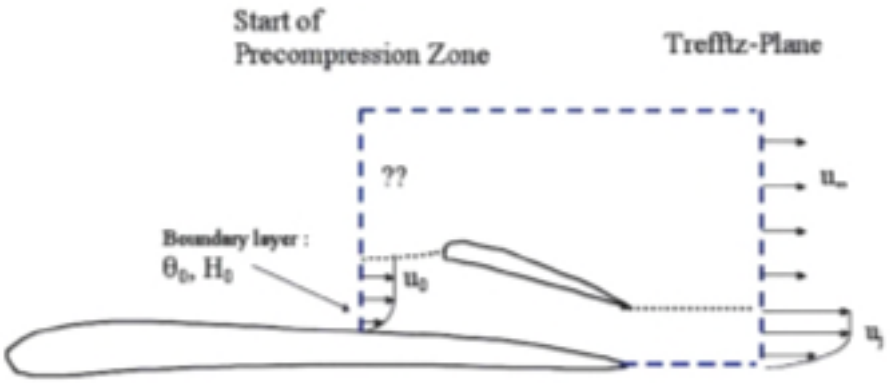

Figure 30: Plas [37] proposed Control Volume 2

Therefore, it is useful and important to define a common control volume to be used consistently in this thesis and to account properly for the thrust and drag definitions resulting from the control volume. Rodriguez [55] perfectly summed up the fundamental differences and usefulness of two such control volumes, external control volume and inner control volume.

4.2.1 External Control Volume

The external control volume is defined as such in Figure 31.

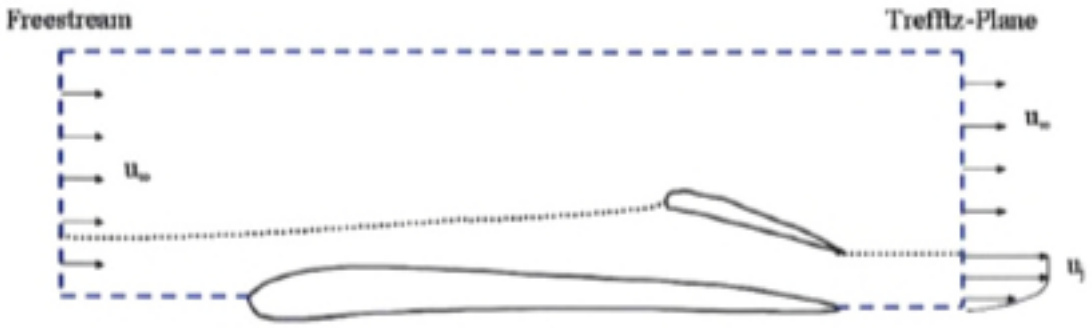

Figure 31: Definition of external Control Volume

The airframe and the engine are both included in such a control volume. The thrust calculations would begin with far upstream freestream conditions to the end which is the Trefftz-Plane. The flow at this plane has a momentum excess over the freestream upstream conditions and is defined as the net thrust below.

$$T_N = \int \rho(u_j - u_\infty)u_\infty dA \tag{4-3}$$

Similarly defined is the net drag which is the momentum deficit and this takes into account the drag of the airframe and nacelle minus the ingested drag which is a result of the fluid that flows over the airframe and into the engine.

$$D_N = D_A + D_{NAC} - D_{ING} \tag{4-4}$$

In trim flight conditions, the net thrust must equate to the net drag and hence

$$T_N = D_N = D_A + D_{NAC} - D_{ING} \tag{4-5}$$

The influence of boundary layer flow in this analysis is displayed in the reduction of the net thrust requirements to trim the aircraft. Hence, differing boundary layer conditions would imply a change in the net thrust requirements of the aircraft.

4.2.2 Inner Control Volume

Another method is the inner control volume as developed by Kim [38]. This method attempts to decouple the propulsion system with the airframe design and hence aerodynamic influences. This is seen in Figure 32.

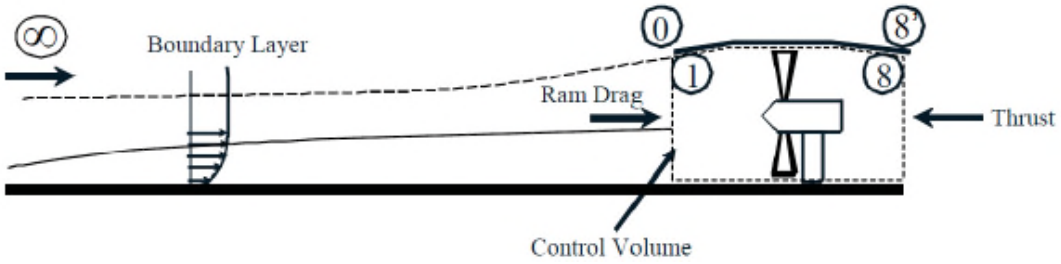

Figure 32: Definition of inner Control Volume

The control volume encloses the propulsor from its intake to its exhaust. The net thrust derived from such a control volume is defined as

$$T_N = W(V_8 - V_1) + \left(P_{S,8} - P_{S,1}\right)A_8 - (P_{S,1} - P_{S.0})A_1 \quad \textbf{(4-6)}$$

The static pressure at the propulsor inlet face does not equate to the ambient static pressure due to the presence of the boundary layer flow. This net thrust is defined as the intrinsic net thrust of the system.

The inner control volume is suitable for the purpose of this thesis due to a few advantages.

- It allows decoupling of the propulsion system with the airframe or aerodynamic performance. The aerodynamic drag determined from the aerodynamics module would be unaffected by such a definition.
- For trim flight conditions, the intrinsic net thrust would equate to the aerodynamic drag, allowing for ease of implementation in the overall scheme.
- The benefits or drawbacks of BLI would be accounted for in the propulsion system design as this is a direct consequence of the reduced inlet momentum drag which is the main emphasis of the work done.

- It allows for a different boundary layer profile in each distributed propulsor and its impact on the propulsion system to be captured more accurately.

A major drawback of this method is the requirements of the boundary layer profile at the inlet to be known. In the context of the work done here however, this would be a useful implementation as it allows for flexibility in placing the inlet location, whether it is longitudinally or laterally and would thus allow investigation into how different location intake would have an impact on various parameters. This however, would still necessitate a methodology to easily obtain the required boundary layer profile which would be covered in later chapters.

Further on from this point in the thesis, all work presented would make use of the inner control volume whereby the intrinsic net thrust produced by the propulsors is defined unless otherwise stated.

4.3 Trim Intrinsic Net Thrust Definition

Using the inner control volume method, the trim intrinsic net thrust that is used in the following studies is defined as

$$T_N = D_N = D_A + D_{NAC} \tag{4-7}$$

An important parameter that will be further discussed later on is the inlet capture sheet height or the intake height for the fan propulsor array. The intake on the N3-X is a mailbox intake with the skin profile following that of the original aircraft design elevated to the intake height. The nacelle drag is assumed constant in the studies and forms part of the aircraft drag for this highly integrated intake. Thus the trim intrinsic net thrust is defined as

$$T_N = W(u_8 - u_1) + (p_8 - p_1)A_8 - (p_1 - p_0)A_1 = D_N = D_A \tag{4-8}$$

At any selected flight condition, the aircraft is considered to be in a trim condition if there are no net forces and moments acting on it [56]. To simplify the analysis, the trim conditions at the ADP for the aircraft are calculated using the defined MTOW of the aircraft. Thus,

$$L = MTOW \quad \textbf{(4-9)}$$

$$T_N = D_N \quad \textbf{(4-10)}$$

$$C_{mcg} = 0 \quad \textbf{(4-11)}$$

It has been shown in previous chapters that the pitching moment is a function of the lift of the aircraft while the aircraft drag follows the drag polar which is a function of the lift. Hence, the MTOW impacts upon trim lift of the aircraft which in turns affects the trim drag of the aircraft and hence the trim intrinsic net thrust of the aircraft.

4.4 Application of Strip Method with Flight Dynamics Modelling

The basic aerodynamic properties obtained from the strip method are incorporated into JSBSim for FDM. At their most basic form, they consist of bare airframe properties:

$$C_{L_0}, C_{L_\alpha}, C_{L_Q}, C_D, C_{D_Q}, C_{Y_\beta}, C_{Y_P}, C_{Y_R}, C_{l_\beta}, C_{l_P}, C_{l_R}, C_{m_\alpha}, C_{m_0} C_{m_Q}, C_{n_\beta}, C_{n_P}, C_{n_R}$$

The main purpose of this thesis concentrates only on the lift, drag and pitching moments which are derived from the strip model. The rest of the parameters are used in its entirety from the output in Tornado.

There are incremental coefficient values for lift, drag and pitching moment as a result of flap deflections and blowing that are similarly derived from the strip method. These are functions of the flap deflection and the blowing coefficients and are used as additional inputs into JSBSim.

CG location and moment reference points are additional outputs from the strip method code and used as inputs into JSBSim. Other defined parameters that are required into JSBSim to fulfil the simulations are the total mass of the aircraft, the blowing coefficient, the TSFC of the propulsion system. It should be noted at this point that the blowing coefficient and TSFC are functions of the propulsion system and can be either defined as constants or in relation to the operating condition of the propulsion system.

It is also important to have a clear idea on the sign conventions and reference frame used in the models to avoid confusion and to accurately model the various forces. Unless otherwise stated, the reference frame used in this thesis is the structural frame whereby the X-axis increases from the nose of the aircraft to the tail, the Y-axis increases from the centreline towards the right when looking forward of the aircraft and the Z-axis is then positive upwards as a result of the right hand rule.

An additional input used in this thesis is the modelling of thrust vectoring for FDM. Each distributed propulsor produces an intrinsic net thrust, $T_{N,prop}$ in the flight direction. Thrust vectoring is modelled as a point thrust in JSBSim and if thrust vectoring is applied at an angle δ_{TV}, the resulting intrinsic net thrust produced in the flight direction is then

$$T'_{N,prop} = T_{N,prop} cos\delta_{TV} \quad \textbf{(4-12)}$$

The resulting change in the Z force as a result from thrust vectoring is modelled in JSBSim as

$$\Delta Z = T_{N,prop} \sin \delta_{TV} \quad \textbf{(4-13)}$$

The additional pitching moment created from this thrust vectoring is then

$$l_{TV} = T_{N,prop} \sin \delta_{TV} \times x \quad \textbf{(4-14)}$$

Whereby x is the distance from the aerodynamic centre of the aircraft defined to the location of the nozzle exhaust.

4.5 Case Study –Flap Size & Location Impact on TSFC of N3-X

The first case study that can be done on the N3-X using a combination of the flight dynamics modelling and aerodynamics module is the determination of the ideal location to locate the flaps and fan propulsor intake. Different lateral location of the intake position would result in different boundary layer profile ingested by the fan array as the aerofoil profile and chord length changes laterally. Similarly, different longitudinal location of the intake would also result in different boundary layer profile ingested due to the continuous development of the boundary layer

profile along the chord. At the same time, the size of the flaps would impact upon the blown aerodynamic properties of the aircraft. Hence, a parametric analysis was done to determine the size of the flaps as well as the lateral location of the intake which would result in the lowest TSFC for the aircraft.

In total, 6 different configurations were studied and these are tabulated in Table 3. The corresponding trim intrinsic net thrust requirements are calculated in the flight dynamics module. Figure 33 shows the various configurations. In this study, the blowing coefficient is assumed to be constant at a value of 0.03. This value in reality, should fluctuate depending on the fan array design and configuration. This value was calculated based on the original thrust requirements and fan configuration from NASA [24]. The intake location and the flap root location are assumed to be the same in this study for two reasons. Firstly, the intake pressure loss is not a variable in this study and assumed to be constant at 1.5%. The length and shape of the intake would invariably affect the intake pressure losses and necessitates in depth study that is not part of the current one. Secondly, by assuming the intake and flap root to be at the same location, it allows a reference point to obtain the boundary layer profile which is ingested into the fan array.

Table 3: Parameters of studied flap configurations

Arrangement	Centre of aircraft				Wing of aircraft	
Intake Span [m]	16		20		20	
Intake/Flap Longitudinal location [m]	33.5	36.5	33.5	35.0	31.0	32.5
Trim Intrinsic Net Thrust [N]	117768	117901	117837	117853	122292	121368
Configuration Number	1	2	3	4	5	6

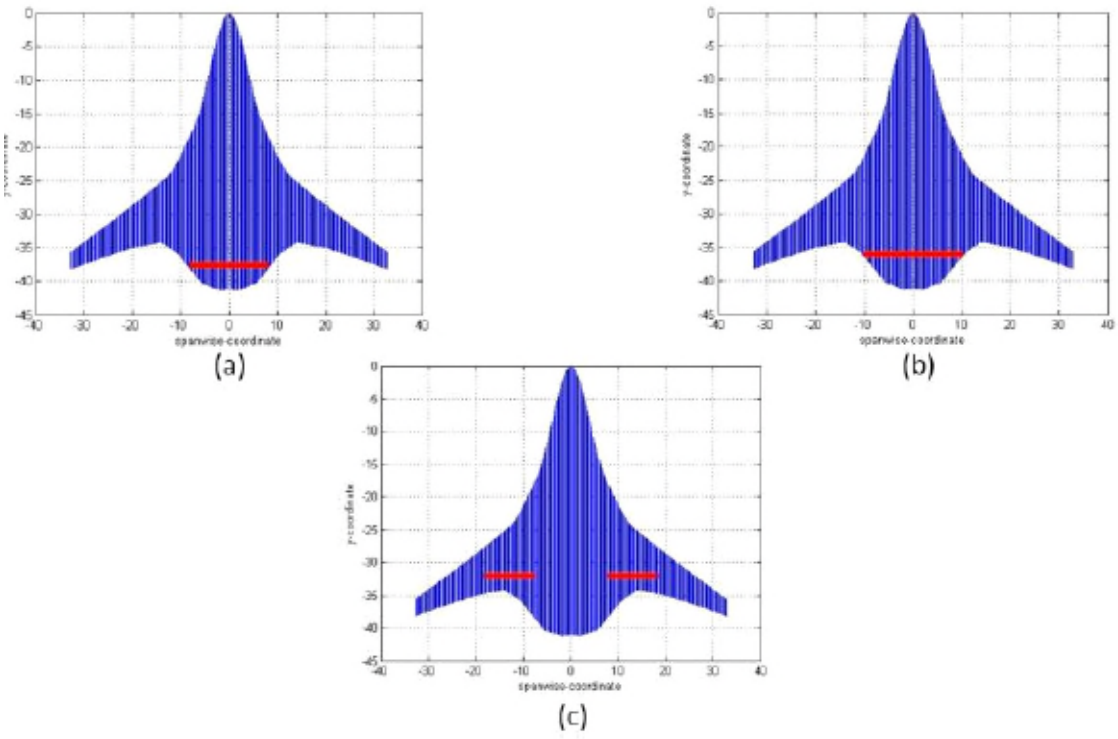

Figure 33: Layout of studied flap configurations

The boundary layer profile in this study is obtained using Javafoil with the aerofoil data of the N3-X. The chord length changes across the span of the intake and the average chord length across each fan array configuration is calculated and

used to derive the boundary layer profile in Javafoil. Figure 34 shows the variation of the boundary layer profile for various aerofoils on the N3-X. These are computed for an AoA of 3 degrees and 3.5 degrees which are representative values of the N3-X trim conditions at the ADP as computed in the flight dynamics module.

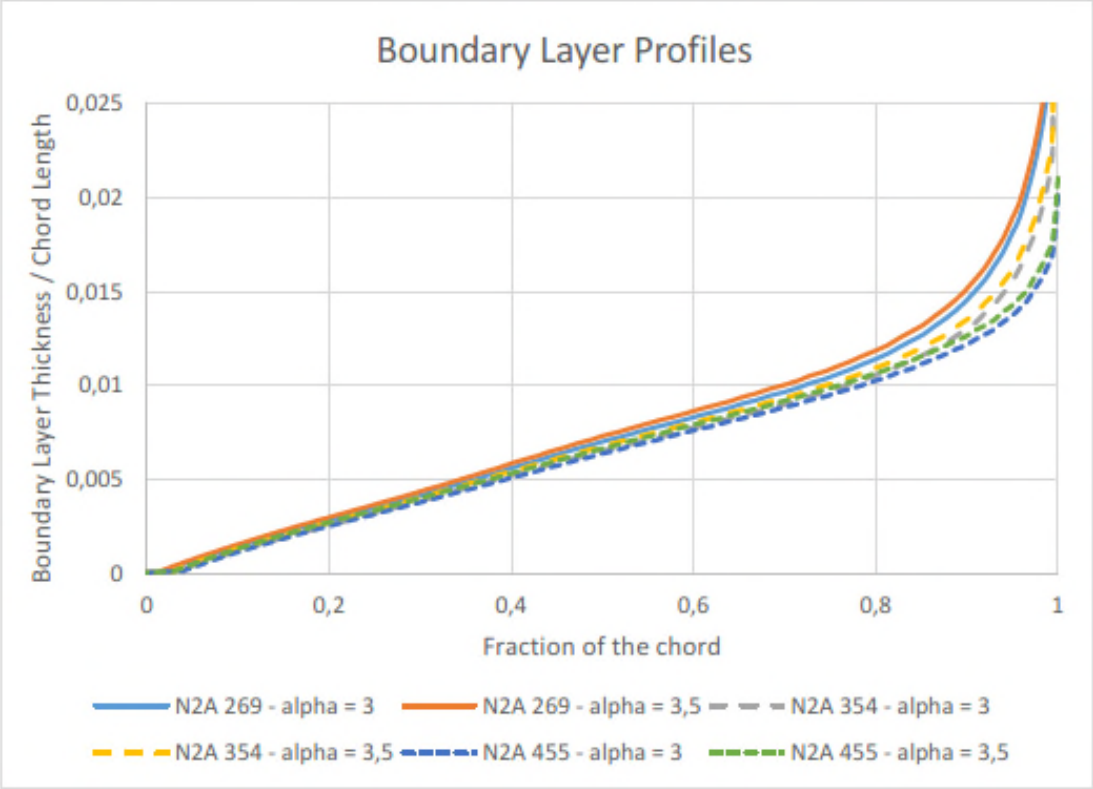

Figure 34: Javafoil output of various boundary layer profiles of N3-X aerofoils

The parallel stream method BLI approach to the fan array design is incorporated in this study. The core engines follow the same assumptions as will be discussed in Chapter Chapter 5 and are modelled in Turbomatch.

For each configuration, the TSFC is calculated and obtained from the core engine design from Turbomatch. The core engines were assumed to be turboshaft engines and a thrust split ratio (TSR) is varied between 75%, 85% and 95%. This is the ratio of the thrust provided by the fan propulsor array to the overall thrust provided by the complete propulsion system. Further explanation of this will be provided in Chapter Chapter 5. Figure 35, Figure 36 and Figure 37 shows the TSFC for a 0%, 1.5%, 3% intake pressure loss system respectively.

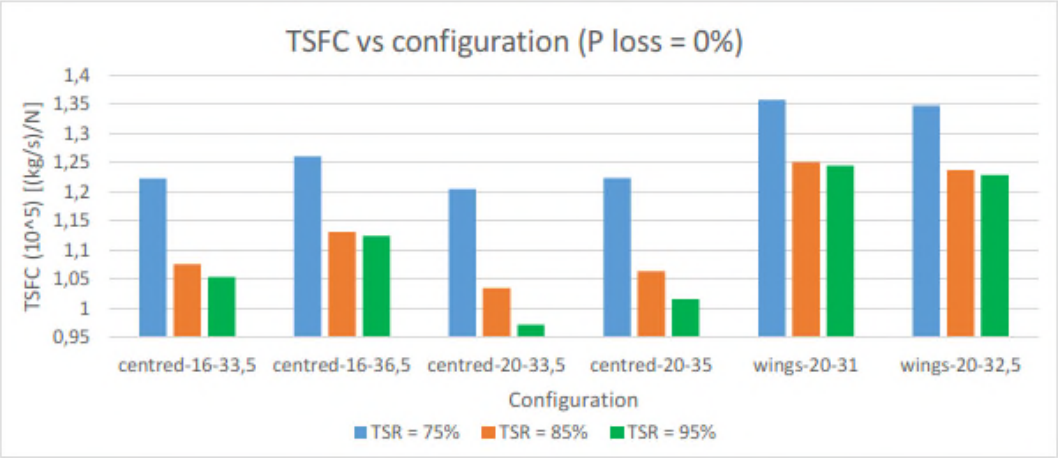

Figure 35: TSFC of configurations with 0% intake pressure loss

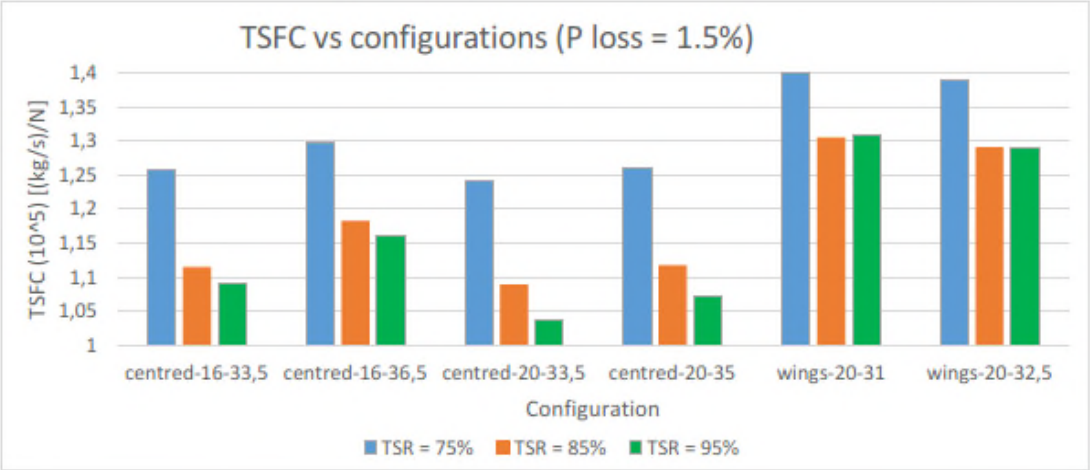

Figure 36: TSFC of configurations with 1.5% intake pressure loss

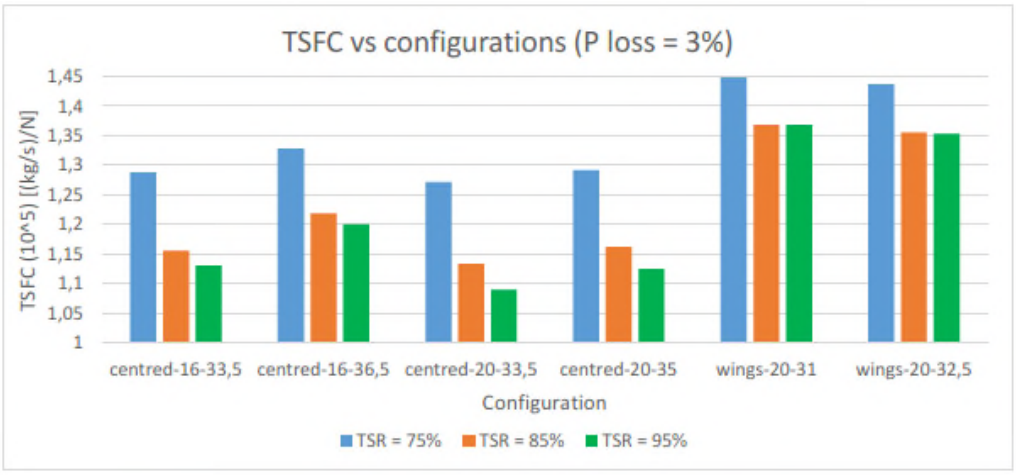

Figure 37: TSFC of configurations with 3% intake pressure loss

The first observation from this study is that the centred fan array configurations achieve significantly lower TSFC as compared to the wing mounted fan array. This is due to the lower intake ram drag reducing the power requirements on the fan propulsor array despite ingesting more distorted flow as compared to that on the wing mounted array.

It would appear that a larger flap chord would beneficial in reducing the TSFC as the benefits of flap blowing are increased with a bigger flap chord. This, however, would mean an intake that is placed further forward on the aircraft and thereby, reducing the benefits of BLI as the intake ram drag increases as the boundary layer profile is less developed further upstream. Furthermore, a big flap chord might not be desirable as there would be much greater requirements and strains on the mechanisms required to rotate the flap. With these considerations in mind, the flap chord and size for the N3-X is selected to be the centred 20m width at a longitudinal location of 35m from this point onwards unless otherwise stated.

4.6 Case Study – Design Point Trim Analysis on N3-X

A case study using the FDM was performed on the N3-X. Whilst the preliminary geometry is easily available from NASA, it lacks crucial information that is requisites for FDM. Table 4 shows the various N3-X flight segment thrust requirements while Table 5 shows the various required inputs that are either available or derived.

Table 4: N3-X thrust requirements at various flight conditions

Flight Condition	Minimum Thrust Required
Aerodynamic Design Point (ADP) (30,000 ft / MN 0.84 / ISA)	26,750 lbf (119 kN)
Rolling Take-Off (RTO) (SL / MN 0.25 / ISA+27 R)	65,000 lbf (289 kN)
Sea Level Static Take-off (T/O) (SL / MN 0.0 / ISA)	90,000 lbf (400 kN)

Table 5: Various N3-X required parameters

Property	Value
Baseline Take-Off Mass	290,000 kg (calculated)
C.G.	27 m aft from nose (assumed)
Neutral Point	25.6 m aft from nose (calculated)
Elevator and propulsor array spanwise location	+-10 m from centreline [24]
Elevator size	35 m aft of centreline nose to tail (assumed)

The ADP trim thrust requirements were defined to be 119 kN when boundary layer ingestion benefits were taken into consideration [24]. The C.G was assumed to be 27m aft from the nose of the aircraft which gives the aircraft a reasonable 5.5% static margin with the neutral point calculated to be at 25.6 m aft from the nose. The flaps or elevators are located +-10m from the centreline of the aircraft along the Y-axis while the flaps were assumed to begin at a location of 35m along the X-axis.

These conditions are used and the total mass of the aircraft iterated in the FDM to obtain a trim intrinsic net thrust requirement of 119 kN at the ADP. The converged iterated mass was then deduced to be 290,000 kg.

At this point, it should also be stated that all models in this thesis are simulated at the ADP unless otherwise stated.

4.6.1 Trim with Pure Thrust Vectoring

A parametric study whereby the N3-X was simulated with thrust vectoring and with varying CG location was conducted. The CG locations were ranged from 23 m to 27 m. All available thrust was assumed to be available for thrust vectoring. It was also assumed that thrust vectoring would replace the flaps for pitching. For this study, the flaps were assumed to be a constant 20% chord length across the entire aircraft span. The studied was conducted to obtain trim status at the ADP.

Figure 38 shows the trim AoA, trim intrinsic net thrust requirements, trim total aerodynamic drag and the trim elevator or TV deflection angle.

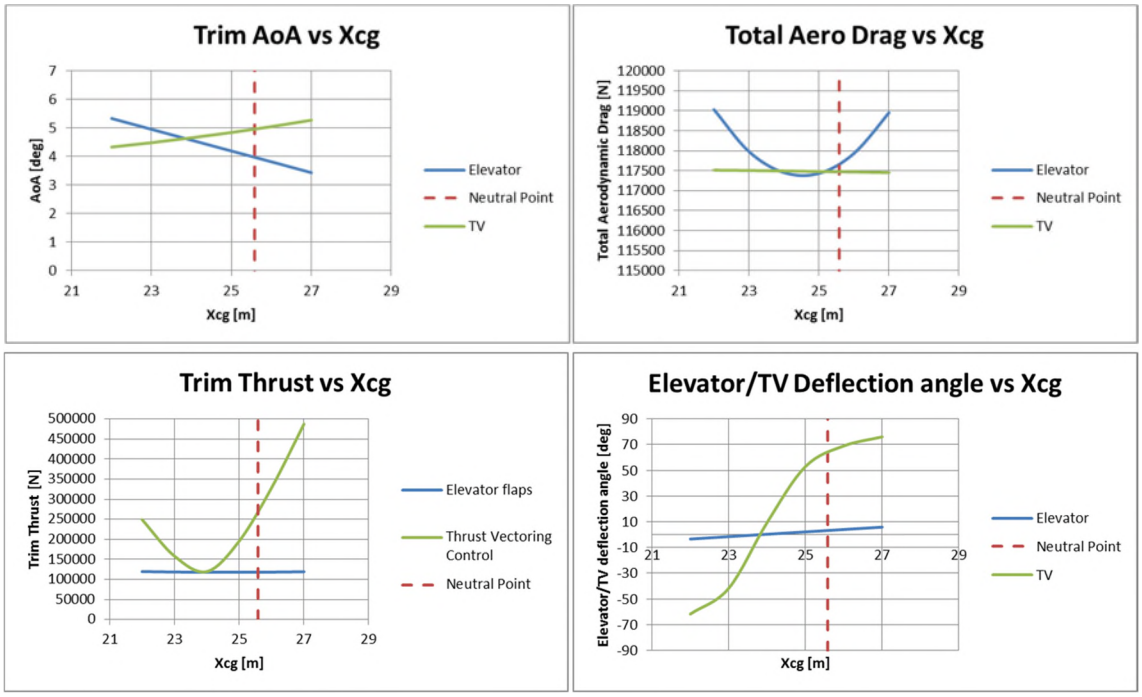

Figure 38: Trim parameters of N3-X at ADP using pure thrust vector control

The most obvious trend in the charts shows that the trim intrinsic net thrust requirements when using pure thrust vector control to replace the flaps become excessively large except within a small range of C.G locations. This occurs because the pitching moment generated by such a BWB aircraft is much larger than a conventional tube and wing aircraft as the whole aircraft is a flying wing which generates lift and hence excessive pitching moment. As such, without the presence of the flaps, a large force is required to produce counteracting moments to maintain zero net pitching moment for trim. As the C.G deviates from the aerodynamic centre of the aircraft, the force requirements to create this counteracting pitching moment increase. This is also seen in the TV deflection angle when the C.G location deviates from the aerodynamic centre of the aircraft. It can also be noted that the TV deflection angles required to trim the aircraft become excessive large. The aerodynamic drag of the aircraft remains constant for TV as the strip method assumes the same drag polar and the trim lift remains constant with constant total mass across the C.G range. For elevator and flap controlled trim, the trim aerodynamic drag increases as flap deflections deviate from 0 deg. There is a small region whereby the absolute flap deflection angles

are very small and the drag is actually reduced which is a well-known phenomenon.

It can thus be concluded that using pure thrust vectoring as a means of control for the N3-X aircraft would not be feasible as the aircraft would have to operate within a very small static margin range unless excessively large thrust can be provided by the propulsion system. Even so, the thrust vectoring deflection angles involved would still render it unfeasible as large losses would be expected in such a system.

4.6.2 Trim with Flap Blowing

The N3-X is now modelled parametrically with various flap blowing coefficients. The assumptions on the structure of the flaps and aircraft follow that of Table 5 as previously mentioned. Once again, the trim requirements at ADP are obtained and seen in Figure 39.

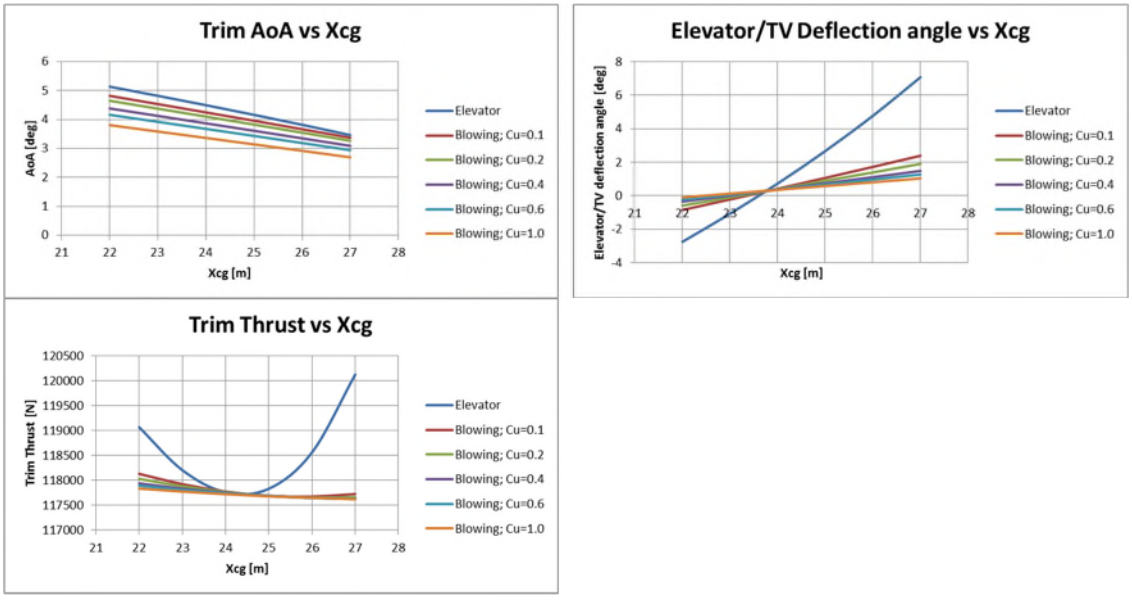

Figure 39: Trim parameters of N3-X using flap blowing

With the additional control power from the flaps due to the blowing effect, the absolute elevator deflection angles are reduced for trim. As the blowing coefficient increases from 0.1 to 1.0, the amount of absolute deflection required is reduced and the amount of intrinsic net thrust required reduces. It should be noted that the trim intrinsic net thrust requirements are equal to the aerodynamic

drag in these cases. The increased control power also allows the aircraft to be trimmed at a lower AoA as compared to a non-blown aircraft. It should also be noted that due to the assumptions made in the strip method code on the drag polar, the amount of drag or intrinsic net thrust reduction shown here is purely due to the reduced flap deflection angles which is a pessimistic opinion as the overall drag of the aircraft is expected to be lower than that predicted by the drag polar. This hence shows great promise for flap blowing on the N3-X as a trim thrust reduction would result in lower fuel consumption during the cruise phase.

4.7 Cruise Phase Simulations

The cruise phase simulation is useful to determine the cruise fuel consumption of the aircraft. While the propulsion system is designed for the ADP trim condition, the aircraft weight reduces as it consumes fuel in the cruise phase. This would hence lead to a decreased requirement for trim intrinsic net thrust as the aircraft completes its cruise segment. This simulation is important as it allows the fuel requirements of the cruise phase to be obtained. To simulate this phase, the ADP TSFC of the propulsion system is used as an input into JSBSim. The simulation is divided into specified time intervals. At each time interval between t_i and $t_{i+\Delta t}$, the fuel consumed by the aircraft and the new overall aircraft weight of the aircraft is calculated respectively by

$$\left(\Delta W_{fuel}\right)_{t=t_i} = TSFC \times (T_N)_{t=t_i} \times \Delta t \times g \quad \textbf{(4-15)}$$

$$(W_{overall})_{t=t_{i+\Delta t}} = (W_{overall})_{t=t_i} - \left(\Delta W_{fuel}\right)_{t=t_i} \quad \textbf{(4-16)}$$

The new overall aircraft weight is then used to obtain the trim intrinsic net thrust requirements in JSBSim for the next time step simulation. For the N3-X case studies whereby the cruise time is approximately 15 hours, a time interval of 60 seconds was assumed and deemed as a reasonable balance between simulation resources and accuracy.

4.7.1 ADP Cruise Simulation of N3-X

The described methodology is applied onto the N3-X to showcase the possible fuel savings obtained when flap blowing is applied to the N3-X aircraft. Several

assumptions were utilized in these simulations and are tabulated in Table 6. The results from the simulations are also tabulated. The empty fuel aircraft mass is calculated based on the BLI fans configuration simulation and is

$$Mass_{empty\ fuel\ aircraft} = 290000 - Mass_{fuel\ consumed\ in\ cruise} \times 1.15 \quad \textbf{(4-17)}$$

The initial aircraft total mass in the FDM simulations for the other configurations are iterated such that the empty fuel aircraft mass remains constant to an accuracy of 0.5%.

Table 6: ADP cruise simulation total fuel consumption for various configurations

	Freestream ingesting fans	BLI fans	BLI fans with blown flaps
Initial total aircraft mass [kg]	304000	290000	288426
Empty fuel aircraft mass	216614.6	216615.4	216616.8
Cruise phase blowing coefficient	0.0	0.0	0.04
ADP TSFC [kg/s/N * 10^-5]	1.156[1]	0.991[2]	0.991[3]
Total Fuel Mass [kg]	87385.4	73384.6	71809.2
% Fuel savings	-	16%	17.8%

The simulations assume the same aircraft design for all configurations whereby there are no changes in the systems weight and structural weight. The only change is the TSFC and total fuel weight in the aircraft. Thus, neglecting any further optimization in terms of structural and design, intake pressure losses or fan performance deficiency, it can be observed that boundary layer has a possibility of reducing the total fuel consumption by approximately 16% while flap blowing further aids in this with an additional 2% reduction in total fuel consumption.

4.8 Off Design Take-Off Modelling

To model off design take-off simulations in JSBSim, it was necessary to include various parameters to have a realistic result. These included the TSFC of the propulsion system as any change in weight in the aircraft would result in a change in the C.G location and the corresponding moments generated by the aircraft, while impacting upon the off design propulsion system performance. At the same

[1] Referenced from [24]with FPR=1.3
[2] Referenced from [24]with FPR=1.3
[3] Assumed to be same as BLI fans without blown flaps

time, take-off runs are generally governed by the flight control system (FCS) of the designed aircraft. This FCS controls the elevator deflections during take-off to ensure the dynamic response of the aircraft follows a pre-defined pitch rate, elevation rate and flight angle. However, there is no universal FCS for all aircrafts and the FCS of each aircraft differs and is guided by general design rules. At the early conception phase of such a futuristic concept aircraft, it becomes impractical to design a FCS due to the constant changes being applied onto the aircraft design. Furthermore, it is not the emphasis of this research to look into the design of such a FCS. As such, a combined methodology involving both FDM simulations in JSBSim and traditional empirical take-off relations were used to capture the effects of thrust vectoring and flap blowing on a TeDP BWB aircraft, whereby there is no need for the design of a FCS.

The take-off phase of an aircraft is generally described as shown in Figure 40. It is divided into 3 main phases, ground run, rotation and transition. For a transport aircraft, take off is completed after the transition phase whereby the aircraft has achieved a vertical height of 50 ft above the ground. This is then followed on by the climb phase.

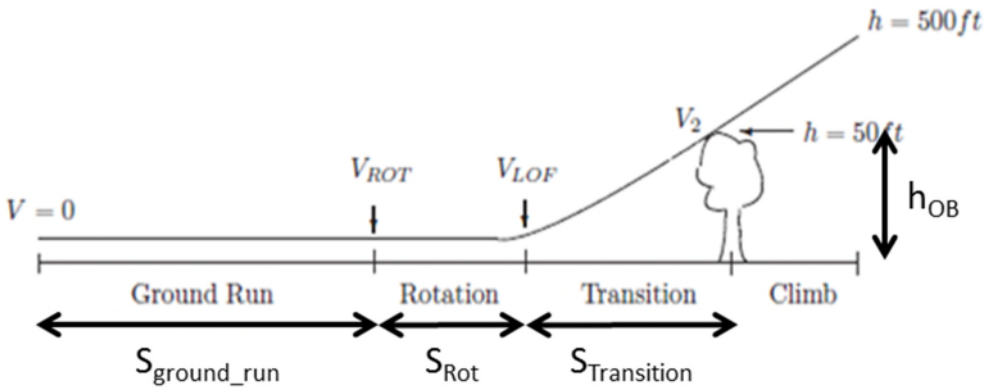

Figure 40: Various phases of take-off

The ground run and rotation phase is simulated using FDM modelling and takes into account the aerodynamic properties, forces of the aircraft and changes to them when thrust vectoring or flap blowing is applied. At the same time, the off design performance of the propulsion system is taken into account in the FDM.

A rotational velocity, V_{ROT}, is defined whereby the elevator flaps and thrust vectoring nozzles are deflected to begin rotating the aircraft. Lift off and its corresponding velocity, V_{LOF} is achieved when the rear aircraft wheels are no longer in contact with ground. The take-off procedure in the FDM analysis is as follows:

1. Flight simulation start, brakes applied.
2. Engines throttled up to 100%.
3. Brakes released.
4. Full flap deflection upwards and TV nozzle deflection at V_{ROT}.
5. Lift off velocity, V_{ROT}, achieved at lift off of plane rear wheels.
6. Check pitch angle to be within pre-defined maximum lift-off pitch angle.
7. If pitch angle is excessive, re-do simulation with lower flap deflection. If pitch angle is acceptable, simulation ends.

In general, the aircraft follows a pre-set pitch angle in the transition phase which is maintained by the FCS. Without the design of the FCS, the transition phase is modelled using empirical take-off relations used for aircraft design [57]. These are functions of V_{ROT}. It should be noted that these relations are developed for traditional tube and wing aircrafts and application of these relations on a BWB would serve as an initial estimate of the N3-X performance during the transition phase.

$$S_{Transition} = R \sin \theta_{OB} \tag{4-18}$$

$$R = \frac{6.96 \left(\frac{V_{Rot}}{1.1}\right)^2}{g} \tag{4-19}$$

$$\theta_{OB} = \cos^{-1}\left(1 - \frac{h_{OB}}{R}\right) \tag{4-20}$$

The overall take-off distance is the sum of the ground run distance, rotation distance and the transition phase. V_{ROT} can be varied to obtain the shortest possible take-off distance achievable for the particular configuration.

4.8.1 Take-Off Analysis on N3-X

The devised take-off analysis methodology was applied parametrically to the N3-X with variations in either blowing coefficient, thrust vectoring angle or a combination of both. The same N3-X properties as previously mentioned are assumed. Additionally, a maximum sea level take-off thrust of 180,000 lbf was assumed. This is similar to the amount of SLS thrust of a Boeing 777 aircraft and the variation in thrust at different Mach and height follows that of the Boeing 777 thrust specifications as modelled in JSBSim.

4.8.1.1 Rotational Velocity

The rotational velocity of a normal passenger aircraft usually ranges between 160-220 knots. It should be noted that this value should be higher than the stall velocity of the aircraft. This can be derived from the max lift coefficient of the aircraft. For the N3-X, the stall velocity is 68 knots. This is comparatively smaller than that of a B777 as the BWB has the characteristic of a much larger lift coefficient. The pilot decides upon the value depending upon the weight of the aircraft, available runway space and the aircraft characteristics. As the N3-X would display differing aerodynamic properties when flap blowing or thrust vectoring is applied, the optimal rotational velocity whereby shortest take-off distance is achieved has to be iterated. Figure 41 shows the variation of V_{ROT} for a non-flap blowing and thrust vectoring case. As V_{ROT} is increased, the ground roll distance required for the aircraft to attain this speed increases. However, the lift force and pitching moment generated as the flaps are deflected are increased and a reduction in the rotation distance is achieved as they are functions of the flight velocity as shown in the below equations. Thus, the opposing impact in terms of ground roll and rotation distances with increasing rotation velocity results in an optimal rotation velocity for minimum take-off distance.

$$L = \bar{q} \cdot S \cdot C_L \quad \textbf{(4-21)}$$

$$M = \bar{q} \cdot S \cdot C \cdot C_M \quad \textbf{(4-22)}$$

$$\bar{q} = \frac{1}{2}\rho V^2 \quad \textbf{(4-23)}$$

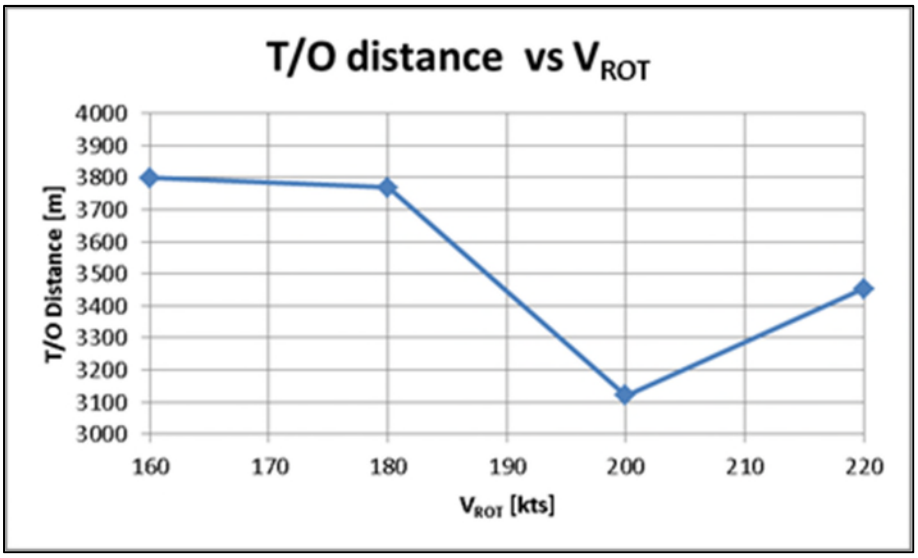

Figure 41: Variation of take-off distance with rotational velocity

4.8.1.2 Impact of Flap Blowing on Take-Off Distance

The blowing coefficient is assumed constant throughout the take-off analysis and parametrically changed between 0-0.8. Figure 42 shows the percentage decrease in the take-off distance as compared to a non-flap blown case for various V_{ROT}.

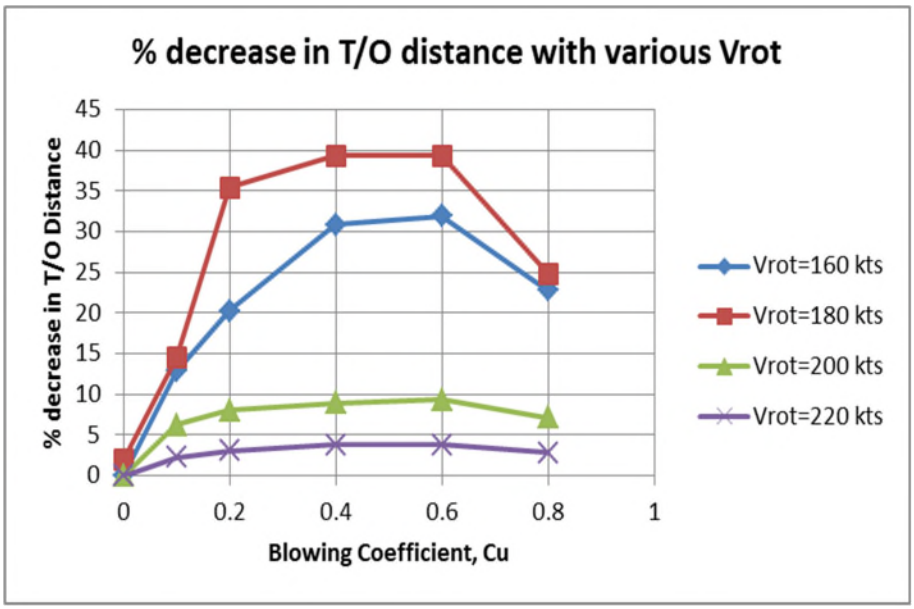

Figure 42: % decrease in take-off distance in the presence of flap blowing

For a specific V_{ROT}, and as blowing coefficient is increased, the take-off distance reduces as the increase in pitching moment is more beneficial than the reduced

lift during the rotation phase as the flaps are deflected upwards. However, the increasing detriment from the reduced lift as blowing coefficient increases becomes more significant and negates the benefits of the increased pitching moment during the rotation phase as blowing coefficient is further increased.

With increasing V_{ROT}, the aircraft gains more lift and velocity before rotation begins. The increased pitching moment coefficient and reduced lift coefficient from flap blowing at lower rotation velocity results in a lower take-off distance. However, as V_{ROT} increases further, the detrimental effect of the reduced lift becomes more significant and negates the positive impact from the increased pitching moment. Hence, there can be an optimal rotational velocity and blowing coefficient for minimum take-off distance.

The shortest possible take-off distance achievable without flap blowing is then used as a reference in Figure 43. The shortest take-off distance achievable across the studied V_{ROT} for each blowing coefficient is shown. This figure shows the percentage decrease in take-off distance and the corresponding take-off length.

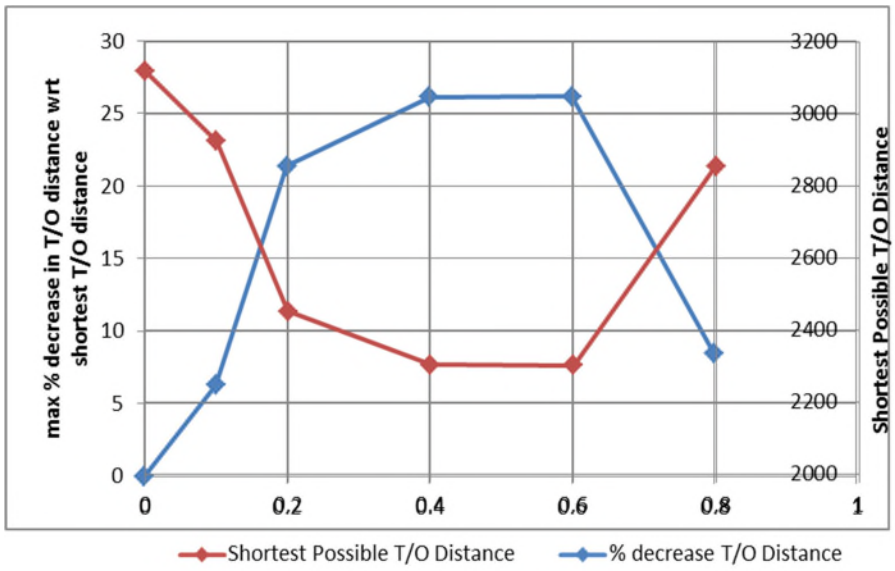

Figure 43: Shortest possible T/O distance and corresponding % decrease with flap blowing

A possible 27% reduction in the take-off distance can be achieved at Cu=0.6.

4.8.1.3 Impact of Thrust Vectoring on Take-Off Distance

A similar study was done whereby the thrust vectoring angle is varied parametrically across a range of rotational velocity. The study assumes all available thrust is deflected upwards during the rotation phase at the rear of the aircraft. The range of study for the thrust vectoring angles is from -50 to 0 degrees. Figure 44 shows the percentage decrease in the take-off distance as compared to a non-thrust vectoring case for various V_{ROT}.

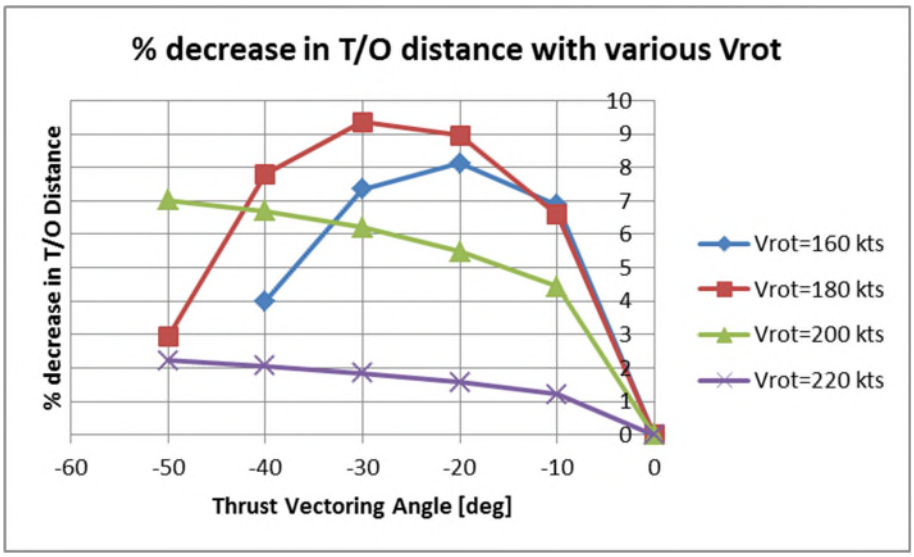

Figure 44: % decrease in take-off distance in the presence of thrust vectoring

The additional pitch up moment generated by TV comes at an expense of a reduction in the net forward thrust force as well as a force component opposing the lift force. This results in an optimal TV angle for every V_{ROT} setting. The effect of increased pitch up moment results in a shorter T/O distance but this effect is diminished as the TV angle increases due to the decreasing amount of net thrust force and net lift force resulting in a slower gain in longitudinal velocity and slower gain in altitude respectively. There is also an optimal rotational velocity as the decrease in rotation distance is negated by the increase in ground roll distance to achieve the rotational velocity.

Similar to Figure 43 for flap blowing, Figure 45 shows the trends when thrust vectoring is applied.

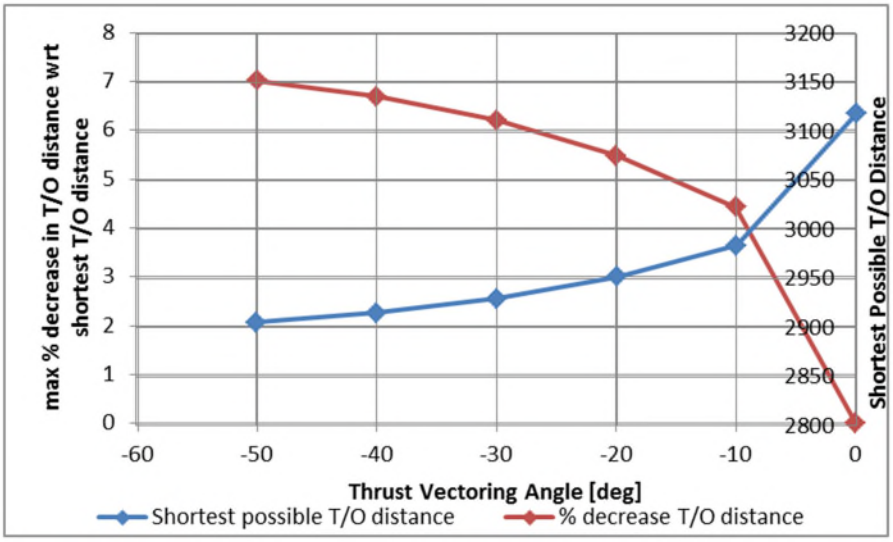

Figure 45: Shortest possible T/O distance and corresponding % decrease with thrust vectoring

It can be observed that throughout the TV angles studied, take-off distances reduce with increasing absolute thrust vectoring angles. There is a possible 7% reduction in take-off distance at the limit of -50 deg TV angle.

4.8.1.4 Combination of Flap Blowing and Thrust Vectoring on Take-Off Distance

Flap blowing and thrust vectoring is both applied to the N3-X for this study. The blowing coefficient is once again varied parametrically across a range of rotational velocity while the thrust vectoring angle is chosen to be constant at a reasonable -30 degrees throughout the simulations.

Figure 46 shows the percentage decrease in the take-off distance as compared to a non-flap blown and non-thrust vectoring case for various V_{ROT}.

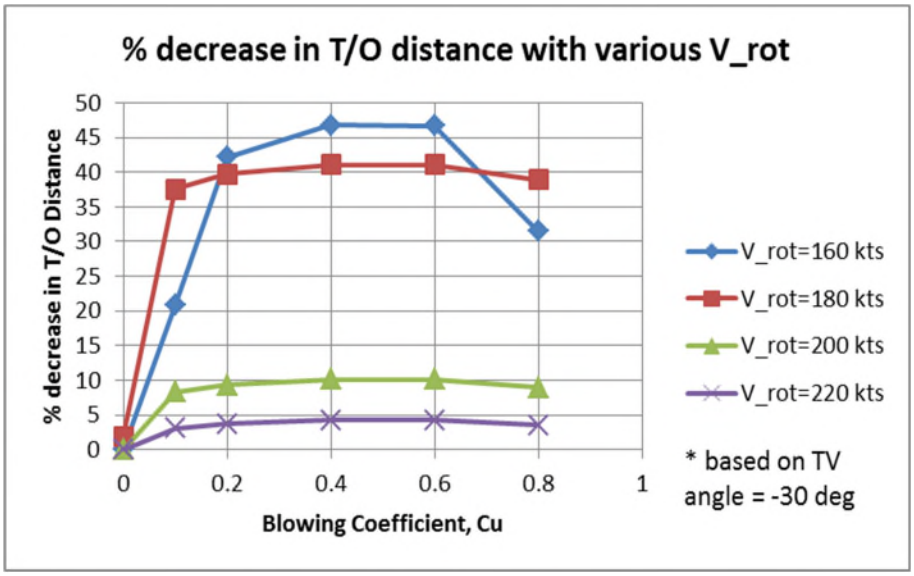

Figure 46: % decrease in take-off distance in the presence of thrust vectoring and flap blowing

Once again, similar trends are observed whereby there is an optimal blowing coefficient as well as an optimal rotation velocity for minimum take-off distance of the N3-X. The presence of an optimal blowing coefficient suggests that for a given aircraft and propulsion configuration, careful control of how much thrust is provided by the fan propulsors to achieve the required blowing coefficient throughout the take-off phase can result in a reduction or optimal take-off distance. This might possibly be achieved through thrust split. Figure 47 shows the trends whereby the shortest take-off distance achievable across the studied V_{ROT} for each blowing coefficient is shown with reference to shortest possible take-off distance achievable without flap blowing and thrust vectoring. This figure shows the percentage decrease in take-off distance and the corresponding take-off length. A possible 35% reduction in take-off distance from 3100m to 2000m is observed.

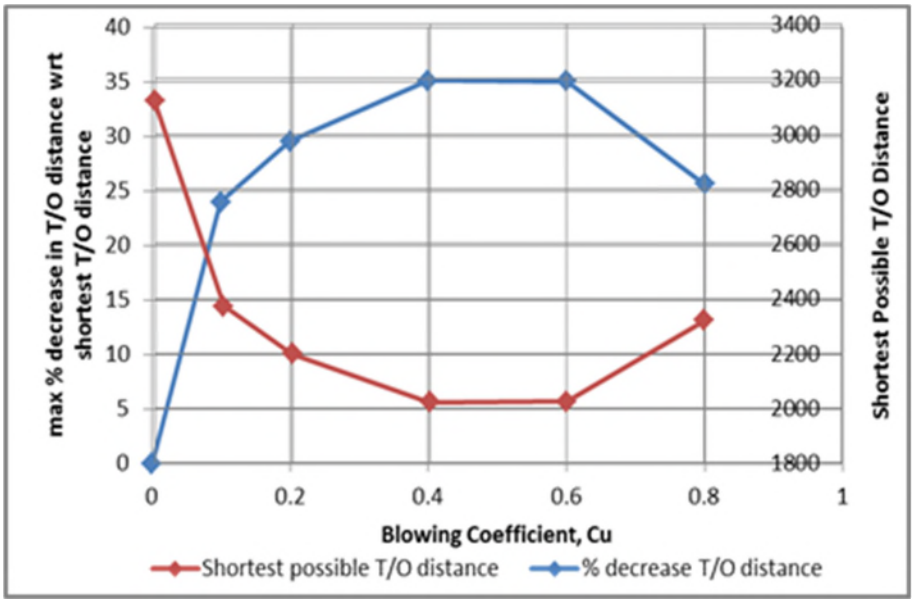

Figure 47: Shortest possible T/O distance and corresponding % decrease with thrust vectoring and flap blowing

4.9 Conclusion

In this chapter, the various modelling pertaining to flight dynamics has been explained. The aerodynamic property and changes due to flap blowing and thrust vectoring has been applied into the FDM code. Thrust definitions has been clearly explained to prevent confusion and parametric studies on the N3-X have been done for design point trim thrust requirements, ADP cruise phase fuel consumption and off-design take-off distance analysis. Baseline aircraft characteristics as well as flap-blowing and thrust vectoring changes have been applied in these case studies. It has been shown that pure thrust vectoring as a replacement for control elevator flaps might not be feasible as the intrinsic net thrust requirements at the design point would become excessively large for trim. Flap blowing on the other hand, reduces the trim intrinsic net thrust and drag requirement through a reduction in the flap deflections. Fuel consumption can be possibly be reduced by 16% with BLI while flap blowing can further reduced fuel consumption in the region of 2%. Both thrust vectoring and flap blowing applied at take-off reduces the take-off distance of the N3-X and a combination of both has potential to reduce the distance by approximately 35%.

Chapter 5

PROPULSION SYSTEM MODELLING

This chapter would discuss the methodology involved in the propulsion modelling. This includes the thrust split, core engine modelling, fan propulsors modelling and the various aspects of the electrical system modelling and assumptions at the design point.

5.1 Introduction

Figure 48 shows the flowchart for the propulsion module modelling.

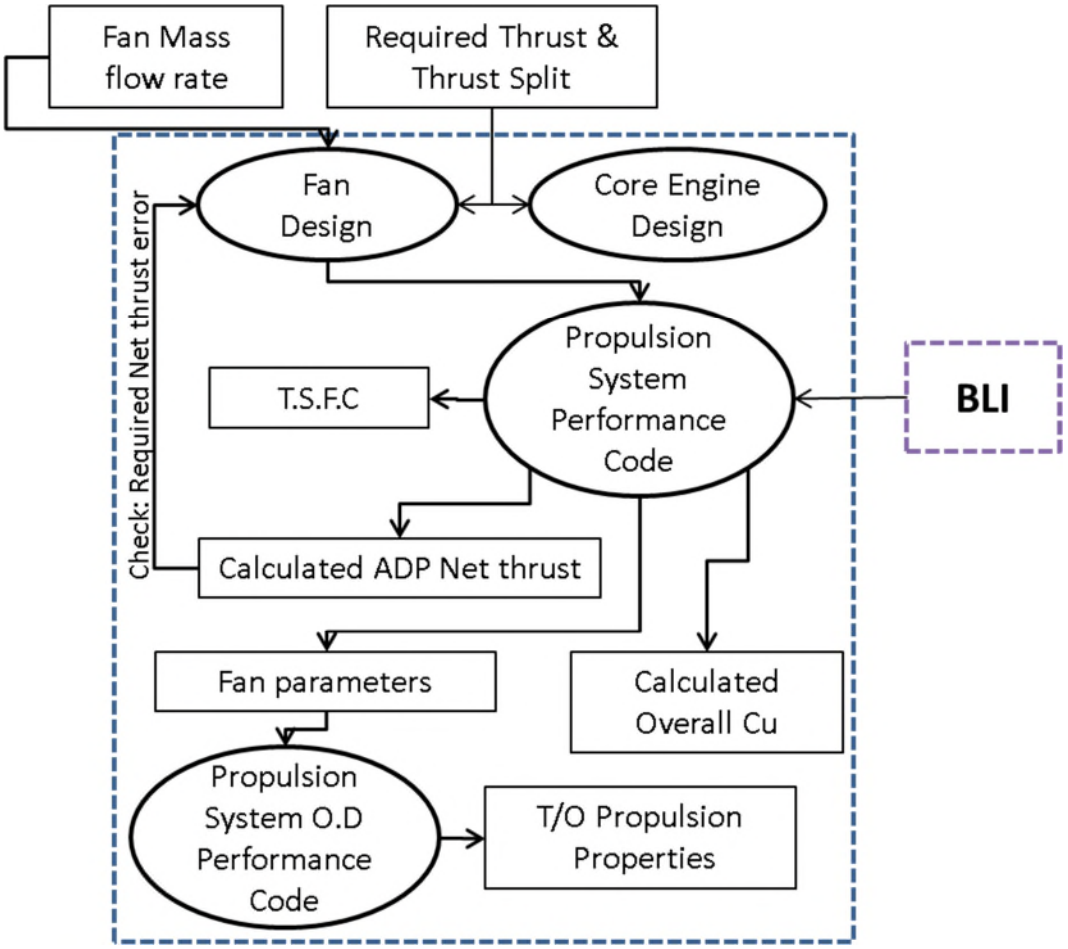

Figure 48: Propulsion module flowchart

The propulsion module consists mainly of the propulsion system performance code. The code takes input from the fan propulsor design and core engine design and calculates the overall thrust produced either at the design point or any off-design condition. At the same time, the overall blowing coefficient is also calculated within the code. The thrust specific fuel consumption at any point is also calculated. The overall process begins with a defined net thrust requirement and thrust split setting. The fan and core engine are then designed and defined. With input from the BLI module, the overall thrust is calculated at the design point. The fan design is then iterated to ensure convergence of the thrust requirements at the ADP.

5.2 Thrust Split

The concept of thrust split is first introduced by Lodesani [10] and is defined as the ratio of the thrust produced by the fan propulsors array to the total thrust produced by the propulsion system.

$$TS = \frac{T_{N,propulsors}}{T_{N,total}} \quad \textbf{(5-1)}$$

This would thus mean that besides the propulsors, the core engines would also be providing some form of thrust to the aircraft. In a 100% TS system, all the thrust would be provided by the propulsor fans while a 50% TS system would imply an equal amount of thrust being provided by the core engines and the fan propulsor array. The advantages of having a thrust split system possibly includes reduced TSFC for the overall system.

5.3 Fan Propulsor Design & Modelling

The fan propulsor array consists of the intake, the fan, electrical motor and nozzle. The various components of a single fan are shown in Figure 49.

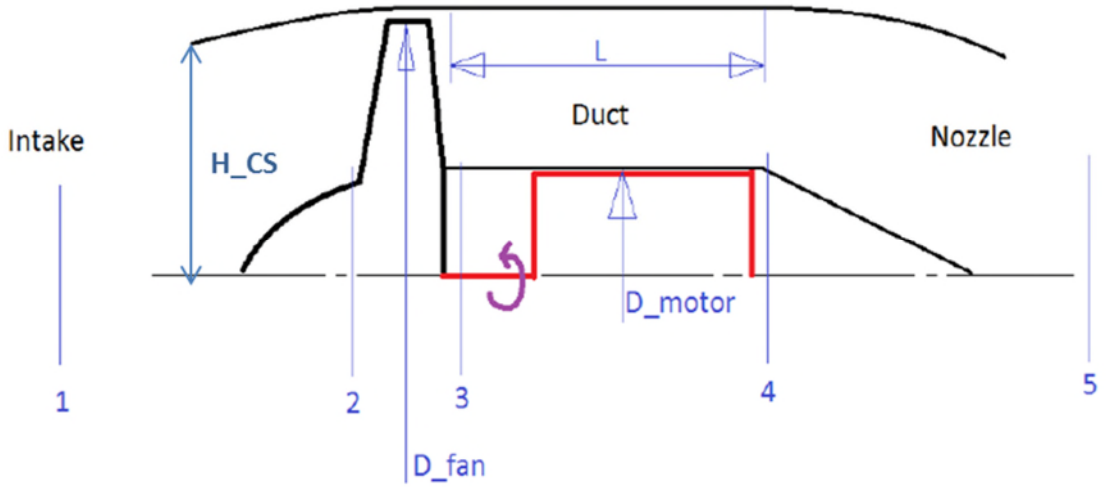

Figure 49: Fan propulsor components and layout

The propulsor fan is driven by an electric motor situated within the hub of the fan design. The complete fan array is situated on the upper surface of the BWB aircraft. The intake is situated at a selected longitudinal location to ingest the boundary layer while the nozzle is placed either at the rear of the aircraft or just fore of the elevator control flaps for flap blowing.

5.3.1 Fan Propulsor Array Design

In the case of the N3-X, the following design assumptions were made:

- Total array width, x_{array} of 20m.
- Fan hub to tip ratio, $\frac{r_h}{r_t}$, of 0.47. This was based on the NASA Rotor 53 [58] design and NASA Rotor 67 [59] design with hub to tip ratio of 0.52 and 0.42 and design pressure ratio of 1.35 and 1.6 respectively. These design pressure ratio are consistent with the performance requirements of the fan propulsor array.
- Minimum hub area is determined by the diameter of the electrical motor. There is also a minimum length involved in the duct to accommodate the motor.
- Minimum separation between each fan propulsor of 0.0254m [24]. The number of fans is the maximum number that can be physically constrained within the array width with the minimum separation fulfilled.

- Rotor inlet face Mach number of 0.62.
- Intake is a 2D mail-slot inlet [24] with a pre-defined intake height with splitters just after the lip to divert the flow to each individual fan.
- Nozzle is a rectangular 2D mail-slot outlet with the splitters from each fan ending just fore of the exit nozzle edge similar to the inlet.
- Variable nozzle area, operating shaft speed, combined with the electric motor power output defining the amount of thrust produced by the propulsors at a given flight condition.

The design adiabatic efficiency and corrected tip speeds of the fan are defined in Figure 50 as a function of the design fan pressure ratio. These are technology trend curves conducted via a study from Aerospace System Design Laboratory (ASDL) at Georgia Tech University for the FAA [24].

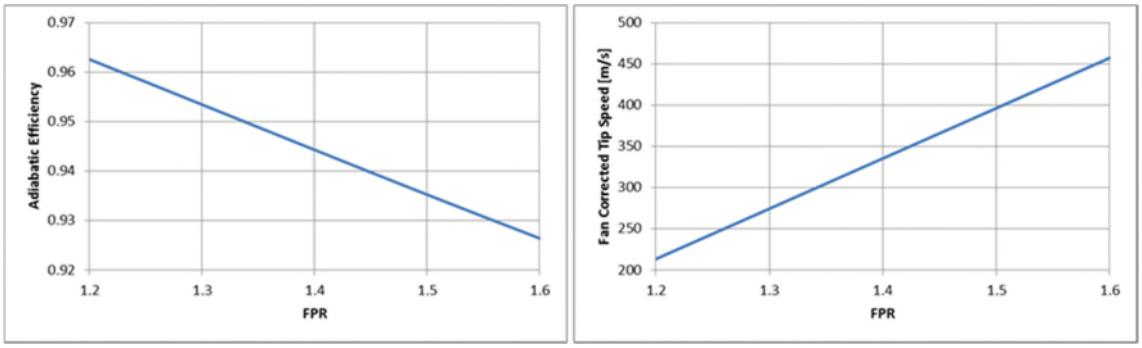

Figure 50: Design fan adiabatic efficiency and corrected tip speed

5.3.2 Fan Propulsor Performance Modelling

The capture sheet height, H_CS, the total array width and the number of fans determines the mass flow that enters each propulsor. To simplify the problem, the intake height is assumed to be the same as the capture sheet height at the design point. At off-design conditions, the capture sheet height is iterated to obtain the required operating mass flow of the fan propulsor.

The gas-turbine engine performance theory [60] [61] is used as a guideline for the calculation of the fan propulsor performance.

5.3.2.1 Intake

Assuming a known boundary layer total pressure, total temperature and Mach profile at station 1 and a varied profile across the span, the total mass flow entering the array can be calculated with a pre-defined H_CS.

$$W_{array} = 2 \times \sum_{0}^{y_{array}} \int_{0}^{H\_CS} \rho \cdot V \cdot (y_{strip} \cdot z) dz \quad \textbf{(5-2)}$$

The total inlet area of the mail slot inlet is

$$A_{1,array} = H\_CS \times |span_{array}| \quad \textbf{(5-3)}$$

If it is assumed that the boundary layer profile across the span is constant and does not vary at each strip location, equation (5-2) reduces to

$$W_{array} = \int_{0}^{H\_CS} (\rho \cdot V \cdot z) dz \cdot |span_{array}| \quad \textbf{(5-4)}$$

The nature of the embedded intake would imply the presence of a S-duct and this itself would present intake pressure losses. To simplify the problem, the intake total pressure losses are defined as follows:

$$\Delta P_{T,intake} = \frac{P_{T,2} - P_{T,1}}{P_{T,1}} \quad \textbf{(5-5)}$$

The mass-averaged total pressure and Mach is computed and used for the fan performance modelling.

5.3.2.2 Fan

The total pressure at the fan inlet face is computed using the intake pressure losses. Isentropic relations for compressible flow, Mach number and ideal gas law equation are then utilised to calculate the other flow properties. The rotor face Mach number is assumed to be 0.62 at the design point [16].

$$\frac{P_{T,2}}{P_{S,2}} = 1 + {M_2}^2 \frac{\gamma - 1}{2}^{\frac{\gamma}{\gamma-1}} \quad \textbf{(5-6)}$$

$$\frac{T_{T,2}}{T_{S,2}} = 1 + {M_2}^2 \frac{\gamma - 1}{2} \quad \textbf{(5-7)}$$

$$\rho_2 = \frac{P_{S,2}}{RT_{S,2}} \quad \textbf{(5-8)}$$

$$V_2 = M_2\sqrt{\gamma RT_{S,2}} \quad \textbf{(5-9)}$$

The diameter of the fan is a function of the area of the rotor inlet face and the hub to tip ratio.

$$A_2 = \frac{W_{array}/NF}{\rho_2 \cdot V_2} \quad \textbf{(5-10)}$$

$$D_2 = 2 \times \sqrt{\frac{A_2}{\pi(1 - \frac{r_h}{r_t})^2}} \quad \textbf{(5-11)}$$

Downstream of the fan, the FPR is defined.

$$P_{T,3} = P_{T,2} \times FPR \quad \textbf{(5-12)}$$

The adiabatic efficiency, η_{clean}, as shown in Figure 50 is utilised to compute the temperature aft of the fan. However, with the flow being distorted due to the presence of the boundary layer, there is an expected deficient in the design efficiency.

$$\Delta\eta_f = \frac{\eta_{f,distorted} - \eta_{f,clean}}{\eta_{f,clean}} \quad \textbf{(5-13)}$$

$$T_{T,ideal,3} = T_{T,2} \cdot FPR^{\frac{\gamma-1}{\gamma}} \quad \textbf{(5-14)}$$

$$T_{T,3} = \frac{T_{T,ideal,3} - T_{T,2}}{\Delta\eta_f \cdot \eta_{f,clean}} + T_{T,2} \quad \textbf{(5-15)}$$

The corrected tip speed, $V_{tip,corrected}$ is obtained from Figure 50 and the tip velocity is then

$$V_{tip} = V_{tip,corrected} \cdot \sqrt{\frac{T_{S,2}}{288.15}} \quad \textbf{(5-16)}$$

The rotational speed, N, is then

$$N = \frac{2V_{tip}}{D_2} \quad \textbf{(5-17)}$$

The power and torque required by one fan are respectively

$$PW_f = \frac{W_{array}}{NF} c_p \left(T_{T,3} - T_{T,2}\right) \quad \textbf{(5-18)}$$

$$TQ_f = \frac{PW_f}{N} \quad \textbf{(5-19)}$$

5.3.2.3 Nozzle

There is a total pressure loss in the nozzle and duct defined as

$$\Delta P_{T,nozzle} = \frac{P_{T,5} - P_{T,3}}{P_{T,3}} \quad \textbf{(5-20)}$$

Once again, with isentropic equations, the static properties can be determined and the total intrinsic net thrust from the propulsor fans can be calculated with the internal control volume.

$$M_5 = \sqrt{\frac{\left(\frac{P_{T,5}}{P_{S,5}}\right)^{\frac{\gamma-1}{\gamma}} - 1}{\frac{\gamma-1}{2}}} \quad \textbf{(5-21)}$$

If $M_5 > 1$, the nozzle is choked and

$$M_5 = 1 \quad \textbf{(5-22)}$$

$$V_5 = \sqrt{\gamma R T_{S,5}} \quad \textbf{(5-23)}$$

$$A_{5,array} = \frac{W_{array} R T_{S,5}}{P_{S,5} V_5} \quad \textbf{(5-24)}$$

$$F_{N,array} = W_{array}(V_5 - V_1) + \left(P_{S,5} - P_{S,\infty}\right)A_{5,array} - \left(P_{S,1} - P_{S,\infty}\right)A_{1,array} \quad \textbf{(5-25)}$$

If $M_5 < 1$, the nozzle is not choked and

$$M_5 = M_5 \quad \textbf{(5-26)}$$

$$V_5 = M_5\sqrt{\gamma R T_{S,5}} \quad \textbf{(5-27)}$$

$$P_{S,5} = P_{S,\infty} \quad \textbf{(5-28)}$$

$$F_{N,array} = W_{array}(V_5 - V_1) - \left(P_{S,1} - P_{S,\infty}\right)A_{1,array} \quad \textbf{(5-29)}$$

This formulation of intrinsic net thrust calculation would require pre-determined values for H_{CS}, NF, FPR. The number of fans selected and utilised must be checked to ensure there is sufficient space in the assumed array width. For a required intrinsic net thrust design, either the H_{CS} or the FPR must be assumed and the other quantity iterated to obtain the required design thrust. The overall fan design modelling is summarised in Figure 51.

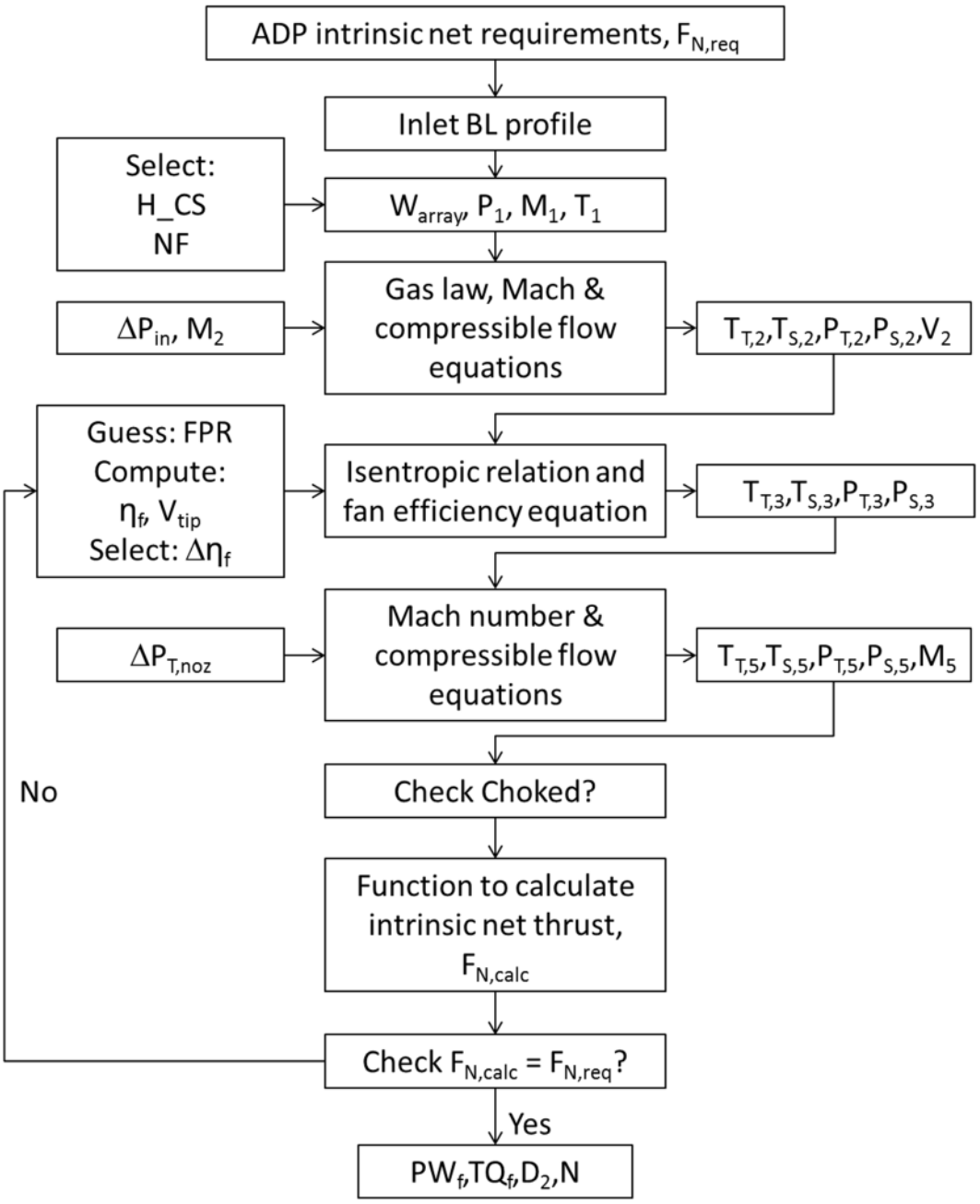

Figure 51: Propulsor fan design flowchart

5.4 Core Engine Design & Modelling

The core engines are modelled using Cranfield University in-house engine design and modelling tool, Turbomatch [62].

5.4.1 Turboshaft Turbogenerator

For a theoretical 100% thrust split design whereby all the required design thrust is provided by the fan propulsor array, the main function of the core engines are to provide electrical power to power the propulsor fans. This is achieved by a two spool turboshaft engine feeding a power turbine. A third shaft would connect the power turbine aft of the low pressure turbine in the engine to the generator. The main function of the power turbine would be to provide the mechanical energy to be converted into electrical energy via the generator. Fig Figure 52 shows the configuration of such a core engine.

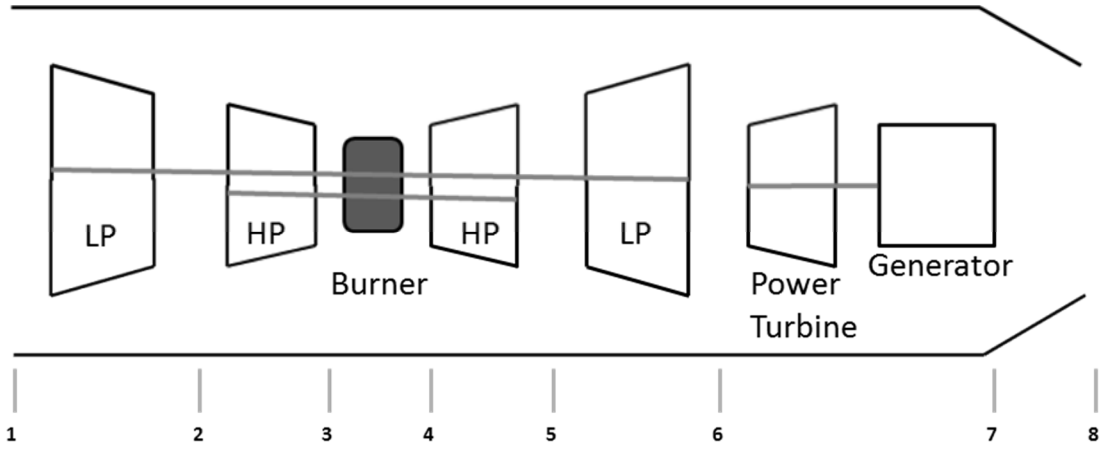

Figure 52: Turboshaft turbogenerator configuration

Besides providing sufficient power for the fan array at the design point, the core engine must also be able to provide enough power to operate the fan array at off-design conditions.

The various design parameters for the core turboshaft engine is shown in Table 7.

Table 7: Turboshaft turbogenerator design parameters

Component	Parameter	Design Value
Low Pressure Compressor (LPC)	Polytropic Efficiency	0.9325
High Pressure Compressor (HPC)	Polytropic Efficiency	0.9325
LPC & HPC	Pressure ratio	OPR varied to equal max T3 with an equal split between compressors
Burner	Inlet Temperature (T_3)	934 K @ ADP
	Exit Temperature (T_4)	1811 K @ ADP 1922 K @ T/O
	Burner Efficiency	0.998
High Pressure Turbine	Polytropic Efficiency	0.93
Low Pressure Turbine	Polytropic Efficiency	0.93
Power Turbine	Polytropic Efficiency	0.924

The turbine inlet temperature, T3, is assumed to be constant at the ADP and not varied. This temperature limit is primarily dependent on the material limits and for the purpose of this study, the technology level is assumed for the N+3 time-frame [24]. Similarly, the efficiencies values utilised in the core turboshaft generators are based on anticipated technology level in the N+3 timeframe.

In such a model, it is not possible practically to produce an engine that produces zero thrust due to the mass flow that would have to exit the engine. As such, the maximum thrust split used for such a configuration is assumed to be 95%.

In Turbomatch, the input handler for the engine simulation is the engine inlet mass flow. Hence, for a specified net thrust requirement from the core engines, the mass flow is iterated to achieve the required net thrust. The convergence criteria for all Turbomatch thrust requirements are assumed to be 0.5% difference.

5.4.2 Turbofan Turbogenerator

A turbofan turbogenerator configuration is also studied with the expectation of lower fuel consumption and higher propulsive efficiency for lower than 95% thrust split settings, thereby allowing the turbogenerator to produce net thrust on top of the power for the fan propulsors. Figure 53 shows the configuration of such an engine.

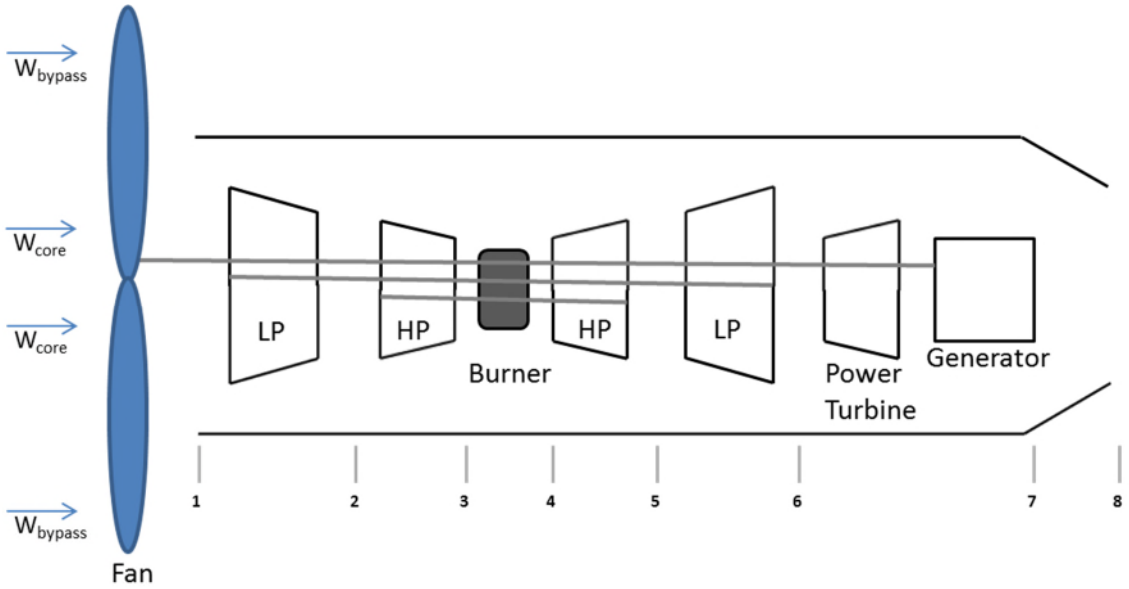

Figure 53: Turbofan turbogenerator configuration

The third spool in such a configuration connects the fan with the power turbine.

The design parameters of the engine are identical to those of the turboshaft turbogenerator with the addition of a few extra parameters. The core bypass ratio, cBPR or $\frac{W_{bypass}}{W_{core}}$ and the core fan pressure ratio, cFPR, are variables which are varied to produce different TSFC.

The TSFC is calculated from the fuel mass flow rate of the turbogenerator, W_{fuel} obtained from Turbomatch.

$$TSFC = \frac{2 \times W_{fuel}}{F_{N,array} + F_{N,core}} \quad \textbf{(5-30)}$$

5.5 Electrical System Modelling

The electrical system modelled in the study assumes the usage of cryocoolers for cooling a HTS system. While other systems have their own advantages, this system is deemed to be suitable for the N3-X and has been used in the preliminary design for the N3-X.

The overall electrical system consists of the fully superconducting generator attached to the core engine, fully superconducting motors driven by cryogenically cooled inverters, superconducting transmission lines and cryocoolers to cool the generators and motors. The usage of inverters allows the propulsor fans to rotate at the desired spool speed without the use of fixed ratio gears.

The overall efficiency of the complete system is assumed to be 99% [14] and this has taken into account the efficiency of the generator with cooler, efficiency of motor and inverter with coolers as well as the transmission line losses for the N+3 timeframe.

It has been noted in previous chapters that the radius of the motor would determine the minimum root or hub radius of the designed propulsor fan as the motor would have to be contained within the hub of the fan. The length of the motor would also determine the length of the duct between the fan rotor face to the nozzle. As such, a motor sizing reference has been implemented in all the studies conducted.

Table 8 describes the characteristics of some of the electrical designs suitable for the use in such a TeDP platform.

Table 8: Characteristic of various electrical generators/motors

Parameter	Homopolar Induction Alternator Electrical Generator	LEI Electrical Generator	HTS synchronous Electrical Motor
Power Density [W/kg]	8000	5281.9	6600
Diameter [m]	-	0.97	0.22
Length [m]	-	1.2	0.76
Power [MW]	4	3	1.5
Torque [N.m]	-	-	4500
Rotational Speed [rpm]	16000	15000	3000

It can be observed that the HTS electric motor can be deemed suitable for the application on the TeDP fan propulsor.

In ref [63], an equation was developed that correlates the radius, length and power of the HTS motor. This is shown below

$$r_{EM}^3 = \frac{0.457\ PW_{EM}^5 - 7.31PW_{EM}^4 + 46.17PW_{EM}^3 - 139.52PW_{EM}^2 + 340.9PW_{EM} + 13.66}{\frac{L}{r\pi}10000} \quad \textbf{(5-31)}$$

The length to radius ratio of the electrical motor is kept constant at 6.909 based on HTS synchronous electric motor in Table 8.

With this, the fan propulsor design model would have an additional design loop to check the root radius of the fan propulsor and iterate if necessary to ensure the minimum hub radius is observed.

$$r_{hub} > r_{EM} \quad \textbf{(5-32)}$$

The length of the duct is then

$$L_{(3-4),fan} = 6.909 \times r_{EM} \quad \textbf{(5-33)}$$

5.6 Case Study on N3-X

The methodology developed in this chapter requires a known boundary layer at the intake face. NASA [24] and Boeing [64] conducted CFD simulations on an earlier version of the N3-X called the N2-A at its flight conditions. Although the N2-A differs from the N3-X in terms of total span and area, it fundamentally utilises the same set of aerofoils across the span. In terms of flight conditions, N2-A's ADP is at 35,000 ft and Mach 0.8 whereas the N3-X's ADP is at 30,000 ft and Mach 0.84. It was judged that the boundary layer conditions at the same percentage chord length for both aircrafts would be very similar. Furthermore, the mass-average Mach number and total pressure profile at each distance, *i,* was obtained from the CFD and calculated as below

$$M_{avg,i} = \frac{\sum_0^i (W_i M_i)}{\sum_0^i W_i} \quad \textbf{(5-34)}$$

$$P_{T_{avg,i}} = \frac{\sum_0^i (W_i P_{T,i})}{\sum_0^i W_i} \quad \textbf{(5-35)}$$

The mass-averaged values obtained were then divided by the freestream Mach and total pressure to yield normalized boundary layer profiles that could be used at other similar flight conditions. Figure 54 shows the normalised profiles at the selected percentage chord length of 0.85. Furthermore, an additional assumption is that there is no total temperature distortion and that remains constant to that of the freestream value. The boundary layer profile is assumed to be constant across the entire span of the intake.

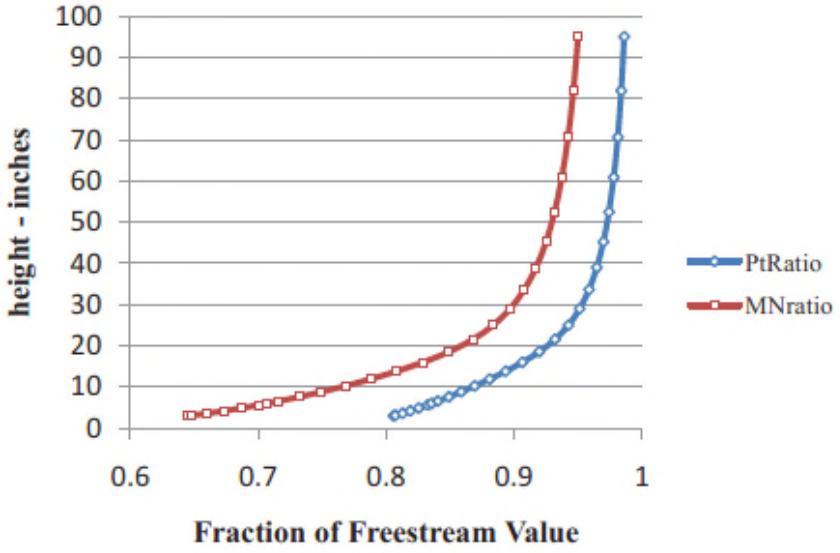

Figure 54: Normalised total pressure and Mach profile at 0.85 chord length

The flight conditions and aircraft variables chosen for this study corresponds to that in Table 9.

Table 9: Assumptions for propulsion module case study

Property	Value
ADP Altitude [m]	9144
ADP Mach	0.84
ADP Thrust requirement [N]	119000
H_CS [m]	0.5 – 2.0
$\Delta P_{T,intake}$	-1.0%
NF	Variable
FPR	Variable
$\Delta \eta_f$	-1%
$\Delta P_{T,nozzle}$	-1%
Thrust Split	95%
Core engine configuration	Turboshaft

The number of fans for each capture sheet height is iterated to obtain the maximum number of fans that can be installed in the constraints previously

mentioned. A parametric study whereby the capture sheet height is varied is conducted.

Fig XX shows the variation of FPR with the capture sheet height.

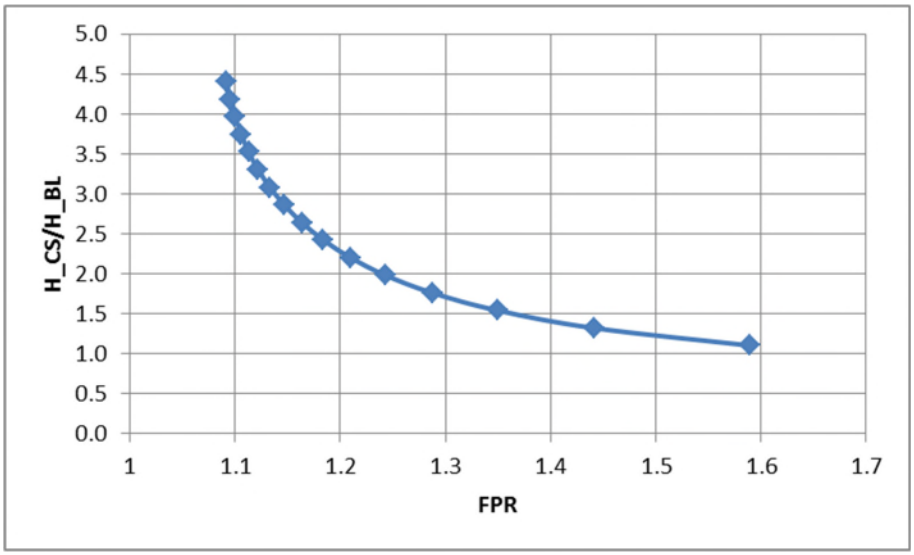

Figure 55: Variation of FPR with capture sheet height

As the capture sheet height decreases, the total mass flow entering the intake reduces. To achieve the same intrinsic net thrust requirements, there needs to be an increase in the FPR. Furthermore, it can be observed that at higher capture sheet height or intake height, the FPR becomes excessively low. At low FPR, the losses associated in the flow would probably negate the pressure gain across the fan and would be impractical to implement. A reasonable minimum FPR would be around 1.2 and that corresponds to an intake height approximately 2.25 times the height of the boundary layer. Such a system on the N3-X would thus require that the intake height be less than 2.25 times the height of the boundary layer.

Fig XX shows the total fan power requirements with varying capture sheet height.

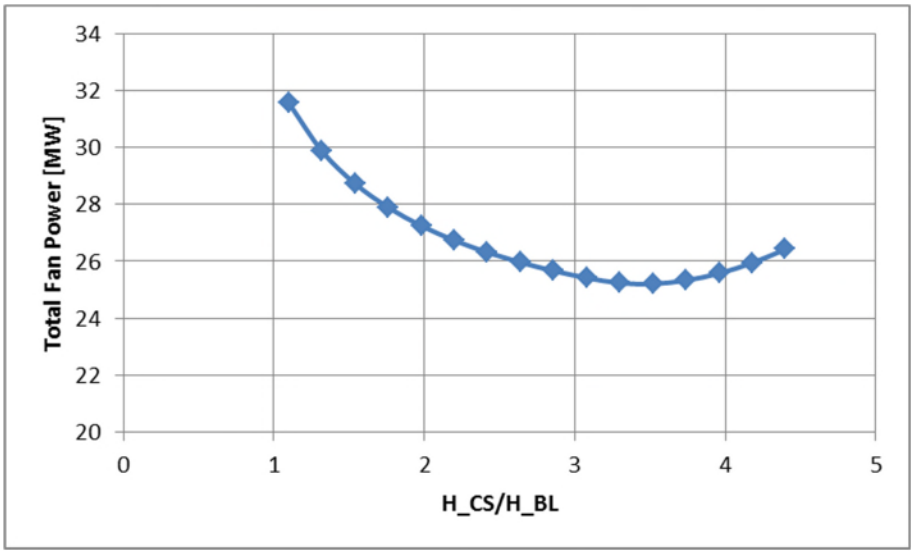

Figure 56: Variation of total fan power required with capture sheet height

Whilst it has just been mentioned that the capture sheet height should be less than 2.25 times the boundary layer height, it is useful to look at the data from high intake heights too. It can be observed that there is a minimum total fan power requirement to drive the N3-X in such a system from Figure 56. This happens as a result of a balance between the positive impact of boundary layer ingestion and the negative impact of higher percentage losses in the flow with decreasing intake height. Further explanation would be given as the boundary layer impacts are further discussed in the thesis. Figure 57 shows the TSFC trends with capture sheet height. It exhibits similar trends to that of the total power requirements as the core turbogenerators have to provide the required power to the fan array at a constant intrinsic net thrust requirement. An increase or decrease in the power requirements would also represent a corresponding change in the core engine mass flow rate and fuel requirements.

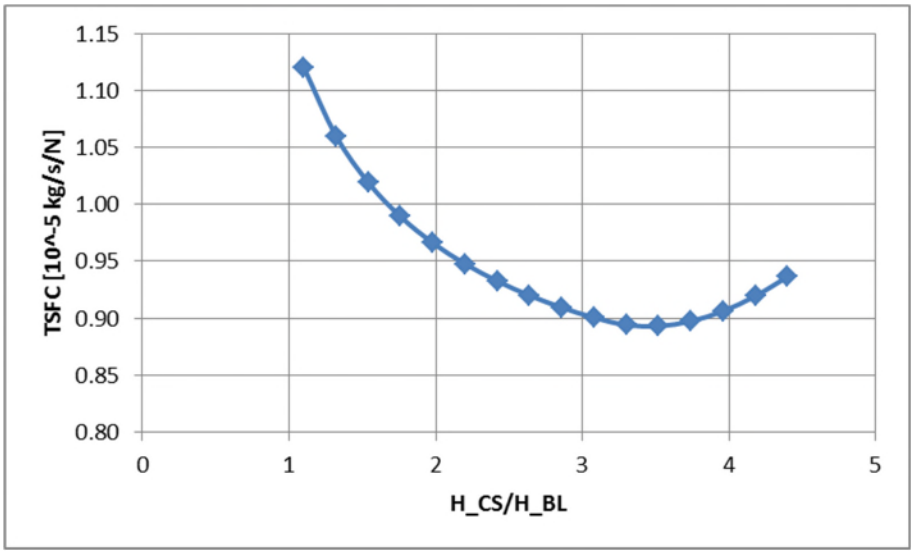

Figure 57: Variation of TSFC with capture sheet height

5.7 Conclusion

In this chapter, the propulsion modelling and design methodologies have been developed. This includes the fan propulsor design variables, fan propulsor performance modelling methodology, core turbogenerators configurations utilising either turboshaft or turbofans and their corresponding design variables. An additional section also described the electrical systems modelling and how it relates and impacts upon the propulsion system design. Lastly, these developed methods were applied onto the N3-X for a case study.

Chapter 6

BOUNDARY LAYER INGESTION MODELLING

6.1 Introduction

The boundary layer ingestion module plays an important role in the overall synergy of the model. It not only impacts upon the mass flow for the fan propulsors, it also impacts upon the efficiency of the fan propulsors due to the distortion in the inlet flow for a fan designed for clean straight airflow. This chapter recognizes the importance of these factors and firstly, introduces a boundary layer profile modelling methodology followed by an adaptation of the Discretised Miller method to model the impacts of flow distortion on the fan performance. The modelling flow of the module is shown in Figure 58. It consists of firstly, generating the boundary layer profile and properties, then defining intake pressure losses and fan efficiency penalty using an adapted version of the Discretised Miller method. The boundary layer module integrates together with the propulsion module as the efficiency penalty on the fan performance and intake losses alters the design of the fan in the propulsion module. An iteration loop is generated until the fan design fulfils the thrust requirements in the propulsion module.

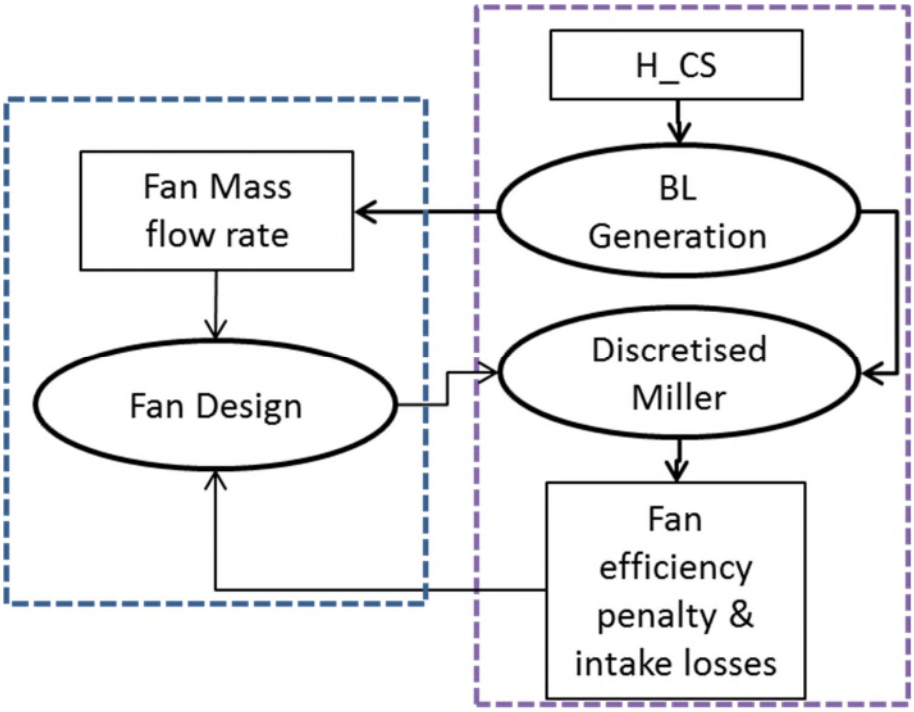

Figure 58: Boundary layer ingestion module flowchart

6.2 Boundary Layer Profile Modelling

It was described in the previous chapter the NASA boundary layer ingestion method whereby the boundary layer profile utilised was that of the N2-A obtained via CFD at a specific chord percentage at the aircraft centreline. This profile was then normalised to its freestream conditions and assumed in the N3-X aircraft as a constant profile across the whole span.

To describe the boundary layer profile, the boundary layer power law is used [65] [66]. The methodology developed here requires a reference boundary layer profile whereby the power law can be applied to model it. If a reference boundary layer profile is not available, the power law indice can be referenced from [65] using the known geometrical and flow properties.

The boundary layer height is defined as

$$\delta_{stirp} = 4.91 \frac{x_{strip}}{\sqrt{Re_x}} \quad \textbf{(6-1)}$$

$$Re_x = \frac{\rho U_\infty x_{strip}}{\mu} \quad \textbf{(6-2)}$$

x_{strip} is the longitudinal distance of the strip surface fore of the intake.

Hence, the boundary layer height at a specific strip is proportional the function

$$\delta_{strip} \propto \frac{\sqrt{x_{strip}}\mu}{\sqrt{\rho U_\infty}} \quad \textbf{(6-3)}$$

Taking a reference known boundary layer profile with a known boundary layer height, the boundary layer height at other flight conditions and longitudinal distance can be calculated. In application to the N3-X aircraft, the reference boundary layer profile and height is the N2-A CFD [24] data at M=0.8 and 35,000 ft with a longitudinal distance of 40m. The corresponding boundary layer height is 0.508m.

The power law is then applied to model the reference boundary layer profile. For the N2-A profile used, this corresponds to

$$\frac{V}{V_\infty} = 0.9725\left(\frac{z}{\delta} + 0.1\right)^{\frac{1}{5.6}} \quad \textbf{(6-4)}$$

Whereby z is the vertical distance from the surface of the profile.

For different boundary layer height as computed in equation (6-3), the same power law profile is applied to compute the boundary layer profile and properties. Such an assumption and derivation of the boundary layer profile allows for more variables to be studied including different flight conditions, different intake longitudinal location and different lateral fan position without the extensive use of time consuming CFD. Figure 59 shows the comparison of the N2-A CFD boundary layer profile to the profile derived using the power law. The boundary layer profile for the N3-X at the ADP is also shown.

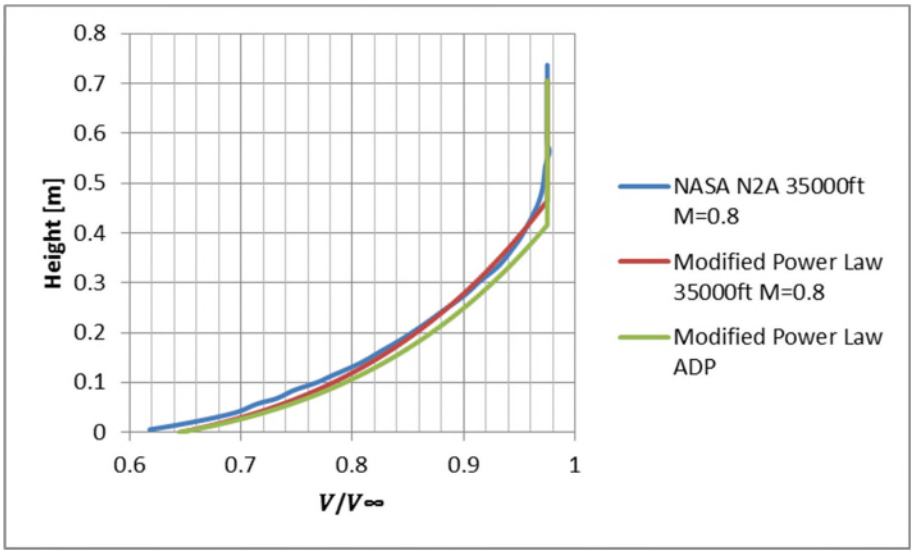

Figure 59: Comparison of boundary layer profile using modified power law

6.3 Intake Pressure Losses and Flow Profile

The intake pressure losses is defined as follows

$$\Delta P_{T,intake} = \frac{P_{T,2} - P_{T,1}}{P_{T,1}} \quad \textbf{(6-5)}$$

As the boundary layer flow enters the intake, there can be expected pressure losses as per any intake flow. However, the presence of low velocity regions in the boundary layer might result in higher pressure losses than those of a straight flow profile. Furthermore, in such TeDP applications, the fan propulsors can be expected to be embedded in the aircraft and this would probably necessitate the usage of S-duct intakes. The low velocity regions coupled with an S-duct might result in excessive pressure losses without a specially designed duct. NASA indicated through design optimization studies that intake pressure losses on an S-duct can be reduced to be as little as between 0.4-0.5% [67]. For the purpose of the study, a parametric application of various intake pressure losses is applied to study the impact of intake pressure losses on the overall synergy and design. The various assumed intake pressure losses would range from 0.2% for a non-boundary layer ingesting or clean flow profile to 2% for a distorted boundary layer ingesting system.

Using the N3-X as a reference, the inlet flow enters a rectangular mail-slot inlet and transits through an S-duct to the round fan rotor face. The flow profile would reasonably be expected to change by the time it is at the rotor face. To simplify the problem, as assumption was made whereby the gradient of the total pressure and Mach number profiles remains the same from the inlet face to the rotor face. The rotor face average Mach number is assumed to be 0.62 as per previous assumptions. Based on these, the inlet Mach number profile is scaled up. There is no total temperature distortion in the flow. This would thus allow mass conservation from the intake face to the rotor face as well as a defined set of flow angles at the rotor face for application of the Discretised Miller method. While a more comprehensive way would be to utilise CFD to simulate the boundary layer flow through the S-duct to the rotor face, such a method would be time consuming and with the lack of a proper designed intake duct, the process would not be suitable for an early design phase study such as that for a future concept aircraft. This would allow a balance between time and accuracy and allows a study for the trends involved in such a design.

6.4 Adapted Discretised Miller Method

Models such as the parallel compressor method consider a 2D inlet plane and distortion effects are captured radially. NASA made use of a 1D methodology whereby a fixed 1% efficiency penalty is applied on the propulsor fans due to the distorted flow. It is opined that the fan efficiency penalty differs at different designed fan pressure ratios.

The effect of distortion on the efficiency of the boundary ingesting fans is captured through an adapted version of the Discretised Miller [41] method. This method is a devised semi-empirical method that discretises the performance of the fan in both the radial and circumferential directions as a function of the inlet velocity and the resulting flow angles. The methodology is shown in Figure 60.

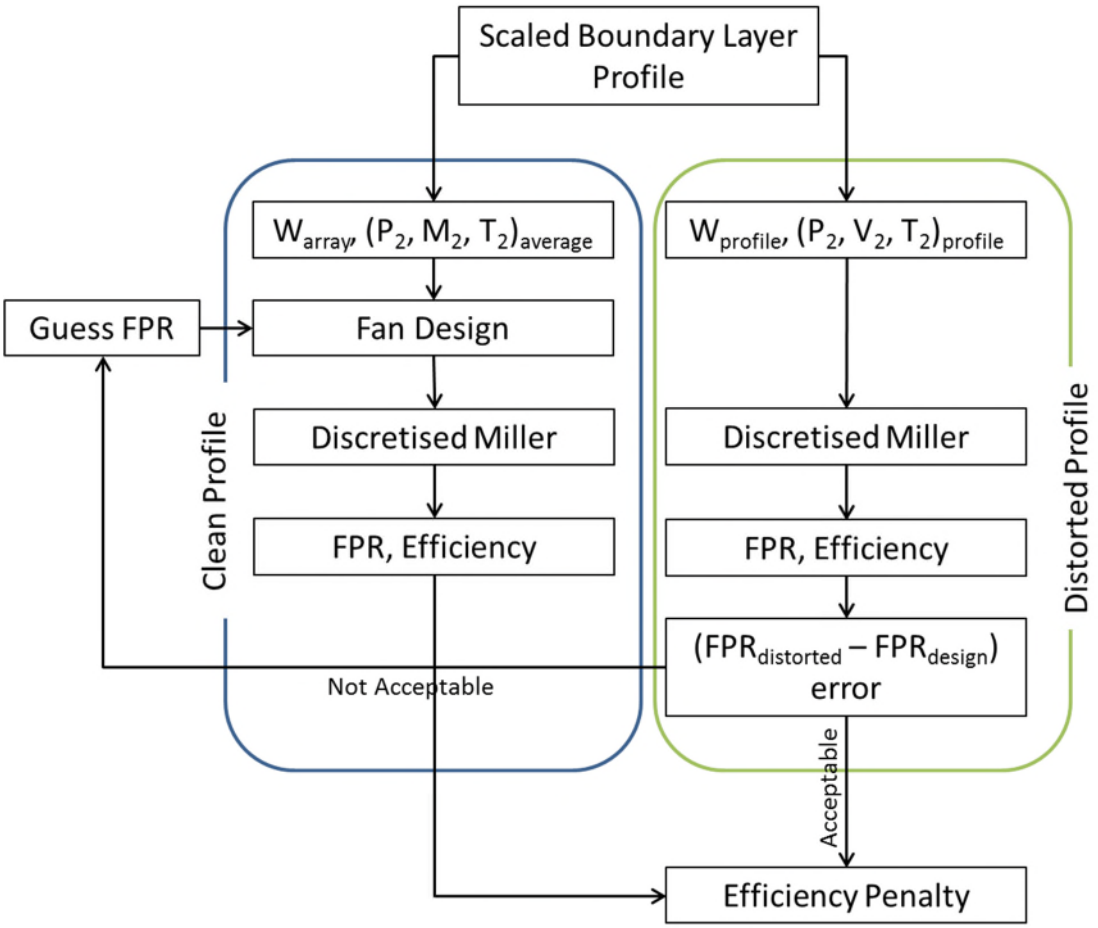

Figure 60: Flowchart for adapted Discretised Miller method

The Discretised Miller method requires a designed fan stage with the fan characteristics known. The fan rotor inlet conditions are obtained from the scaled boundary layer profile. To design the fan stage, the mass-averaged values of the total pressure, total temperature and Mach number is used to assume a constant profile.

To obtain a basic fan stage design, the design process in reference [60] is used. This is a mean-line design methodology, employing Euler equations and velocity triangles to calculate the air angles before and after each blade. The design assumes a free vortex condition and a constant axial velocity. This simplifies the model at an expense of accuracy. It should however, be noted too that the entire adapted Discretised Miller method is to obtain an estimated efficiency penalty on the designed fan stage and the designed fan stage in this model is not physically used in the overall methodology. The pitch-to-chord ratio is defined using

reference [60] and the blade geometry is determined using the Carter's rule for deviation angle [68].

With defined blade geometry, the Discretised Miller method is applied. The fan rotor inlet area is first discretised in both the radial and circumferential directions and is assumed constant from the inlet rotor face to the stator exit face. The circumferential direction is discretised into the number of blade passages. Figure 61 shows the fan rotor inlet discretised area.

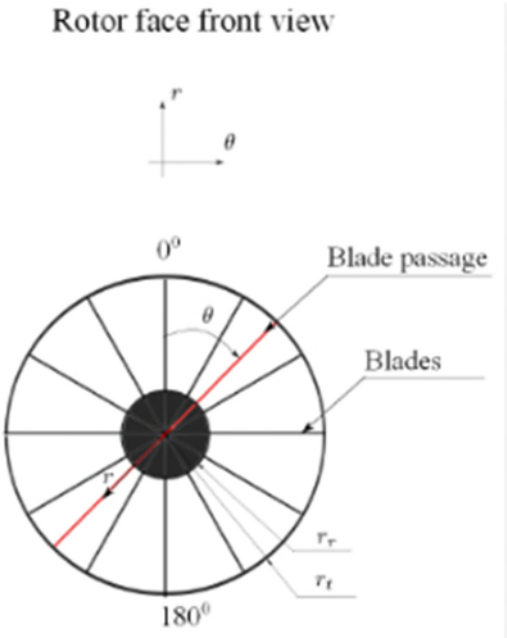

Figure 61: Fan rotor inlet discretised area

At each discretised area, the deviation angle is calculated as a function of the stagger and camber angles using charts from reference [69] [70]. The deviation angle is then used to calculate the minimum loss, optimum stall and choke incidence angles across each discretised stream. The stream loss coefficient is calculated using the approach as described in [69] [70] [71]. The various loss coefficients empirical data used are summarized in Table 10.

Table 10: Summary of loss coefficients empirical relations used in D.M

Parameter	Reference method
Minimum loss coefficient	Miller [70]
Deviation Angle	Miller [70]
Total loss coefficient	Miller [70]
End wall loss coefficient	Wright [72]
Profile loss coefficient	Wright [72]
Shockwave loss coefficient	Schwenk [73]

The density changes and blockage effects are neglected in this approach as the fan stage is expected to operate at a low pressure ratio [60] and allows the simplification of the model to allow the use of incompressible flow equations. The static pressure increment is thus calculated across each discretised stream and together with the loss coefficient, can be used to calculate the isentropic efficiency across the stream. The empirical relations applied in the methodology are developed for mean-line analysis and in this case, adapted for a discretised stream in terms of radial and circumferential position. The interactions between the streams are neglected in the methodology and deemed effective enough.

The overall FPR and the isentropic efficiency is a mass average of all the individual streams. Several validation cases were applied by Esteban [41] that compares results of both clean and distorted cases. Figure 62 [41] shows the comparison of the stage total pressure increment and isentropic stage efficiency along the span of one flow passage on the NASA designed Rotor 53 [58] using experimental data and the Discretised Miller method. The results are based on clean airflow entering the fan stage and shows good promise in the method. While it can be observed that there is an offset in the static pressure increment prediction and isentropic stage efficiency especially in the hub and tip regions, the balance between speed, resources and accuracy is deemed adequate in application on such early design phase. It also cannot be emphasised enough that the Discretised Miller method is in this instance, is adapted to only predict the efficiency penalty for a generic designed fan with a design FPR when subjected to a set of described distorted flow conditions.

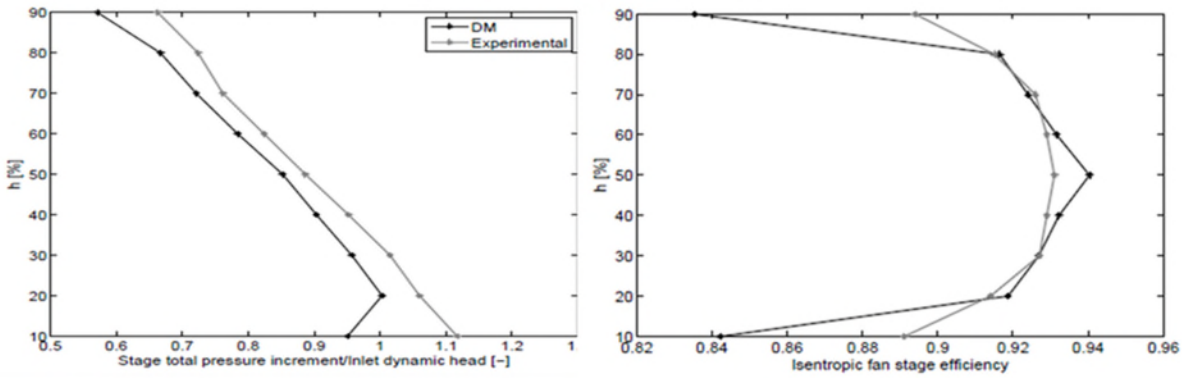

Figure 62: Sample validation of the D.M method

It can thus be seen that the FPR and isentropic efficiency is different when clean flow conditions and distorted flow conditions are applied on a designed fan stage with the adapted Discretised Miller method. The design FPR is the FPR required by the fan propulsors to produce the required intrinsic net thrust. Thus, iterations are conducted on the fan stage design to obtain the required FPR under distorted flow conditions.

Once converged, the efficiency penalty is determined as below

$$\Delta\eta_f = \frac{\eta_{f,distorted} - \eta_{f,clean}}{\eta_{f,clean}} \quad \textbf{(6-6)}$$

This penalty can be applied on the future fan design efficiency as described in Chapter Chapter 5 for the propulsion design.

6.5 Case Study on N3-X

Two sets of parametric studies were done on a case study on the N3-X. The intake pressure losses is first varied parametrically to observe the trends involved with changing intake total pressure loss and the second is the application of the adapted Discretised Miller method to determine the impact of fan efficiency losses in the overall design.

The assumptions made in these simulations are tabled in Table 11.

Table 11: Assumptions for boundary layer ingestion module case studies

Property	Value
ADP Altitude [m]	9144
ADP Mach	0.84
ADP Thrust requirement [N]	119000
H_CS [m]	1.6 – 2.6
$\Delta P_{T,intake}$	-0.2%, -1.0%, -2%
NF	Variable
FPR	Variable
$\Delta \eta_f$	0%, Discretised Miller
$\Delta P_{T,nozzle}$	-1%
Thrust Split	95%
Core engine configuration	Turboshaft

6.5.1 Impact of Intake Pressure Losses on N3-X

For an embedded fan propulsor system, the distortion of the flow in the embedded intake duct would possibly result in significant pressure losses. Coupled with the ingestion of the boundary layer flow, this might cause further distortion and further losses in the inlet stream. This loss in pressure is essentially a loss in the potential energy of the flow entering the fan propulsors. The flow would then have to be further re-energised via the fan propulsors to provide the required intrinsic net thrust. This would result in an increase in the power consumption or requirement of the fan propulsor array.

Figure 63 shows the total power requirements of the fan propulsor array with respect to different capture sheet heights with varied intake pressure losses while Figure 64 shows the required design FPR with respect to different capture sheet heights. No fan efficiency penalty is applied such as to isolate the effects resulting from intake pressure losses.

It can be observed that if the intake pressure losses are kept minimal and constant as that of the freestream configuration, the power requirement reduces significantly. This is due to the much lower inlet momentum drag of a BLI

configuration, resulting in less propulsive force required to be produced by the array for the same intrinsic net thrust requirement. As we recall from the intrinsic net thrust equation for the fan propulsor below

$$T_N = W(u_8 - u_1) + (p_8 - p_1)A_8 - (p_1 - p_0)A_1 \quad \textbf{(6-7)}$$

A lower inlet velocity due to the boundary layer flow would mean a lower inlet momentum drag. Hence, the FPR required of the fan propulsor is lower and the energy imparted to the flow via the propulsor is less, resulting in a lower power requirement.

As the inlet pressure losses are increased for the same capture sheet height, the inlet flow itself has less energy and there is now further requirement by the fan propulsor to re-energise the flow through a higher fan pressure ratio to obtain the intrinsic net thrust required.

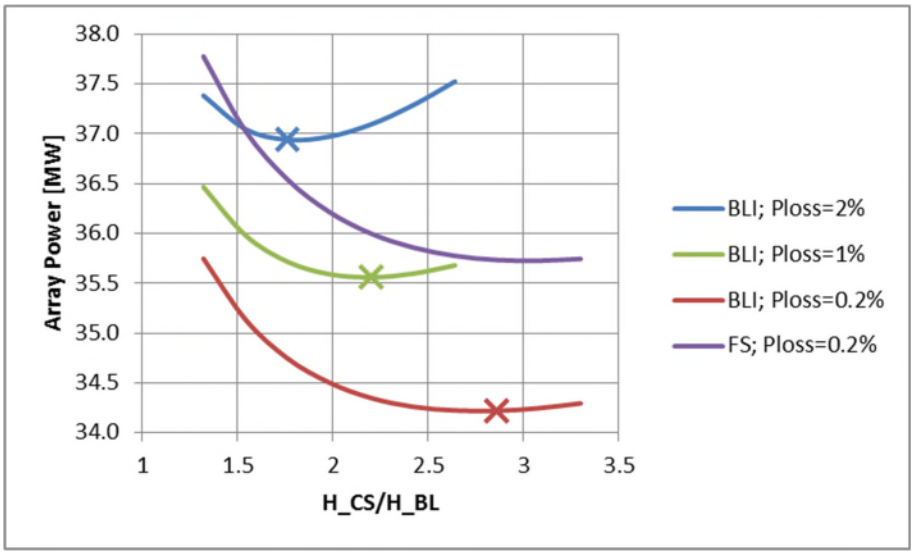

Figure 63: Array required power variation with capture sheet height for various intake pressure loss

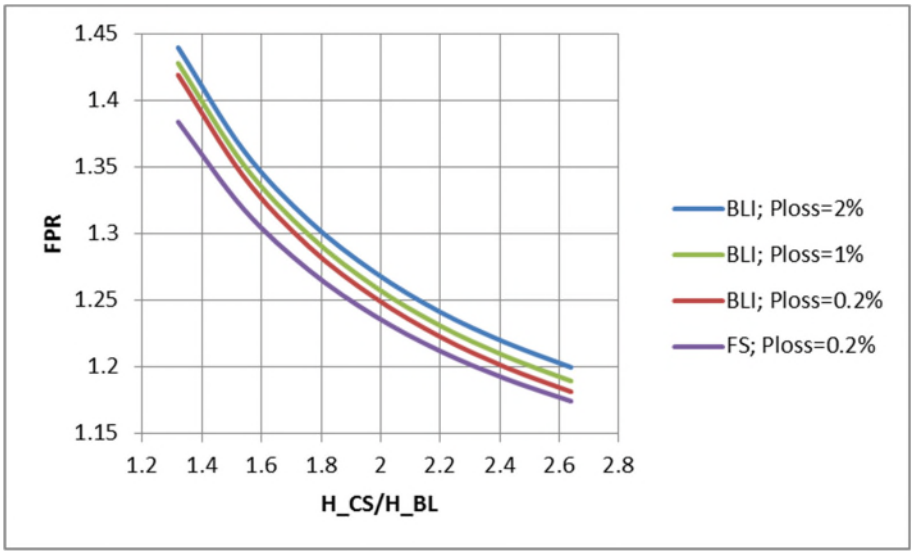

Figure 64: FPR variation with capture sheet height for various intake pressure loss

For each defined intake pressure loss, there now exists an optimal capture sheet height where minimal power is required. This can be attributed to two opposing effects. BLI reduces the energy required to be imparted to the flow while the presence of pressure losses increases the energy requirements. As the capture sheet height increases, there are more energy losses in the intake with a higher mass flow rate for a fixed intake pressure loss percentage. There would be a point whereby the energy losses would negate the positive impact of inlet drag momentum reduction and further increasing the capture sheet height would no longer result in a lower array power requirement. This also explains why a higher intake pressure loss percentage would result in a lower optimal capture sheet height. The higher percentage intake pressure losses would negate the positive impact of boundary layer ingestion at a lower capture sheet height as more energy is required to be imparted to the flow as compared to a lower intake pressure loss percentage.

Lastly, the importance of reducing the intake pressure losses can be observed. While a similar 0.2% pressure loss similar to the freestream intake pressure loss is applied in a BLI system would significantly reduce the total array power requirements by about 4-5%, a 1% intake pressure loss would only reduce the array power requirements by 1-2%. A 2% intake pressure loss would have totally

negated the positive impact of BLI through power requirements reduction and would instead require more power than a freestream system. Thus, reducing the intake pressure losses is of utmost priority in such a BLI system.

6.5.2 Impact of Fan Efficiency Detriment on N3-X

A decrease in the fan adiabatic efficiency would result in an increase in the total temperature across the propulsor fan for a fixed FPR. This increase would hence lead to an increase in the propulsor array power required. Figure 65 shows the total propulsor array power when no efficiency penalty is applied and when the penalty derived from the discretised miller method is applied as well as their corresponding FPR. As expected, the power requirements increase across all the capture sheet height.

The optimum or lowest power capture sheet height also changes. The increase in power requirements when the fan efficiency penalty is applied for the optimum lowest power configuration is around 1%.

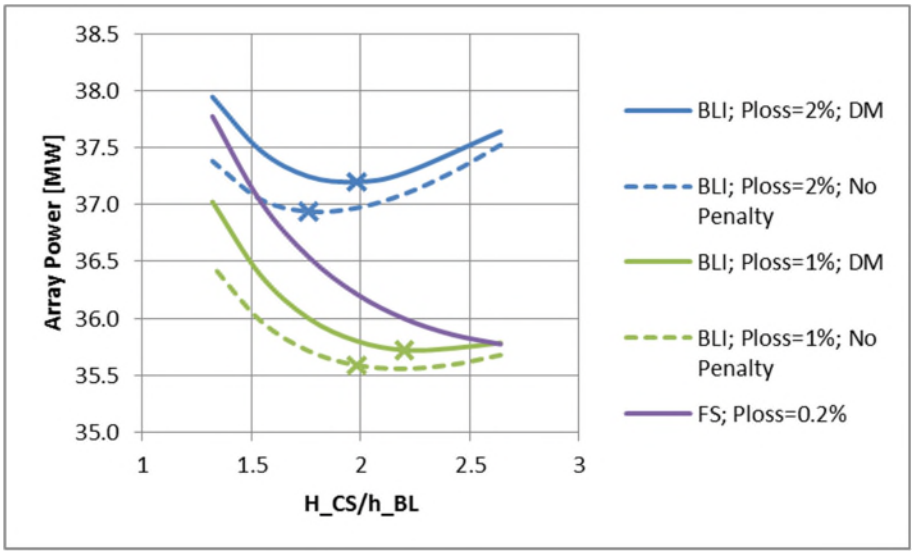

Figure 65: Impact of fan efficiency penalty on array power requirements

Figure 66 shows the adiabatic efficiency of the designed fan with respect to the design FPR. The adapted Discretised Miller used is compared to the simple NASA 1% efficiency penalty applied. The design FPR changes are a result of the different capture sheet height for the fixed intrinsic net thrust requirement. It can be observed that at lower design FPR, the efficiency penalty is less and

increases as the design FPR increases when using the adapted Discretised Miller method. This is attributed to the fact that at lower FPR or higher capture sheet height, the distortion effect on the flow reduces as the inlet flow ingests more and more freestream clean flow. With less percentage of distorted flow in the inlet, the adapted method predicts a lower efficiency penalty as expected.

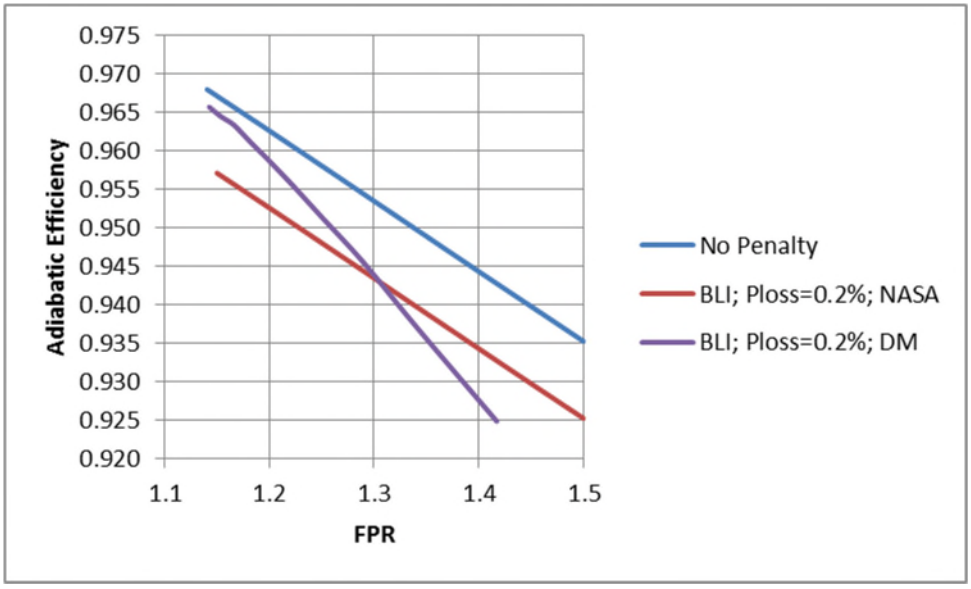

Figure 66: Comparison of the adapted D.M method and NASA based fan adiabatic efficiency

6.6 Conclusion

This chapter introduced and explained the boundary layer ingestion modelling work done. These include the modelling of the boundary layer profile, modelling the intake pressure losses and the flow profile after the intake at the rotor face, the adapted Discretised Miller method to account for the fan efficiency penalty from distorted flow ingestion and the application of the models on the N3-X aircraft as a case study. Reducing intake pressure losses have been shown to be of paramount importance to the effectiveness of a BLI system as even a 2% intake pressure loss on the N3-X would have negated any power reductions benefits from BLI. Fan efficiency penalty has also shown to change across the design FPR on the N3-X and the efficiency penalties result in around 1% increase in the total power requirements of the fan propulsor array.

Chapter 7

WEIGHT MODEL

7.1 Introduction

A weight model for the various components is necessary in the overall modelling and synergy as different overall aircraft weight would result in a different trim intrinsic net thrust requirement at the ADP. This in turn would lead to different design conditions for the propulsion system and resulting different component mass. An overall iteration loop is created to model the weight of the various components and the corresponding intrinsic net thrust requirements as shown in Figure 67.

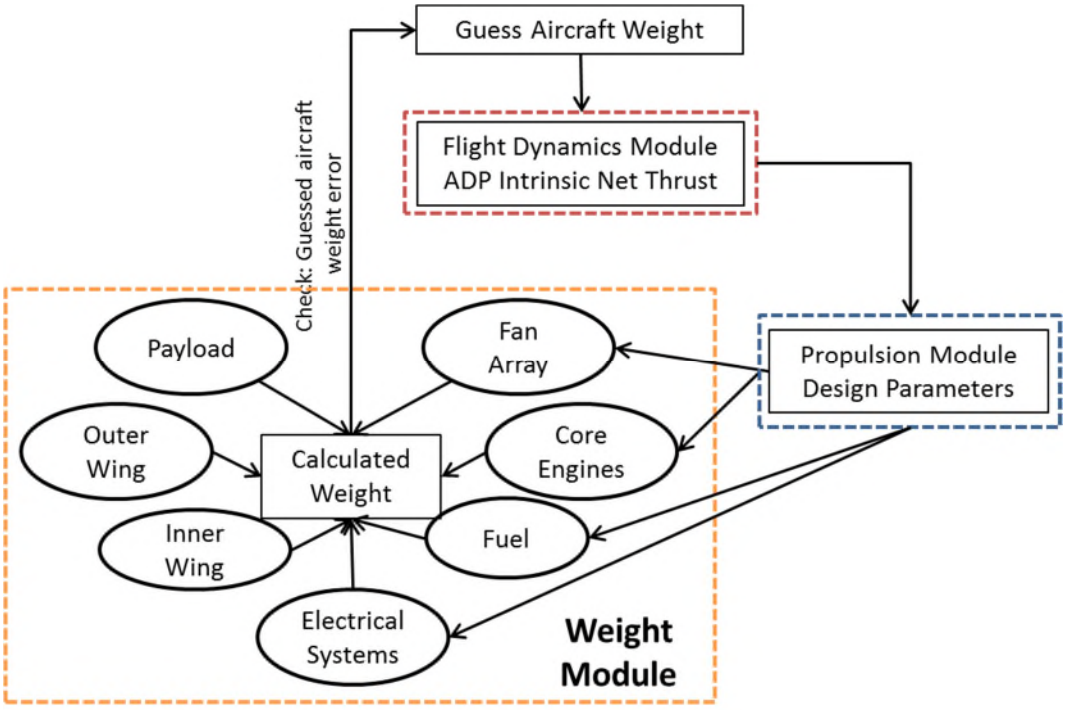

Figure 67: Weight module flowchart

The weight module consists of 7 main components. Figure 68 shows how some of the components are identified on the N3-X aircraft although the same classification can be used on another BLI BWB aircraft.

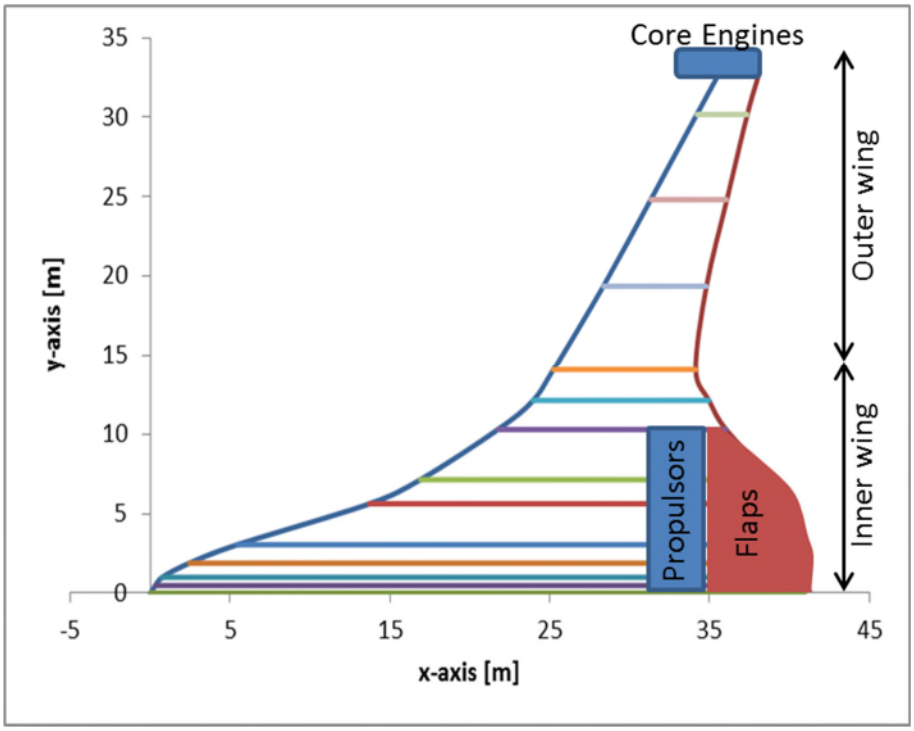

Figure 68: Some components of the weight module

The fan propulsors consists of the whole fan propulsor array including the intake and the nozzle structure. The core engines are for both turbogenerators mounted on the wing tips. The payload is fixed and constant as per the design requirements and positioned within the inner wing area. The electrical system consists of the generators, motors, inverters, coolers and the transmission lines. The fuel is the overall fuel requirements for the complete aircraft mission and positioned within the inner wing area. The outer wing consists of the wing-like structure on the aircraft away from all the auxiliary systems and propulsor array. In the case of the N3-X, it is defined as being from Y-axis location of 15m to the wing tip. The inner wing of the N3-X is defined as being from Y-axis location of 0m to 15m. It also consists of all other auxiliary systems such as the landing gear and electronics. The elevator flaps also form part of the inner wing structure.

7.2 Fan Array Weight Prediction

The fan propulsor array consists of the fans, the fan ducting including the casing and acoustic lining and the nozzle. The length of the duct is determined in the propulsion module as a function of the electrical motor radius as previously seen in equation (5-33). The weight of the each individual fan is scaled as follows from reference [74] in relation to the diameter, pitch-to-chord ratio, tip velocity and blade aspect ratio.

$$W_{fan} = 85.4\left(D_{tip}\right)^{2.7} \cdot \left(\frac{\sigma_{tip}}{\sigma_{tip,ref}}\right)^{0.3} \cdot \left(\frac{V_{tip}}{V_{tip,ref}}\right) \quad \textbf{(7-1)}$$

The fan casing weight is calculated as follow assuming it is aluminium material

$$\mathrm{W}_{casing} = \pi(D \cdot L \cdot \rho \cdot t)_{duct} \quad \textbf{(7-2)}$$

The weight of the acoustic lining wall is calculated as follows

$$\mathrm{W}_{lining} = \pi[(L \cdot D)_{inner\ wall} + (L \cdot D)_{outer\ wall}] \cdot \rho_{wall} \cdot t_{wall} \quad \textbf{(7-3)}$$

The various constants and assumed values are shown in Table 12.

Table 12: Various assumptions and reference values for the fan array weight calculations

Parameter	Value
$\sigma_{tip,ref}$	1.25
$V_{tip,ref}$ [m/s]	350
t_{duct} [m]	0.0013
t_{wall} [m]	0.0010
ρ_{wall} [kg/m^3]	2770
ρ_{duct} [kg/m^3]	2770

7.3 Core Engines Weight Prediction

The core engine weight calculations are based on a power law scaling methodology developed in reference [75]. Various difference complexities methodologies are available in predicting the weight of turboshaft and turbofans

[76] [77] that can be applied in this study. However, this scaling methodology was selected for its simplicity in application while taking into consideration both bypass ratio and diameter. The balance of simplicity and accuracy is deemed appropriate for such an early design phase model. The calculation is based on the following

$$Mass_{total,2} = \left(BPR_{ref} + 1\right) Mass_{core} \quad \textbf{(7-4)}$$

$$Mass_{eng} = Mass_{eng,ref}\left(0.9 + 0.1\frac{{D_{eng,2}}^2}{{D_{eng,ref}}^2}\right) \cdot \frac{{D_{eng}}^{2.7}}{{D_{eng,2}}^{2.7}} \quad \textbf{(7-5)}$$

$$W_{eng} = Mass_{eng} \times 9.81 \quad \textbf{(7-6)}$$

The various constants and assumed values are shown in Table 13.

Table 13: Various assumptions and reference values for the core engine weight calculations

Parameter	Value
BPR_{ref}	15
$Mass_{eng,ref}$ [kg]	6900
$D_{eng,ref}$ [m]	2.565

7.4 Electrical Systems Weight Prediction

The electrical systems consists of the propulsor fans' motors, inverters and respective coolers, core engines' generators, inverters and respective coolers as well as transmission lines. All of these were calculated based on scaling with respect to their power and shaft speed. The baseline values were based on NASA reports [23] and shown in Table 14.

$$\mathrm{W}_{motor/generator} \propto \left(\sqrt{\frac{Power}{Shaft\ speed}}\right)_{motor/generator} \quad \textbf{(7-7)}$$

$$\mathrm{W}_{motor/generator\ cryocooler} \propto (Power)_{motor/generator} \quad \textbf{(7-8)}$$

$$\mathrm{W}_{inverter} = \mathrm{W}_{inverter,ref} \quad \textbf{(7-9)}$$

$$W_{inverter\ cryocooler} = W_{inverter\ cryocooler,ref} \quad \textbf{(7-10)}$$

$$W_{transmission} = W_{transmission,ref} \quad \textbf{(7-11)}$$

Table 14: Various assumptions/reference values for the electrical systems weight calculations

Parameter	Value
$W_{motor,\mathrm{ref}}$ [N]	1397.2
$Power_{motor,ref}$ [MW]	3.138
$Shaft\ speed_{motor,ref}$ [rpm]	4500
$W_{motor\ cryocooler,ref}$	414.0
$W_{generator,ref}$ [N]	5268.5
$Power_{generator,ref}$ [MW]	22.371
$Shaft\ speed_{generator,ref}$ [rpm]	3600
$W_{generator\ cryocooler,ref}$ [N]	2581.0
$W_{inverter,ref}$ [N]	889.8
$W_{inverter\ cryocooler,ref}$ [N]	298.2
$W_{transmission,ref}$ [N]	4449.8

7.5 Fuel Weight Prediction

To estimate the total fuel weight of the aircraft, as assumption is made that the overall fuel weight is 115% of the weight of the fuel consumed during the cruise phase. This would imply that an additional 15% of fuel above the cruise requirements is required to cater for the other flight segments including spare fuel. The flight dynamics module is utilized to compute the cruise phase fuel consumption. Various relations exists for a more comprehensive prediction of fuel weight at the various flight regimes but an initial approximation of 15% additional of fuel is deemed sufficient for the study.

To simulate this phase, the ADP TSFC of the propulsion system is used as an input into JSBSim. The simulation is divided into specified time intervals. At each

time interval between t_i and $t_{i+\Delta t}$, the fuel consumed by the aircraft and the new overall aircraft weight of the aircraft is calculated respectively by

$$\left(\Delta W_{fuel}\right)_{t=t_i} = TSFC \times (T_N)_{t=t_i} \times \Delta t \times g \quad \textbf{(7-12)}$$

$$(W_{overall})_{t=t_{i+\Delta t}} = (W_{overall})_{t=t_i} - \left(\Delta W_{fuel}\right)_{t=t_i} \quad \textbf{(7-13)}$$

The new overall aircraft weight is then used to obtain the trim intrinsic net thrust requirements in JSBSim for the next time step simulation. The cruise phase fuel weight is then

$$W_{fuel,cruise} = \sum_0^t \Delta W_{fuel} \quad \textbf{(7-14)}$$

The total fuel weight is then an additional 15% to cater for the other flight segments.

$$\mathrm{W}_{fuel,total} = W_{fuel,cruise} \times 1.15 \quad \textbf{(7-15)}$$

7.6 Outer Wing Weight Prediction

The outer wing weight is calculation is based on a fairly detailed analytical method from Toreenbeek [78] that caters for differences in leading edge and trailing edge support structures as well as loading, stresses and bending dependent on the MTOW and velocities. The level of detail in the method is suitable for this instance as the outer wing area will be modified in the studies as part of the optimisation process.

7.7 Payload Weight Prediction

The payload of the aircraft was assumed to constant throughout the studies as per the design requirements of the aircraft. For the case of the N3-X aircraft as primarily used in this thesis, this value was kept constant at 525070.4 N.

7.8 Inner Wing Weight Prediction

The inner wing weight would be expected to change as the weight of the aircraft changes and the loading requirements on the structure changes. It is assumed,

however, that as the payload remains constant, the inner wing area which houses the payload would not be expected to change in any optimization study done in this thesis. In this respect, the weight of the inner wing which includes all other subsystems is assumed to be a constant ratio with respect to the overall MTOW of the aircraft. This would thus allow the inner wing weight to change with respect to the overall weight and loading requirements on the aircraft without going into too much detail in the sizing and weighing of the subsystems such as the landing gear as the detailed design of the aircraft is not a priority in such an early design phase. This ratio of the weight is determined at the ADP conditions of the flight.

$$\left(\frac{W_{inner\ wing}}{MTOW}\right)_{ADP} = constant \tag{7-16}$$

For the N3-X aircraft, this ratio was calculated to be 0.37

7.9 Case Study on N3-X

Two different case studies utilizing the weight modules are presented here. Firstly, the impact of number of fans on the overall weight and fuel requirements is shown. Secondly, the impact of the overall weight on the thrust requirements as well as fuel consumption and propulsion design is shown.

7.9.1 Impact of Number of Fans

As has been previously shown, boundary layer ingestion helps in lowering the overall TSFC and hence total fuel consumption. There exists an optimal boundary layer ingestion capture sheet height whereby the TSFC is at a minimal. An important assumption during those studies was the maximization of the available array width to fit in as many propulsors as possible as this was assumed to be the most beneficial layout. The impact of the number of fans on the overall mass or weight of the aircraft for a fixed inlet capture sheet height is assessed here.

The following conditions in Table 15 were assumed in the simulations.

Table 15: Assumptions for impact of number of fans case study in weight module

Property	Value
ADP Altitude [m]	9144
ADP Mach	0.84
ADP Thrust requirement [N]	Varies
H_CS [m]	0.6
$\Delta P_{T,intake}$	-1.0%
NF	10 -16
FPR	Varies
$\Delta \eta_f$	Discretised Miller
$\Delta P_{T,nozzle}$	-1%
Thrust Split	95%
Core engine configuration	Turboshaft
Blowing Coefficient	0

Figure 69 shows the variation of the fan propulsor array mass, electrical system mass and the combined mass of the two with respect to the number of fans fitted in the array. The electrical system weight is inexplicably linked to the number of propulsors as the number of inverters and motors as well as their cooling systems increase with the increase in propulsor fans. While the overall array mass decreases with increasing numbers in the system, the electrical system mass increases. The combined weight of the array and electrical systems actually increases with the number of fans. This would thus mean an overall increase in the weight of the aircraft and the required intrinsic net thrust for trim at the ADP. The result is an increase in the overall fuel weight as seen in Figure 70. It should also be noted that the increase in fuel consumption is minimal.

While this implies that reducing the number of fans in a selected capture sheet height is the most beneficial in terms of reducing the fuel consumption, it must be noted that the inlet pressure losses is kept constant in this simulation regardless of the number of fans. A reduction in the number of fans in the same inlet width would result in a larger fan diameter which would have to be embedded in the

aircraft. This would mean a greater 'distorted' S-duct inlet which would inexplicably lead to more inlet pressure losses. If an additional 0.5% intake pressure loss is applied for the low fan number selection, the total fuel consumption would be significantly larger than a 1% intake pressure loss with higher number of fans. As have been previously mentioned, design of the S-duct would play an important role in reducing the inlet pressure losses and a low fan number, large fan diameter S-duct requirement would make the design all the more difficult.

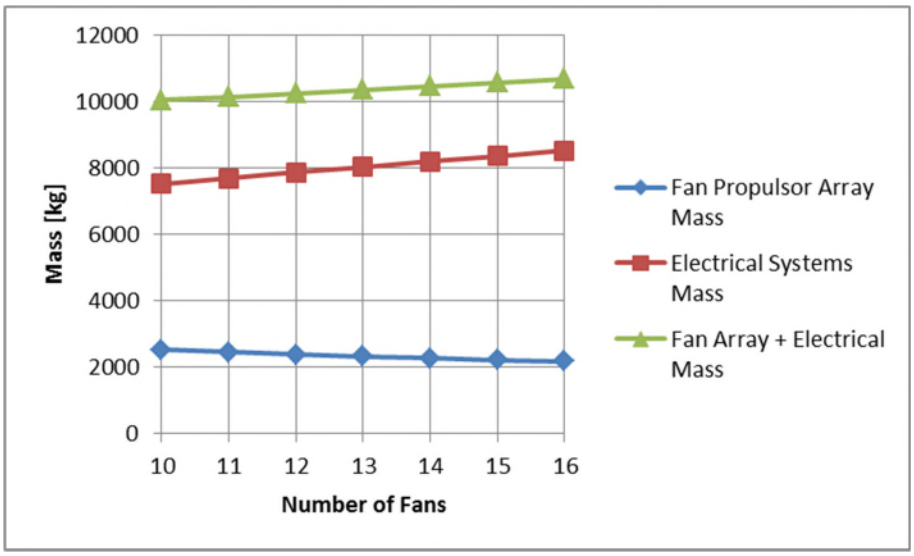

Figure 69: Variation of fan mass, electrical system mass and combined mass with number of fans

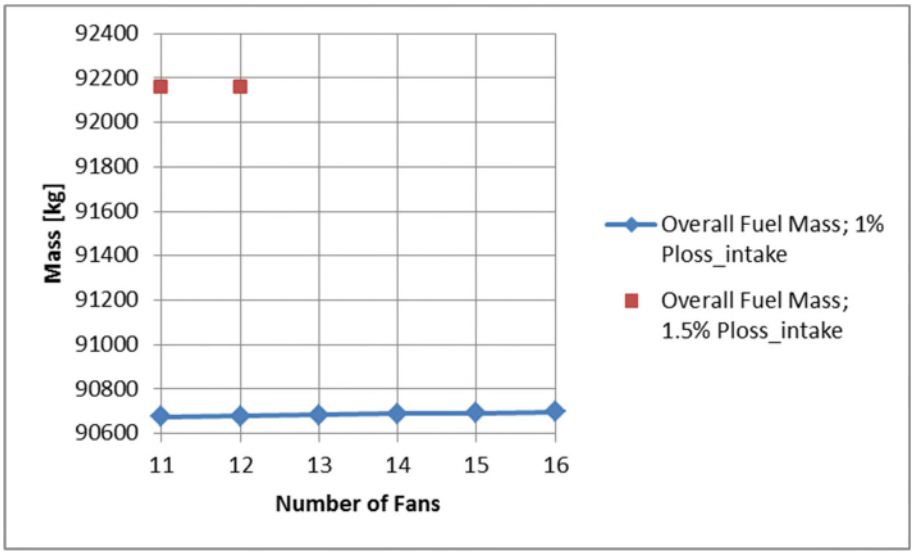

Figure 70: Comparison of overall fuel mass against the number of fans for different intake pressure loss assumption

7.9.2 Impact of Overall Weight on Design

The relation of the overall weight on the design is of interest as while it would seem straightforward that an increase in the overall weight of the aircraft would thus imply a greater intrinsic net thrust requirement at the ADP and hence, greater fuel consumption, it might also lead to increased flap blowing coefficient in the design iteration as the fan propulsors produce more thrust in a non-thrust-split system. The increased flap blowing coefficient might lead to a reduction in drag greater or smaller than the increased in intrinsic net thrust requirements due to the increased weight. Hence, it might be beneficial to study the trends involved when there is an increased aircraft weight. In this study, the overall aircraft weight is varied parametrically while the propulsion system is designed based on the resulting thrust requirements and blowing coefficient. The assumptions are shown in Table 16.

Table 16: Assumptions for overall weight impact case study in weight module

Property	Value
ADP Altitude [m]	9144
ADP Mach	0.84
ADP Thrust requirement [N]	Varies with respect to weight
Aircraft Mass	95%, 100%, 105%
H_CS [m]	0.6 – 1.2
$\Delta P_{T,intake}$	-1.0%
NF	Varies
FPR	Varies
$\Delta \eta_f$	Discretised Miller
$\Delta P_{T,nozzle}$	-1%
Thrust Split	95%
Core engine configuration	Turboshaft
Blowing Coefficient	Varies

Figure 71 shows the overall fuel mass for an assumed 100% original design weight, 105% original design weight and 95% original design weight condition. Although a higher overall weight results in a higher blowing coefficient, the reduction in the drag and hence fuel consumption is not significant enough to impact upon the trends involved. It can thus be interpreted that reducing the overall mass of the aircraft remains a priority over increasing the blowing coefficient in terms of benefits to overall fuel consumption.

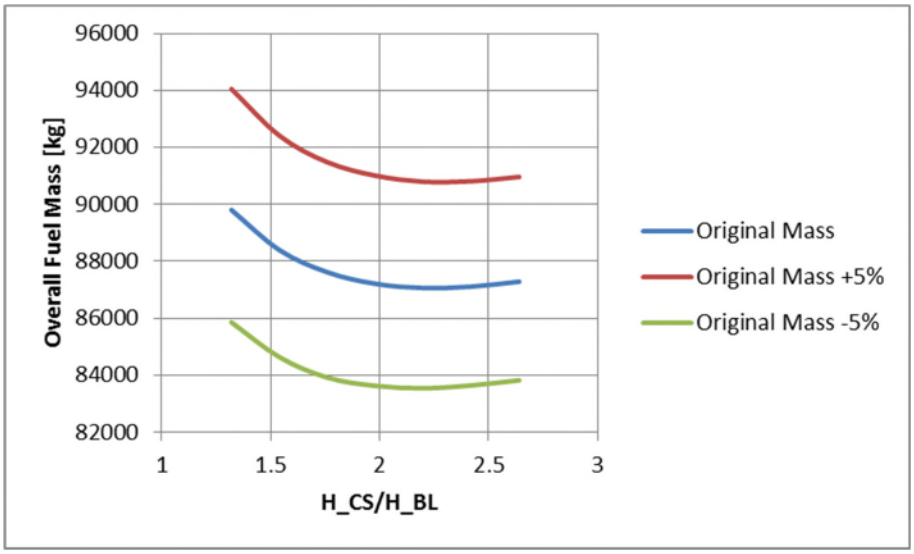

Figure 71: Comparison of overall fuel mass for different total aircraft mass assumed

7.10 Conclusion

Overall, in this chapter, the weight module has been developed and incorporated together with the other modules. The various assumptions and relations to predict the mass of the defined components of the BWB has been explained. Whilst decreasing the number of fans in a fixed array width and fixed capture sheet height seems to lower the overall weight of the aircraft and would seem beneficial in terms of reducing fuel consumption, the overall weight decrease is minimal. Care instead, must be taken as the intake pressure losses play a more significant role. A reduction in number of fans would mean a bigger fan diameter and more distortion associated in the intake. This would lead to significant increase in the overall fuel consumption. Hence, overall, it would probably be more beneficial in maximizing the number of fans in a defined array width.

Also, it has also been shown that the corresponding increase in blowing coefficient from the fan propulsor when overall weight is increased has little benefits in terms of reducing the overall drag and fuel consumption. Hence, priority should remain in reducing the overall weight of the aircraft despite a lower blowing coefficient produced by the fan propulsors.

Chapter 8

INTEGRATION & SYNERGY OF ALL MODELS

8.1 Introduction

The previous chapters have introduced each and every aspect whereby blowing would have an impact on. These include aerodynamics, flight dynamics, propulsion system design, boundary layer ingestion as well as weight. The main contribution of the work done is to showcase a methodology to synergize all these aspects whereby blowing coefficient can be utilized as a reference to determine the impact on the overall performance of the aircraft as well as the impact on aerodynamic or propulsion design. The overall methodology to incorporate all these components is shown in Figure 72.

It can be seen that the blowing coefficient impacts upon the aerodynamic properties of the aircraft as well as the propulsion system design. These two aspects are integrated together in the flight dynamics module to determine the intrinsic net thrust required at the ADP. Meanwhile, the boundary layer ingestion module takes into account the impact on fan propulsor performance due to the distorted boundary layer profile inlet flow. The weight is estimated based upon the design parameters from the various modules and this is in turned used as an input for determination of the intrinsic net thrust in the flight dynamics module. Overall iterations are carried out to ensure convergence of the weight as well as the blowing coefficient which are guessed estimates initially.

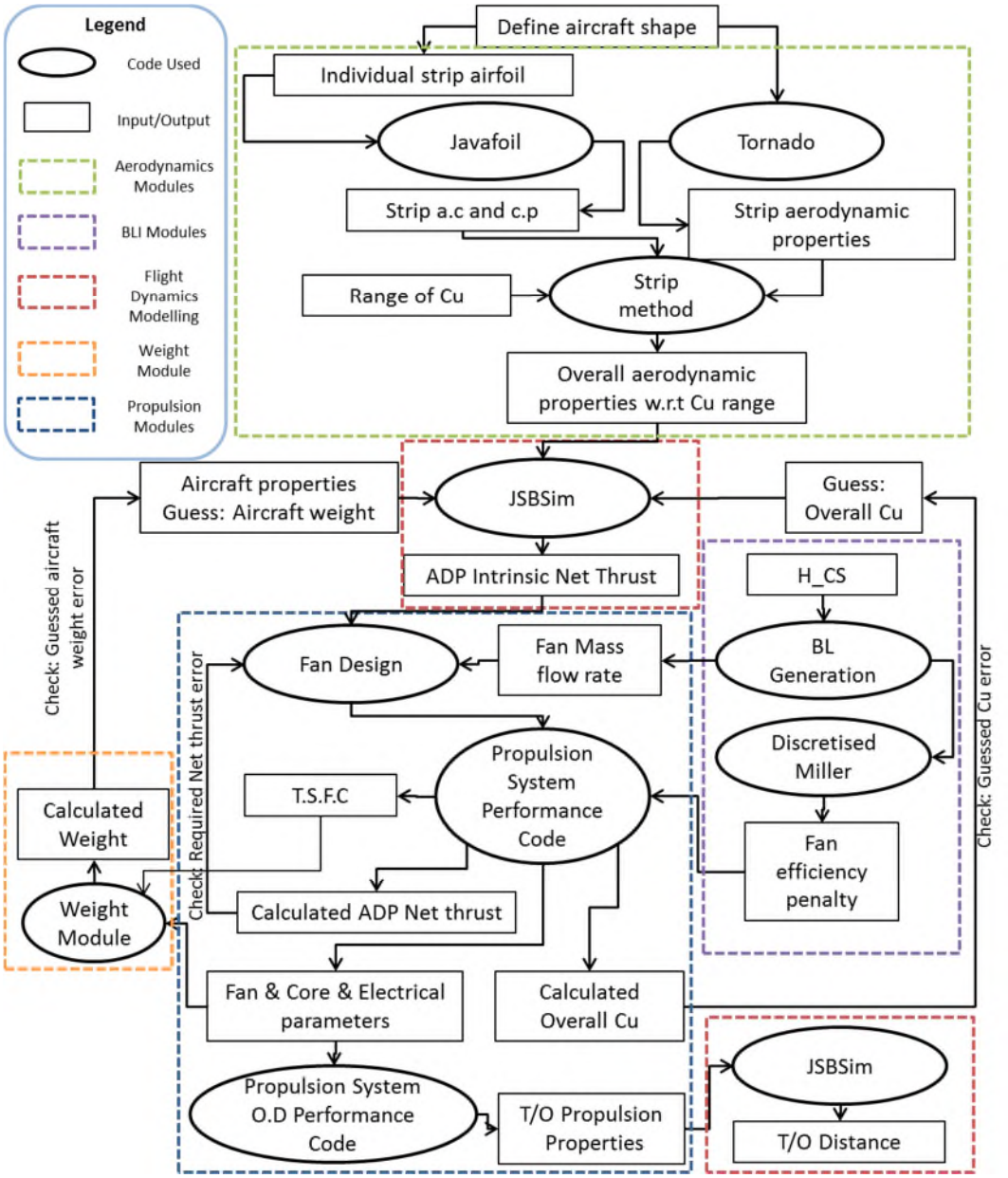

Figure 72: Overall methodology flowchart

The overall methodology is applied onto the N3-X aircraft and some of the previous studies done individually in each module are revisited to observe the overall trends when the complete methodology is applied. Thrust split is then applied with a turbofan core engine propulsion system to observe the impact of thrust split on the designs.

8.2 Turboshaft Case Study on N3-X

The application of the developed methodology is applied on the N3-X aircraft for more detailed studies. The impact on the various design criteria due to boundary layer ingestion, flap blowing, secondary weight impact and the overall impact from the various modules on the N3-X are assessed.

8.2.1 Impact of Boundary Layer Ingestion

While previous chapters isolated and analysed the impact of intake pressure losses and fan efficiency penalty individually, this section will analyse the overall impact of boundary layer ingestion while taking into consideration secondary weight change and hence ADP trim intrinsic net thrust requirements effects as well. Table 17 shows the assumptions for the simulations.

Table 17: Assumptions for BLI impact case study in overall integration and synergy

Property	Value
ADP Altitude [m]	9144
ADP Mach	0.84
ADP Thrust requirement [N]	Varies with respect to weight
Aircraft Mass	Varies
H_CS [m]	0.6 – 1.2
$\Delta P_{T,intake}$	-0.2%, -0.5%, -1.0%, -2%
NF	Varies
FPR	Varies
$\Delta \eta_f$	Discretised Miller
$\Delta P_{T,nozzle}$	-1%
Thrust Split	95%
Core engine configuration	Turboshaft
Blowing Coefficient	0.0

Figure 73 and Figure 74 shows the total fan array power requirements and total overall fuel consumption respectively and Figure 75 shows the TSFC with changing capture sheet height at various intake pressure loss settings. The

trends observed largely follows that as previously described and explained. Both intake pressure losses and fan efficiency penalty combine to lower the benefits of fuel consumption reduction derived from boundary layer ingestion.

Once again, it must be emphasized that the main contributing factor for negating the benefits of BLI is the intake pressure losses. A 2% intake pressure loss totally negates the benefits of boundary layer ingestion in terms of power and fuel consumption. The presence of an optimal intake height is once again observed and differs depending on the intake pressure loss. As explained previously, this is attributed to two opposing effects. BLI reduces the energy required to be imparted to the flow while the presence of pressure losses increases the energy requirements. As the capture sheet height increases, there are more energy losses in the intake with a higher mass flow rate for a fixed intake pressure loss percentage. There would be a point whereby the energy losses would negate the positive impact of inlet drag momentum reduction and further increasing the capture sheet height would no longer result in a lower array power requirement. The corresponding trend is similarly observed in the total fuel consumption.

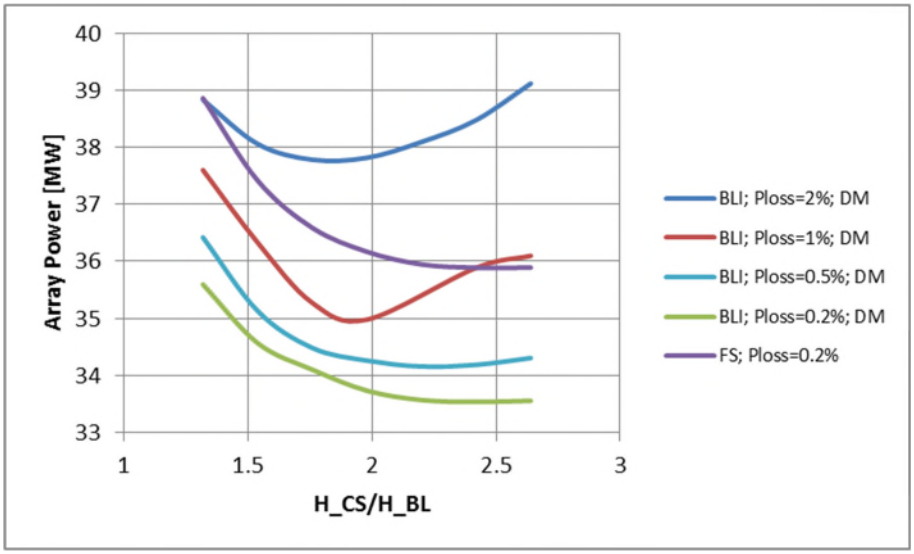

Figure 73: Array required power variation with capture sheet height for various intake pressure loss BLI and freestream conditions

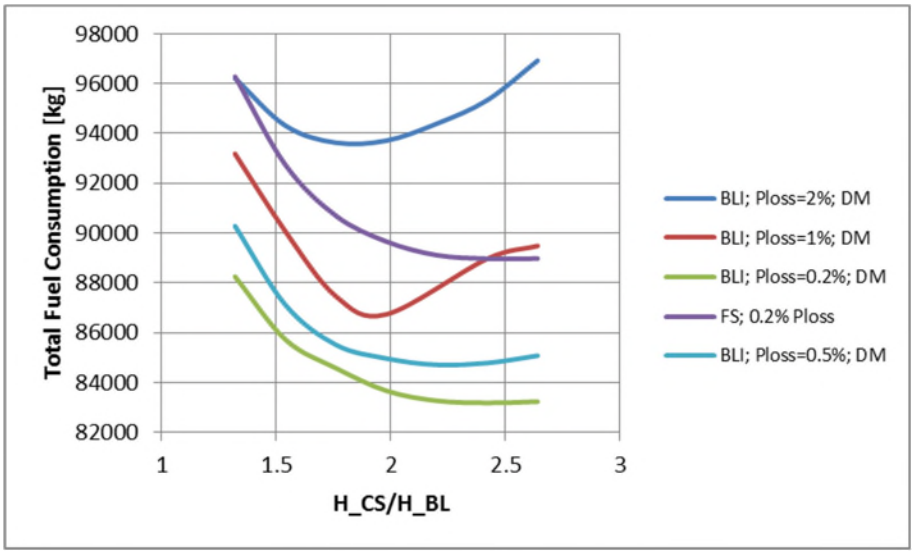

Figure 74: Total fuel consumption variation with capture sheet height for various intake pressure loss BLI and freestream conditions

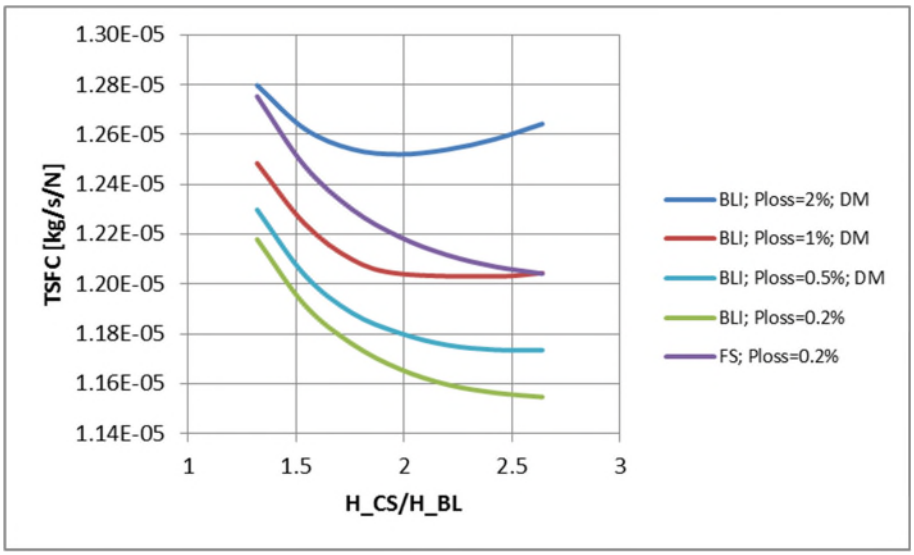

Figure 75: TSFC variation with capture sheet height for various intake pressure loss BLI and freestream conditions

As the total weight for each configuration studied changes, the trim intrinsic net thrust requirements differ as well. An increase in the overall weight would indicate an increase in the trim intrinsic net thrust requirements and hence, higher power requirements. Figure 76 shows the weight breakdown of the optimal lowest power requirement configuration of each intake pressure loss assumption.

Boundary layer ingestion lowers the converged total weight of the aircraft but as the intake pressure losses are increased, the converged overall weight of the aircraft increases as well as more power is required, resulting in bigger and heavier components. This inexplicably leads to more trim intrinsic net thrust required and increased fuel consumption. The weight changes thus act as a secondary impact in the designs of such BLI aircrafts.

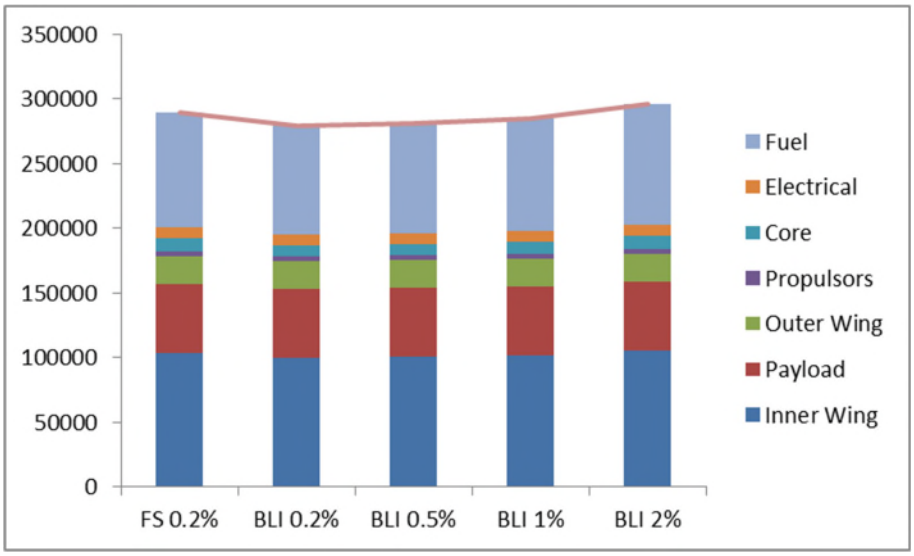

Figure 76: Total and component weight breakdown for various intake pressure loss BLI and FS conditions

8.2.2 Impact of Blown Flaps

In terms of blown flaps, the impact on the overall design and trends are a result of a change in the ADP trim intrinsic net thrust requirements as well as secondary weight change impact. With an assumed constant aircraft weight and hence a constant lift requirement for trim, utilizing flap blowing would allow the aircraft to trim at a lower AoA with a lower flap deflection as the pitching moment coefficient of the aircraft is increased with flap blowing. This results in a reduction in the overall drag of the aircraft and hence, a lower trim intrinsic net thrust requirement. Table 18 shows the assumptions made in the simulations for the blown flap without any consideration for the secondary weight changes. The flap blown aircraft is assumed to be ingesting freestream air and hence no distortion and efficiency penalty is applied at the fan stage.

Table 18: Assumptions for impact of blown flaps with no secondary weight change considerations case study in overall integration and synergy

Property	Value
ADP Altitude [m]	9144
ADP Mach	0.84
ADP Thrust requirement [N]	Varies
Aircraft Mass [kg]	29000
H_CS [m]	0.6 – 1.2
$\Delta P_{T,intake}$	-0.2%
NF	Varies
FPR	Varies
$\Delta \eta_f$	0%; freestream inlet profile
$\Delta P_{T,nozzle}$	-1%
Thrust Split	95%
Core engine configuration	Turboshaft
Blowing Coefficient	Varies

Figure 77 shows the trim intrinsic net thrust requirements and the corresponding blowing coefficient with respect to change in capture sheet height. For a non-flap blowing aircraft, the trim intrinsic net thrust requirements remain constant as the overall weight of the aircraft is assumed constant. The flaps deflection required to trim the aircraft remains constant throughout the inlet capture sheet height. However, in the case of flap blown aircraft, the change in capture sheet height would result in changes in the design of the fan propulsor, resulting in a change in the flap blowing coefficient. This would result in a change in the flap deflection angles required to trim the aircraft and thereby affecting the trim drag and intrinsic net thrust requirement of the aircraft. As the capture sheet height increases, the blowing coefficient increases as well. This is attributed to the increased mass flow rate through the nozzle. While the nozzle jet velocity decreases with increasing fan size, the increase is mass flow rate is more significant, resulting in an increase in the blowing coefficient.

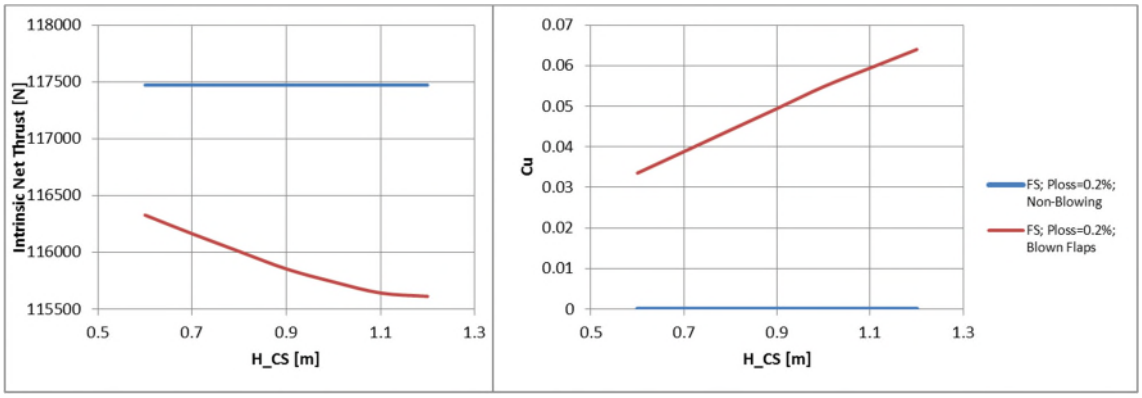

Figure 77: Comparison of trim intrinsic net thrust requirements and corresponding blowing coefficient at various capture sheet height between blown and non-blown flap configurations

Figure 78 shows the fan array power requirements. The total array power requirements decreases with increasing capture sheet height and blowing coefficient. There appears to be a minimal at a comparatively high capture sheet height. This minimal occurs as increasing blowing coefficient would reduce the trim flap deflection and as it approaches zero trim flap deflection, this would result in the minimal trim intrinsic net thrust requirement. Any further increase in the blowing coefficient would result in the flap being deflected in the opposite direction and further increasing the blowing coefficient would result in a bigger flap deflection in that direction, resulting in increasing trim drag and intrinsic net thrust requirements. This would then translate to a higher array power requirement and fuel consumption.

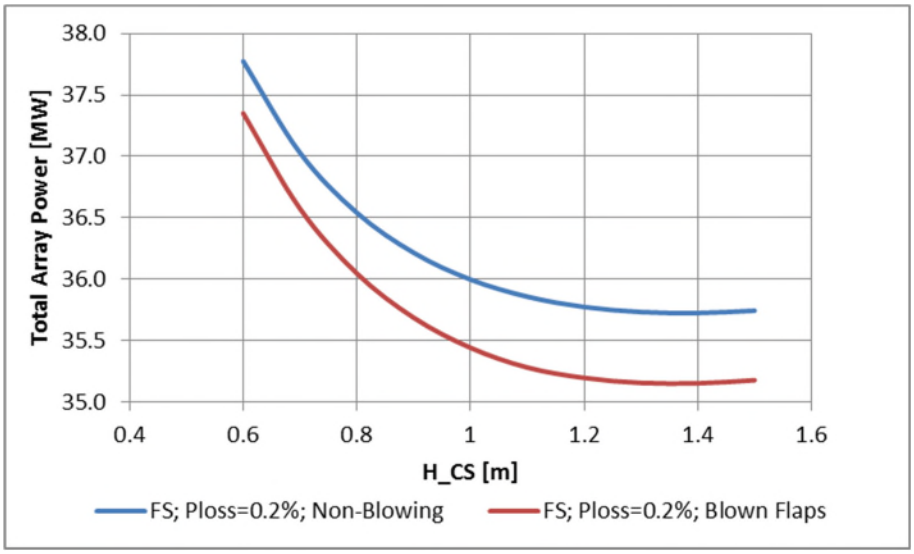

Figure 78: Comparison of total array power requirements for blown and non-blown flap configurations

Figure 79 and Figure 80 shows the total fuel consumption and the corresponding percentage change in fuel consumption respectively of the flap blown system when compared to the non-flap blown system at the corresponding capture sheet height. The fuel consumption is reduced by approximately 1.1% at low capture sheet heights up to a maximum of about 1.6% at higher capture sheet heights. Further increasing the capture sheet height beyond that would not be beneficial in terms of reducing fuel consumption due to the increase in the flap deflection angle in the opposite direction.

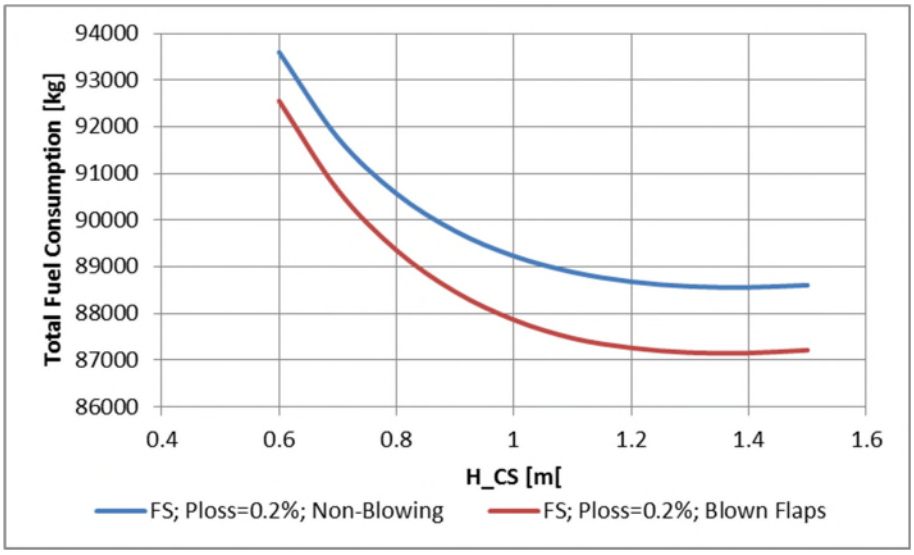

Figure 79: Comparison of total fuel consumption between blown and non-blown flap configurations

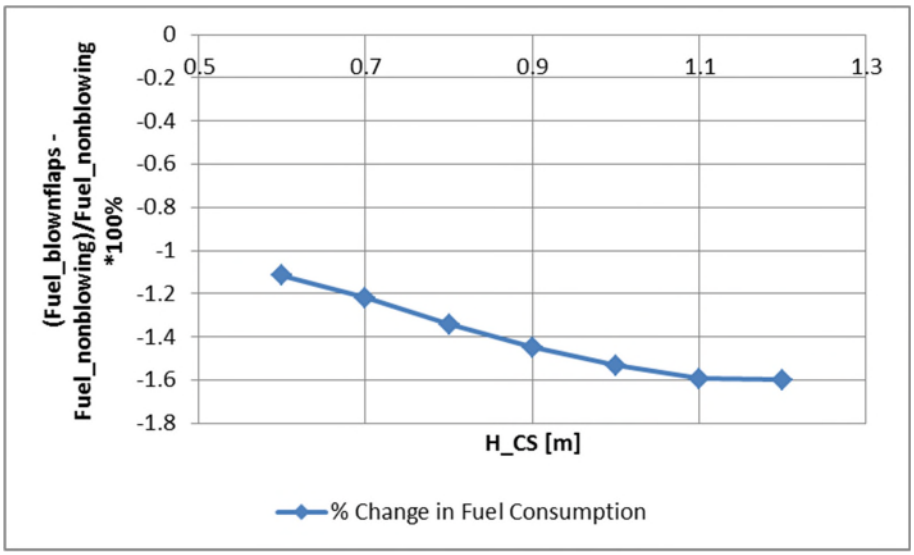

Figure 80: % change in total fuel consumption with varying capture sheet height for a blown flap configuration

The inclusion of secondary weight change with flap blowing is then further investigated. The assumptions made in the simulations are shown in Table 19.

Table 19: Assumptions for impact of blown flaps with secondary weight change considerations case study in overall integration and synergy

Property	Value
ADP Altitude [m]	9144
ADP Mach	0.84
ADP Thrust requirement [N]	Varies
Aircraft Mass [kg]	Varies
H_CS [m]	0.6 – 1.2
$\Delta P_{T,intake}$	-0.2%
NF	Varies
FPR	Varies
$\Delta \eta_f$	0%; freestream inlet profile
$\Delta P_{T,nozzle}$	-1%
Thrust Split	95%
Core engine configuration	Turboshaft
Blowing Coefficient	Varies

Figure 81 shows the thrust specific power across the capture sheet height range. The thrust specific power for a flap blown system is lower than that of the non-flap blown system, thereby reaffirming the advantage of reducing array power requirements using such a system. Figure 82 shows the trim intrinsic net thrust changes throughout the capture sheet height range. Once again, there is a minimal trim intrinsic net thrust in the capture sheet height range attributed to the change in direction of the flap deflection. The secondary weight change makes this trend more obvious as a reduction in trim thrust requirements is coupled with smaller sized components and an overall lower mass which then reduces the trim thrust requirements further. The opposite occurs when trim thrust requirements are increased.

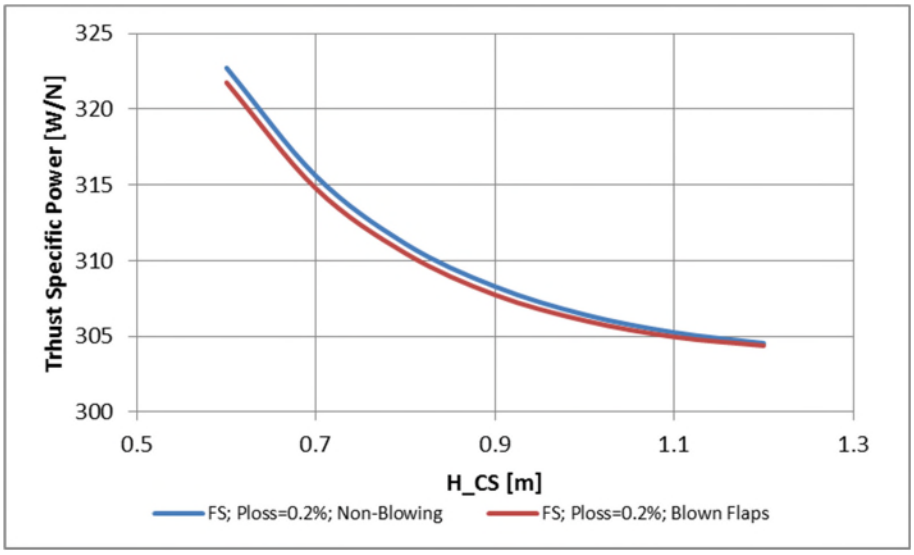

Figure 81: Comparison of thrust specific power for a blown and non-blown flap configuration with secondary weight change

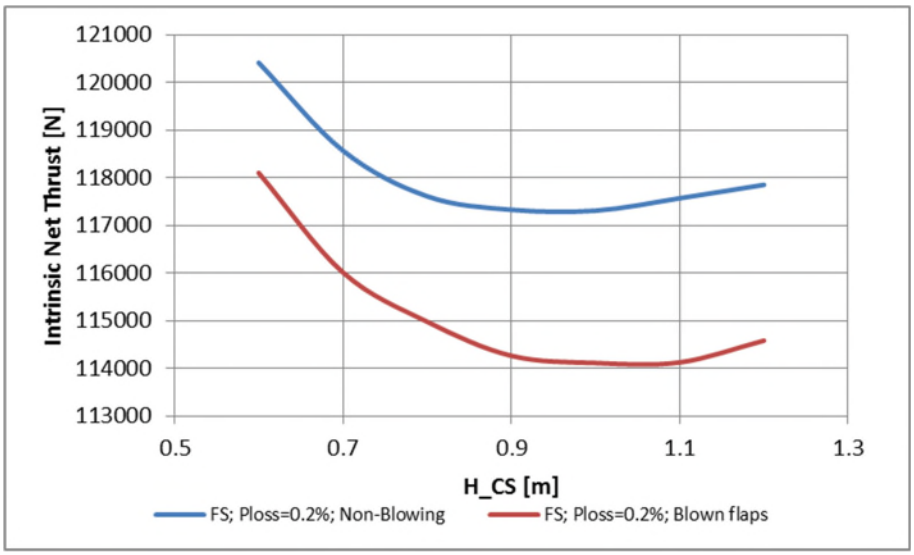

Figure 82: Comparison of trim intrinsic net thrust for a blown and non-blown flap configuration with secondary weight change

The total fuel consumption and the percentage change in fuel consumption of the flap blown system when compared to the non-flap blown system at the corresponding capture sheet height is shown in Figure 83 and Figure 84 respectively. The fuel consumption of the flap blown system is reduced by between 2.1% to 3%. Thus, depending on the capture sheet height selected in the overall design, flap blowing would provide benefits in terms of reducing the

fuel consumption. It should also be worth reminding that, in the formulation of the strip method code, the original aircraft drag polar was used to estimate the drag of the aircraft even with flap blowing. This is probably an over-estimate in the drag calculation of flap blown systems as explained previously, and hence, there is a probability of a higher potential in reducing the fuel consumption through flap blowing as that estimated in the works carried out here.

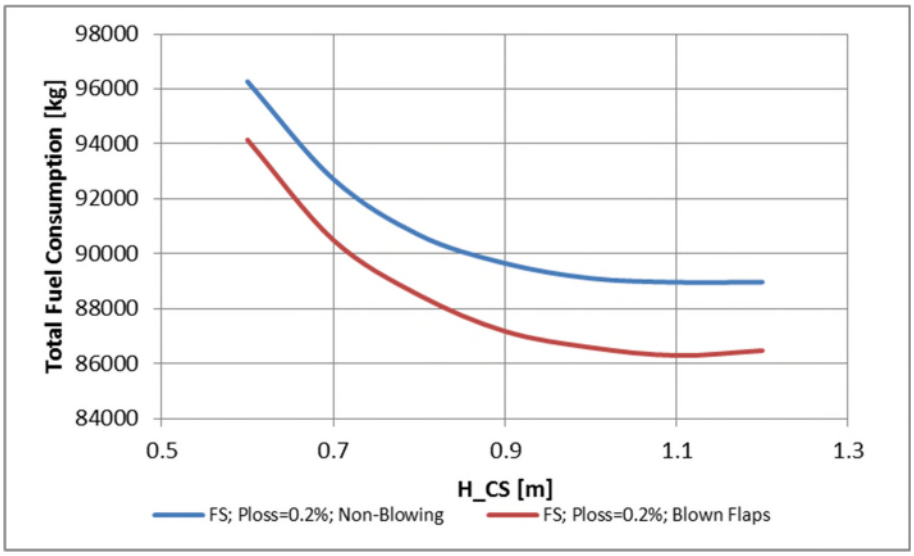

Figure 83: Comparison of total fuel consumption for a blown and non-blown flap configuration with secondary weight change

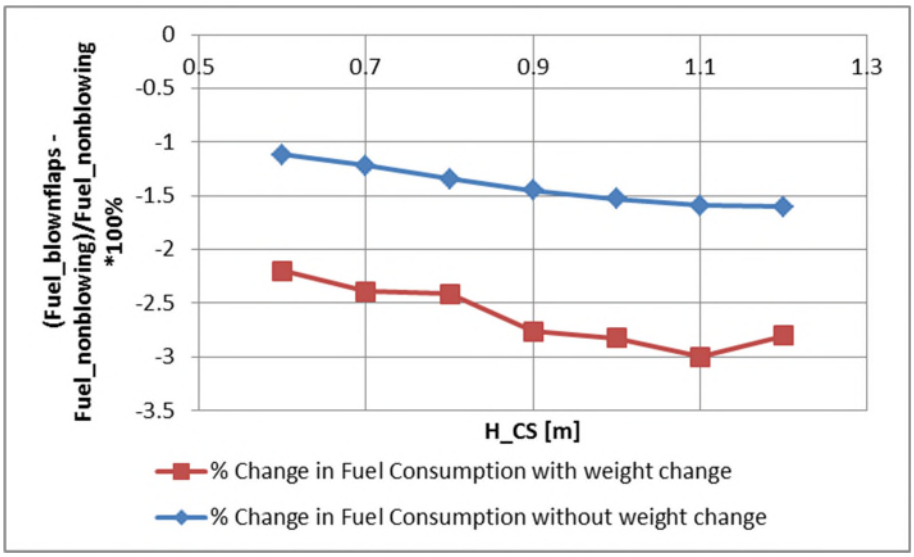

Figure 84: Comparison of % change in total fuel consumption between blown flap systems with and without secondary weight change considerations

8.2.3 Combined Impact

The benefits in terms of fuel consumption due to boundary layer ingestion as well as flap blowing have been individually assessed. The combined impact of both is now integrated together and assessed on the N3-X aircraft. The assumption used for these simulations are shown in Table 20.

Table 20: Assumptions for combined impact case study in overall integration and synergy

Property	Value
ADP Altitude [m]	9144
ADP Mach	0.84
ADP Thrust requirement [N]	Varies
Aircraft Mass [kg]	Varies
H_CS [m]	0.6 – 1.2
$\Delta P_{T,intake}$	-0.2%, -0.5%, -1%, -2%
NF	Varies
FPR	Varies
$\Delta \eta_f$	Discretised Miller
$\Delta P_{T,nozzle}$	-1%
Thrust Split	95%
Core engine configuration	Turboshaft
Blowing Coefficient	Varies

Figure 85 shows the total array power requirements for the various intake pressure losses across the capture sheet range. While flap blowing reduces the overall array power requirements, the reduction of intake pressure losses still take utmost priority. A 2% intake pressure loss would once again totally negate the benefits derived from boundary layer ingestion and flap blowing.

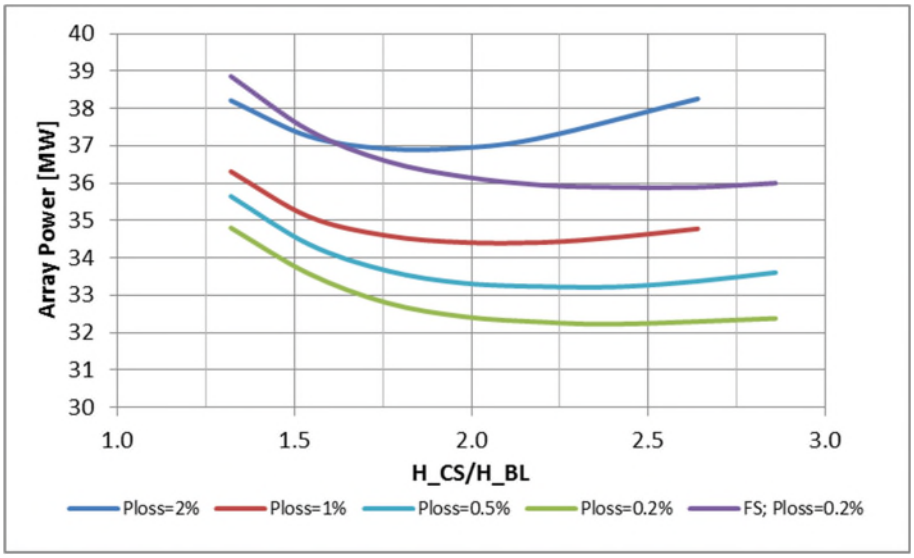

Figure 85: Total array required power variation with inlet capture sheet height for various intake pressure loss BLI and FS configurations

Once again, there exists an optimal capture sheet height for each selected intake pressure loss whereby total array power is at a minimal due to the balance of mass flow pressure losses in the intake and lower inlet ram drag with increasing capture sheet height. The total fuel consumption is used as the figure of merit to assess the benefits and Figure 86 shows the percentage change in the overall fuel consumption for various intake pressure losses when compared to the optimal lowest possible fuel consumption capture sheet height for the case of a freestream ingestion. Overall, a boundary layer ingesting, flap-blown N3-X aircraft can possibly derive 10% fuel savings if the intake pressure losses remain the same as that of a freestream ingesting intake. A 0.5% intake pressure loss as estimated possible by NASA reports [67] would result in a lower fuel savings of around 8%. A 2% intake pressure loss would negate all benefits of flap blowing and BLI and would instead see an increase in the total fuel consumption for such a system.

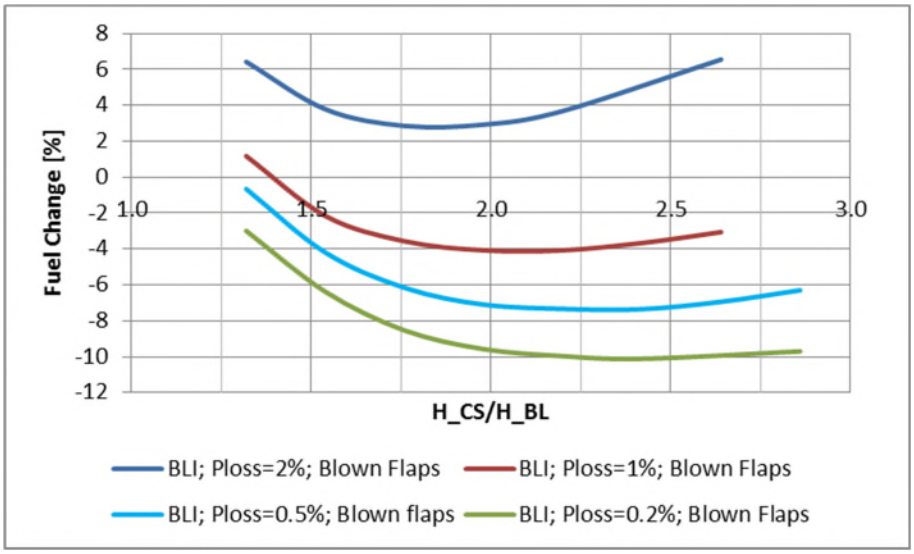

Figure 86: % change in total fuel consumption in comparison to lowest fuel FS configuration for different intake pressure loss BLI configurations

As the weight and trim thrust requirements of the aircraft at ADP changes due to the presence of flap blowing in such a highly synergized aircraft, the total fuel consumption was chosen as a figure or merit instead of the TSFC. Nevertheless, it is interesting to look at the TSFC comparison. Figure 87 shows the TSFC percentage change when compared to the corresponding FPR freestream ingesting system for a range of FPR. NASA estimated a 15-18% reduction improvement [24] in TSFC across a FPR of 1.15-1.5 on the N3-X aircraft with 0.2% intake pressure loss whereas the models used here predicted a significantly lesser improvement of between 4-5%.

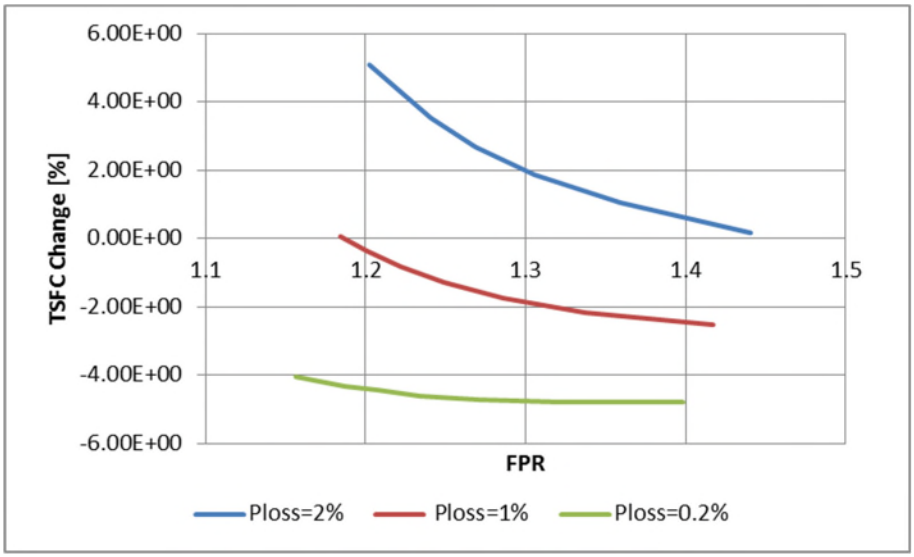

Figure 87: % change in TSFC as compared to FS configuration for various intake pressure loss BLI configurations

This can be attributed to a few factors. The first is the differences in the boundary layer profile used. Any change in the boundary layer profile has a significant impact on the study as the change in inlet ram drag is significant across the whole mailbox inlet. This thus also signify the importance of understanding the synergy of the various aspects of such a highly integrated aircraft as the aerodynamic design of the aircraft would play an important role in determining how much benefit can be derived from the BLI system. Similarly, the placement of the intake and the boundary layer profile ingested would also highly impact upon the benefits of a BLI system. As a comparison, the intake location is now shifted 10% further aft of the aircraft and hence ingesting a more developed boundary layer profile. Figure 88 shows the total fuel consumption when comparing a 0.5% intake pressure loss system. The total fuel consumption is further reduced when the intake is shifted back. An important trend in this is thus to recognize that the intake should be placed as further back as possible and the length reduced if the intake pressure losses can be maintained at the same level, thereby maximizing the benefits of BLI.

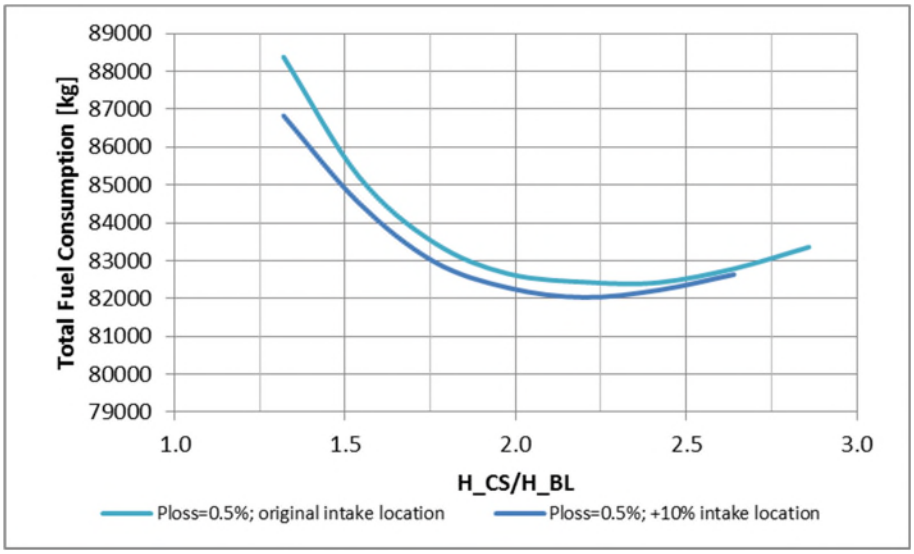

Figure 88: Comparison of total fuel consumption for different intake locations

Second, the differences can also be attributed to the level of fidelity in modelling the fan efficiency when ingesting a distorted profile. It has previously been discussed that NASA used a constant 1% deficiency in the fan efficiency as a result of the flow distortion due to BLI. The adapted Discretised Miller predicted a higher fan efficiency loss as the FPR increases, thereby reducing the overall benefits of BLI.

8.3 Thrust Split Turbofan Case Study on N3-X

The same overall study and synergy was applied onto a thrust split system whereby the core engines are turbofans and provide a portion of the thrust in the propulsion system. Since less net thrust is required from the fan propulsor array, the power requirements from the array and the power generated by the core engines would reduce as the TSR increases. This is shown in Figure 89 for a cBPR=4 thrust split system.

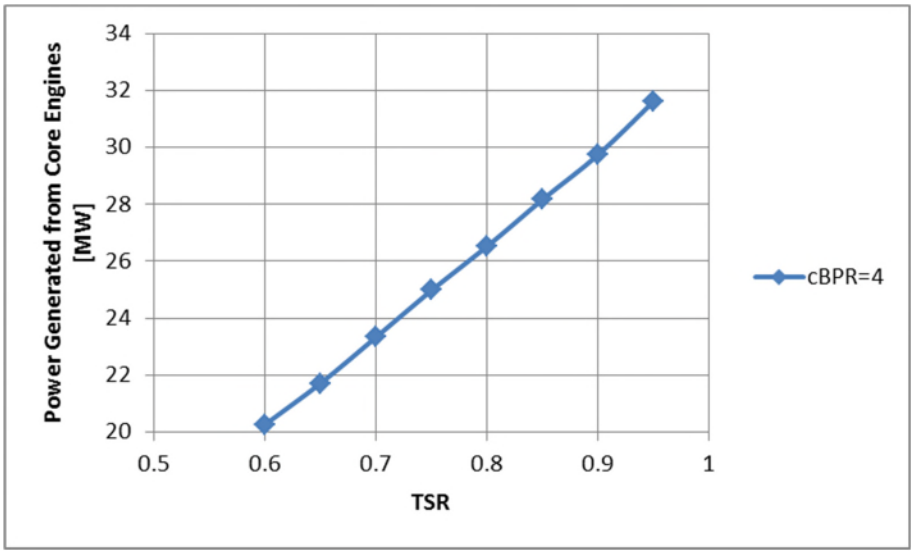

Figure 89: Variation of power generated by the cBPR=4 core turbogenerators with different TSR

For a thrust split system, there are more additional variables to consider. The first is the core turbofan bypass ratio (cBPR). For a conventional turbofan, an increment in bypass ratio reduces the specific thrust and increases the fuel savings due to the improvement in propulsive efficiency. The second variable to consider is the core fan pressure ratio (cFPR).

To optimize the system to obtain the lowest fuel consumption, basic turbofan design concepts [60] [79] are employed. This involves varying the core fan pressure ratio for a selected thrust requirement, TSR and core bypass ratio. In the overall methodology, these changes impact upon the weight of the components and hence the overall required intrinsic net thrust, thereby creating an iteration loop for convergence of the design. Figure 90 shows the TSFC for varying cFPR at various TSR and a selected cBPR=4. As can be seen and expected, there is an optimal cFPR for that specific power requirement and net thrust requirement by the core engines that results in a minimal TSFC.

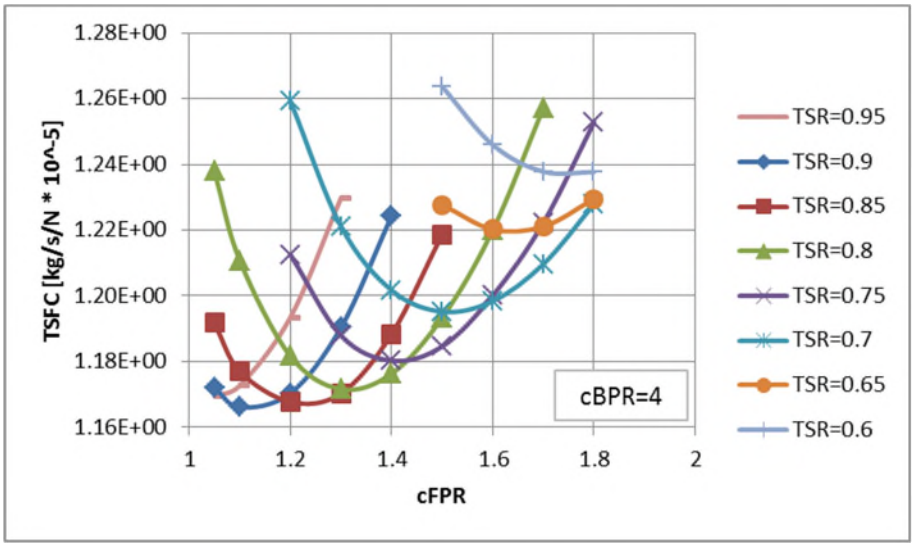

Figure 90: Variation of TSFC of cBPR=4 turbogenerators with different cFPR for different TSR

Figure 91 shows the impact of cBPR and cFPR on the TSFC of the system at 80% and 60% thrust split. These two cases were utilized to illustrate the optimization and impact of the variables on the design of the propulsion system. Three core bypass ratios were utilized with a maximum cBPR=12. Assuming a fixed constant core size that corresponds to current technology level, a higher cBPR would result in a bigger turbofan engine and higher nacelle drag. It is possible that for future technology to allow a further reduction of core size and possibly increasing the cBPR above 12 without any drag penalties. It should also be noted that it might not be geometrically feasible to have a small core in the turbofan with such a high cBPR as the size of the low pressure turbine might be much bigger than the core engine size. However, the focus of the work here is on the performance of the synergized system and would assume there are no geometrical constrains. As one would expect, there is an optimum cBPR and cFPR for the main engine and this differs at each thrust split level. As the TSR decreases, the optimal cBPR would change as the specific thrust produced by the core engine changes and the lowest TSFC configuration would be dependent on the core engine design.

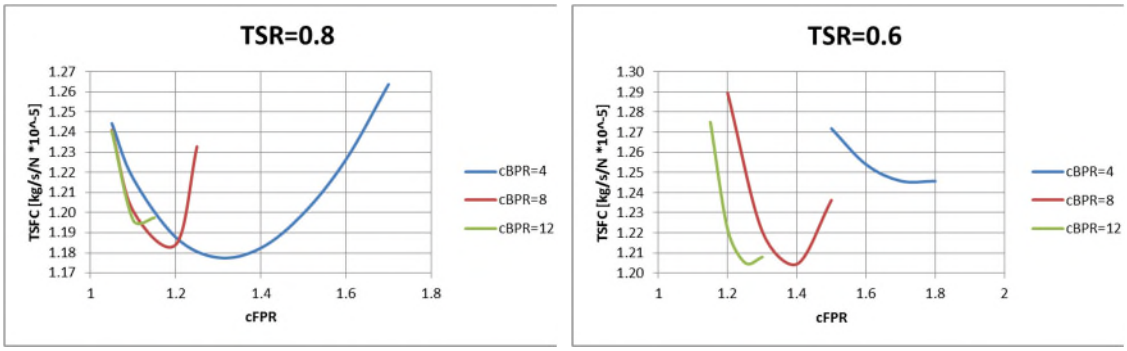

(a) TSFC at TSR=0.8 **(b) TSFC at TSR=0.6**

Figure 91: Variation of TSFC with different cFPR and cBPR

There are a few reasons to utilize a thrust split propulsion system in such a TeDP system. Firstly, it would minimize the detrimental effects of intake pressure losses as lower mass flow is required for the fan propulsor array. This is especially significant when intake pressure losses are high. By reducing the mass flow through the fan array intake and utilizing the core turbofan engines to provide the balance thrust required, there would be a possible overall improvement in the TSFC. As an example, the TSFC and total fuel consumption of a thrust split system and that of a non-thrust split system is compared in Figure 92 and Figure 93 respectively. The various assumptions utilized are shown in Table 21.

Table 21: Assumptions for turbofan turbogenerator case study in overall integration and synergy

Property	Value
ADP Altitude [m]	9144
ADP Mach	0.84
ADP Thrust requirement [N]	Varies
Aircraft Mass [kg]	Varies
H_CS [m]	Optimal Configuration
$\Delta P_{T,intake}$	-1.0%,
NF	Optimal Configuration
FPR	Optimal Configuration
$\Delta \eta_f$	Discretised Miller
$\Delta P_{T,nozzle}$	-1%
Thrust Split	50% - 100%
Core engine configuration	Turboshaft & Turbofan
Blowing Coefficient	Varies

Only the optimal cFPR configuration which corresponds to either the lowest TSFC or lowest total fuel consumption is shown in the figure. For a minimal 1.0% intake pressure loss, a turbofan thrust split system would also allow for some savings in terms of fuel consumption when comparing the optimal configuration between the turbofan and turboshaft configurations. The percentage savings would be expected to amplify with increasing intake pressure losses and the optimal TSR would decrease as more of the required net thrust is produced by the core engines while minimizing mass flow through the fan array intake. Optimal cBPR and cFPR would also be expected to change when TSR decreases as described previously from Figure 91. It can also be observed that a turboshaft configuration is beneficial for the high thrust split cases (>95%) for fuel consumption. This signifies that the larger transmission losses associated with the turbofan engine becomes more significant and relevant when the net thrust requirement from the core engines is low, thus resulting in a higher total fuel consumption in the use of turbofan core engines.

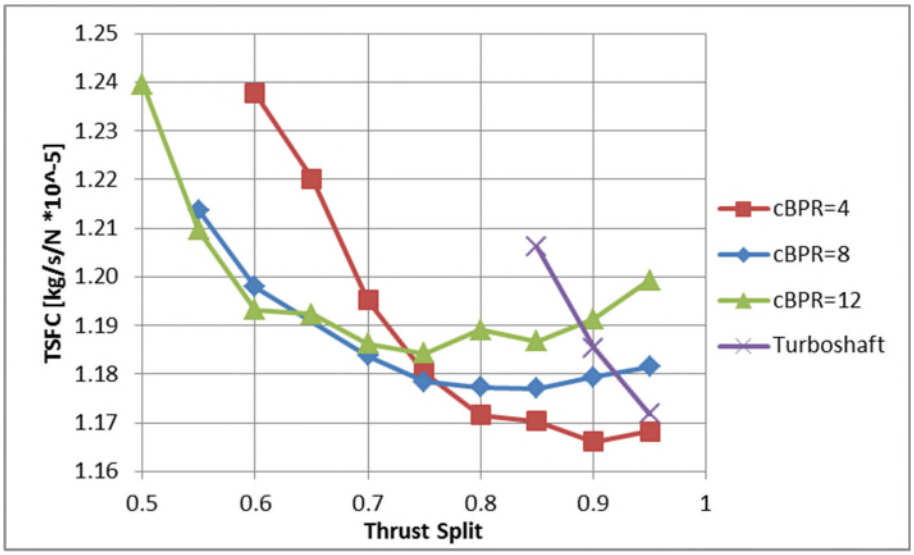

Figure 92: Comparison of TSFC between turboshaft and turbofan turbogenerators with varying TSR

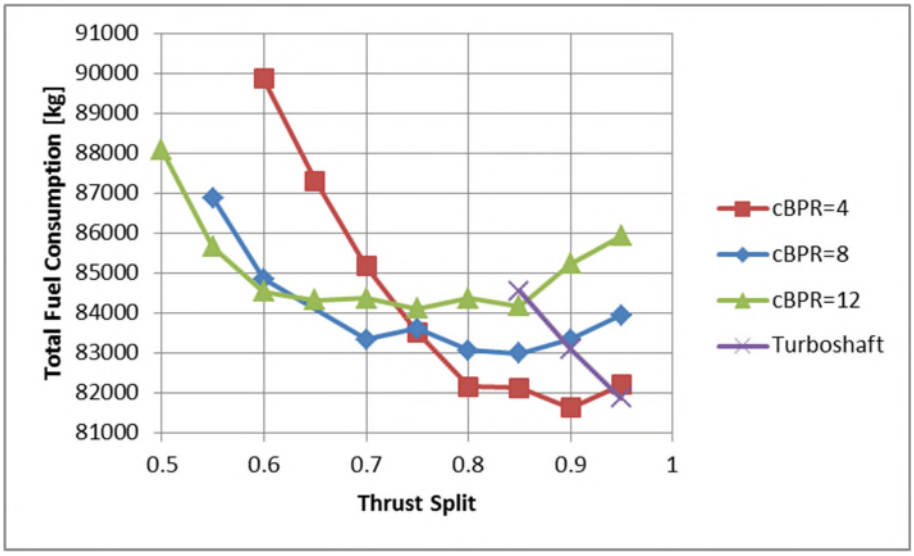

Figure 93: Comparison of total fuel consumption between turboshaft and turbofan turbogenerators with varying TSR

A second reason why a turbofan thrust split system might be beneficial is in its off design motor performance. It can be recalled that in the design of a non-thrust split system, the electrical motors and generators as well as the core engines are designed to provide enough power for the maximum power requirements condition which would be during take-off. Thus, at the design point conditions whereby the aircraft would spend the most significant amount of time, these

electrical components are oversized. This results in inefficiencies while operating as well as heavier components, thereby contributing to additional thrust requirements and fuel consumption. A thrust split system on the other hand, is sized to its ADP conditions. The amount of power available at take-off is utilized for the fan propulsors while the core engines provide additional thrust at the take-off conditions. The impact of this on the take-off performance is further discussed in later chapters. As a comparison, Table 22 shows the difference in weight of the electrical components between a turboshaft 95% - 100% TS system and that of a turbofan thrust split system ranging 0.8<TS<0.95. The electrical systems weight for that of a turbofan is significantly smaller when comparing the same thrust split level and this would have a secondary impact on the trim intrinsic net thrust requirements as well as the total fuel consumption.

Table 22: Electrical system weight of various configurations

	Turboshaft		Turbofan			
Thrust Split	1.0	0.95	0.95	0.9	0.85	0.8
Electrical Systems Weight [kg]	8825	8736	7897	7740	7779	7581

As an overall comparison between the various configurations discussed and compared, some important parameters are shown in Table 23 comparing that of the optimal configurations between a freestream system, a turboshaft system utilizing flap blowing and a thrust split turbofan system utilizing flap blowing. However, bearing in mind that a cFPR=1.1 is unlikely to be achievable, as is the case of the optimal solution for a turbofan system, the next most suitable configuration whereby the cFPR=1.3 is also included for comparison.

Table 23: Important parameters for optimal fuel consumption configurations

	Turboshaft	Turbofan		Freestream
$\Delta P_{T,intake}$	-1.0%	-1.0%	-1.0%	0.0%
BLI	Adapted D.M	Adapted D.M	Adapted D.M	-
Capture Sheet Height [m]	1.00	0.90	0.80	1.10
cBPR	-	4.00	4.00	-
cFPR	-	1.10	1.30	-
Thrust Split	0.95	0.90	0.85	0.95
Total Power Requirements [MW]	31.35	29.74	28.17	34.09
Number of Propulsors	10	11	13	9
Propulsor Diameter [m]	1.89	1.65	1.44	2.04
Propulsor FPR	1.20	1.22	1.23	1.19
Rotational Speed [rpm]	2316.63	2781.83	3309.96	1857.38
Trim Intrinsic Net Thrust [N]	111436	111655	112012	117567
Trim Blowing Coefficient	0.047	0.042	0.038	0.000
TSFC [kg/s/N *10^-5]	1.1719	1.1686	1.1780	1.2069
Fuel Mass [kg]	81872.9	81803.3	82728.3	88962.9
Total Mass [kg]	275599.1	276206.6	276926.2	290109.7

In the case whereby the intake pressure losses for a BLI system is being kept to a minimal of 1.0%, there is an approximately 9% possible fuel consumption reduction by incorporating a BLI, flap blown thrust split turbofan system. A turboshaft system achieves approximately the same amount of fuel savings. However, bearing in mind that at higher intake pressure losses for a BLI system,

the overall fuel savings would be reduced as previously discussed, a turbofan thrust split system becomes more viable as the mass flow through the fan propulsors are reduced and a higher proportion of the required net thrust is produced by the turbofans. A lower optimal thrust split level would thus be expected for higher intake pressure losses system.

8.4 Conclusion

Overall, in this chapter, the multi-fidelity and multi-disciplinary overall methodology has been applied on the N3-X aircraft and the synergy of the various aspects of such a highly integrated aircraft investigated. This included the weight and trim intrinsic net thrust, the aerodynamic impact from flap blowing, the impact on propulsion system design as well as boundary layer ingestion. Various optimization methodologies have been looked at which included that for a thrust split system utilizing core turbofan engines. The advantages of a boundary layer ingesting system as well as a flap-blown system in reducing the overall fuel consumption are clear. The emphasis remains on reducing the intake pressure losses to make a BLI system viable. The negative impact of high intake pressure losses can be mitigated by utilizing a thrust split system when high intake pressure losses cannot be avoided. A thrust split system also brings about advantages in terms of designing and sizing the electrical components to the ADP conditions instead of take-off conditions, thereby maximizing their efficiencies and reducing overall weight and thrust requirements.

Chapter 9

OFF DESIGN TAKE-OFF ANALYSIS of N3-X

9.1 Introduction

In this chapter, the off-design take-off analysis is applied onto the N3-X using the overall methodology. To apply this, an explanation on the method to model the performance of the fan and superconducting motor at off-design conditions is provided. The impact of flap blowing and thrust split on the N3-X take-off performance is detailed.

9.2 Superconducting Motor Modelling

Superconducting motors are AC synchronous motors using high temperature superconductor windings instead of conventional copper coils. These windings are able to transmit larger currents as compared to the copper coils. As such, they generate higher power magnetic fields in a constrained volume. The motor rotating speed is

$$\omega = \frac{120 \times Frequency}{number\ of\ motor\ windings} \quad \textbf{(9-1)}$$

For a traditional motor, the maximum power produced increases with increasing shaft speed to its limiting design maximum output power. Further increasing the shaft speed beyond this point would reduce the power produced by the motor. For superconducting motors, this value is assumed to remain constant beyond the limiting design shaft speed [74]. Figure 94 shows a sample torque and power working line of a superconducting motor. The output power of the motor can be calculated as

$$Power = \frac{\omega}{\omega_{max}} \times Power_{max} \; ; \; \omega < \omega_{max} \tag{9-2}$$

$$Power = Power_{max} \; ; \; \omega < \omega_{max}$$

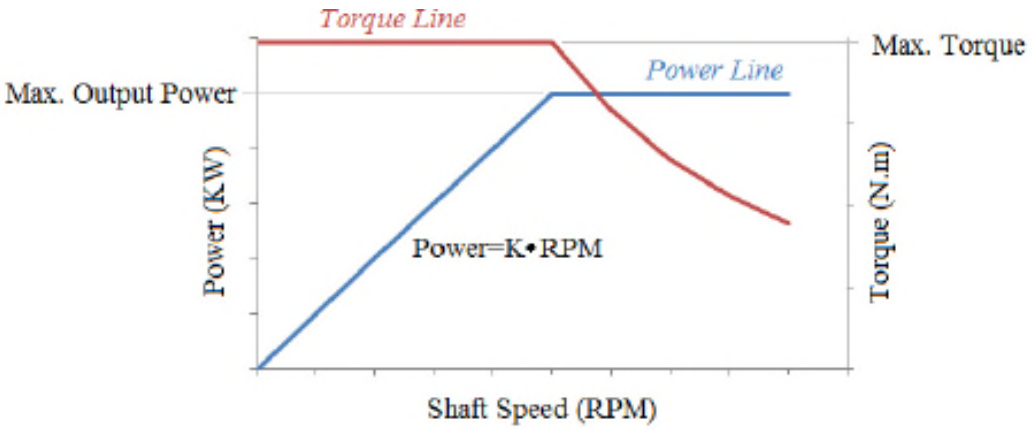

Figure 94: Superconducting motor working line

The superconducting motors are assumed to be able to working at variable frequency [74]. Therefore, the working shaft speed is thus limited only by the load torque and the fan tip speed. Increasing the shaft speeds reduces the fan loading coefficient but would lead to a higher fan tip speed and lower output torque. In a superconducting motor, the maximum torque is significantly higher than traditional motors [14] and it is thus assumed that the motor can produce sufficient torque as long as it can produce the required power.

9.3 Motor and Fan Propulsor Off Design Performance

Liu [74] introduced a method to match the performance between the fan and the motor at off-design conditions. This requires special attention as the motor performance is defined by torque and power while the fan performance is defined by its pressure ratio and shaft speed. One of the advantages of using a TeDP system is the ability to control the generator and fan motors independently to change the shaft load without changing the speed or to change the speed without changing the loading. The torque provided at take-off can be kept constant as the torque required at the ADP. As the superconducting motor is assumed to be able to provide the required torque as long as it can provide the required power,

only the power needs to be taken into consideration when matching the performance. The motor output power can be controlled by its working voltage and current.

Liu [74] introduced a term called the Non-Dimensional Power (NDP) for the fan which can be used to map a traditional fan map onto a power based fan map.

$$NDP = \frac{Power}{C_p T_S} \frac{\sqrt{\frac{T_S}{T_{S,sls}}}}{\frac{P_S}{P_{S,sls}}} = \frac{CMF}{Eff}\left(FPR^{\frac{\gamma-1}{\gamma}} - 1\right) \quad \textbf{(9-3)}$$

With the NDP for the fan performance, the NDP fan map can be plotted together with the motor performance map and the possible working zone of the fan can be determined. Figure 95 shows a sample of a NDP fan map together with the motor map. The grey zone thus represents possible working conditions of the fan propulsor. The fan propulsor can change its running line within the grey zone by changing the shaft speed while the working point along the specified running line can be controlled by changing its nozzle area and thus mass flow.

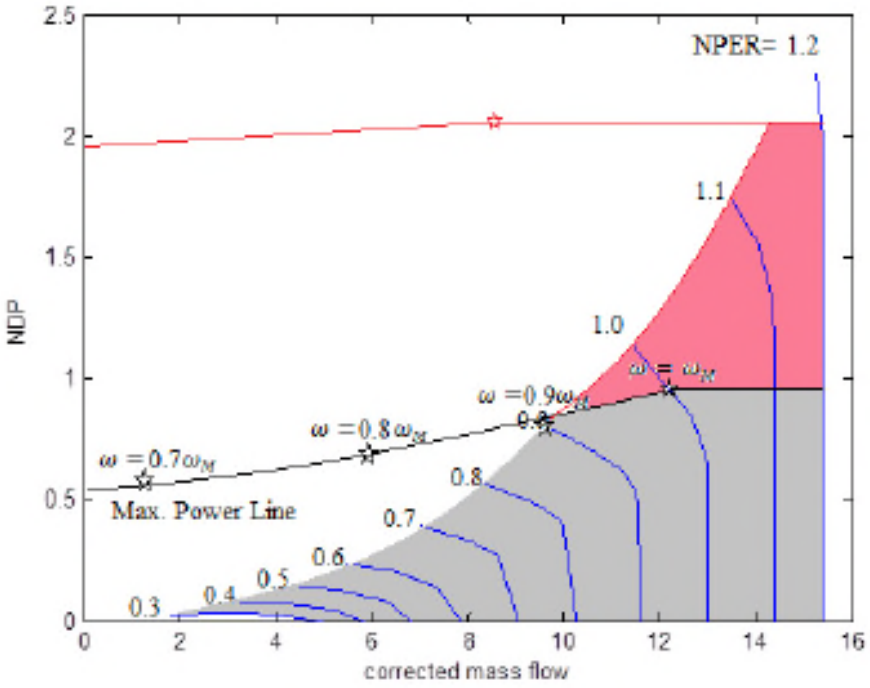

(a) NDP vs CMF

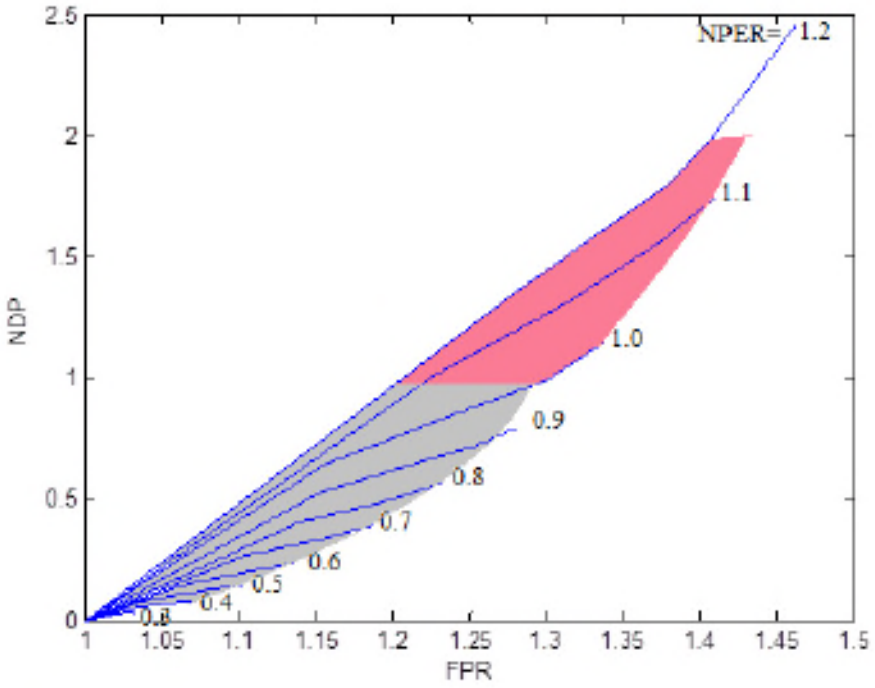

(b) NDP vs FPR

Figure 95: Sample NDP based fan performance map [74]

9.4 Overall Off Design Performance Modelling

Besides obtaining the fan and motor performance map, another factor to take into consideration for an aircraft such as the N3-X is the distorted fan profile and mass flow parameters at off-design. The adapted D.M method as described previously is used. Bearing in mind that the D.M method can be utilized to obtain fan performance parameters due to distorted flow not only on design point but also on off-design conditions, the same methodology is adapted to obtain the deficiency in fan efficiency in off-design conditions. The inlet boundary layer profile is described with the same methodology in Chapter Chapter 6 and varies with differing flight conditions. The capture sheet height is determined via mass conservation at the inlet to have the same mass flow rate as that defined by the nozzle area. The thrust calculation is similar to that as explained in Chapter Chapter 5. Figure 96 shows the overall methodology in the off-design phase.

The running line and nozzle area are iterated to obtain the maximum thrust possible within the grey zone constrains or possible working zone within the plotted map.

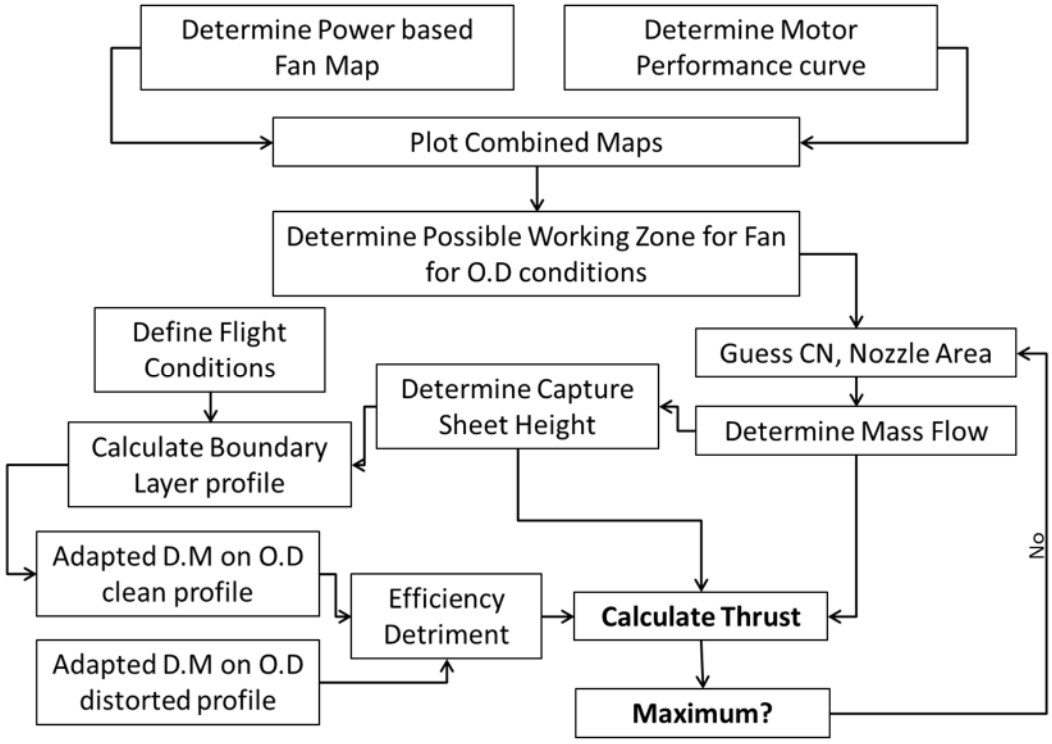

Figure 96: Off-design thrust calculation methodology

For the core engines, the off-design thrust is determined using Turbomatch.

9.5 Case Study on N3-X

The take-off performance of the N3-X is determined using the overall methodology to design the aircraft at the ADP and using the take-off modelling method previously described in tandem with the off-design propulsion modelling. A baseline study is done whereby no flap blowing is applied to the N3-X aircraft before a comparison is done on the N3-X with flap blowing. Further on, thrust split propulsion system is applied on the N3-X for it off-design take-off performance.

9.5.1 Turboshaft N3-X Case Study

The designed turboshaft N3-X system is described and summarized in Table 24 and is used for this take-off analysis. An important point to note is that the electric motors and generators are sized based on the assumption that enough power must be available for the fans to operate at the peak efficiency point for corrected speed line=1 for take-off conditions. This assumption is made as in such a design process; the thrust requirements for take-off are not yet defined.

Table 24: Assumed parameters for Turboshaft turbogenerator case study in off-design take-off analysis of N3-X

	Turboshaft
Intake Ploss	1.0%
BLI	Adapted D.M
ADP Capture Sheet Height [m]	1.00
Thrust Split	0.95
ADP Total Power Requirements [MW]	31.35
Number of Propulsors	10
Propulsor Diameter [m]	1.89
ADP Propulsor FPR	1.20
Propulsor nozzle Area [m^2]	1.64
Trim Intrinsic Net Thrust [kN]	111.44
MTOW [kN]	252.90

Table 25 shows the various important parameters obtained from the converged solution of the take-off simulations for the N3-X aircraft using the above described propulsion system for both non flap blowing and flap blown system.

Table 25: Parameters for non-flap blown and flap blown system at take-off

	Non Flap blown system	Flap blown system
Rotational Velocity [m/s]	104.9	93.1
C_u at V_{ROT}	0.0	0.503
Ground run + Rotational distance [m]	5833	4265
Transition distance [m]	371	329
Total take-off distance [m]	6204	4594
Total SLS Thrust [kN]	563.75	563.75

As a reference, the blowing coefficient at the rotational velocity is tabulated. The blowing coefficient changes as the flight conditions changes and is a constantly changing variable in the simulation. The blowing coefficient at the rotational velocity gives an idea of the impact of flap blowing on the overall take-off distance. For the flap-blown system, the blowing coefficient as a result of the operation of the fan propulsors is 0.503. This is significantly higher than that at the ADP trim point and provides significant additional control power to the aircraft. This is reflected in the reduction of the ground run and rotational distance. To recall, it has been previously mentioned that the rotational velocity is iterated in the simulations to achieve the lowest possible ground run and rotational distance. The impact of flap blowing reduces the rotational velocity as the same control power to rotate the aircraft is achieved at a lower velocity and the aircraft also rotates at a faster rate with the additional control power from flap blowing despite a decrease in the lift on the aircraft as the elevators are rotated upwards. Overall, flap blowing reduces the take-off distance of the N3-X by approximately 26%.

9.5.2 Thrust Split Turbofan N3-X Case Study

In the case of the turbofan thrust split N3-X, the motor and generators are designed and sized for the ADP cruise condition. At the take-off condition, the motors operate at a condition whereby it uses all the power available to it through the generators but limited by the design power of the motor. There are multiple points within the grey zone of the map that it can operate on and the shaft speed and nozzle area are iterated to obtain the highest possible thrust output.

As been previously mentioned, for each turbofan cBPR and each thrust split level, there is an optimal cFPR whereby the TSFC or fuel consumption is lowest. Each of these designed optimal configurations is used to simulate the N3-X take-off performance. Figure 97 shows the take-off distance of the N3-X for the 3 simulated cBPR at various thrust split levels. The diagram also depicts how the take-off distance changes with respect to the optimal TSFC configuration in each cBPR. The corresponding parameters for the optimum TSFC thrust split take-off performance is tabulated in Table 26.

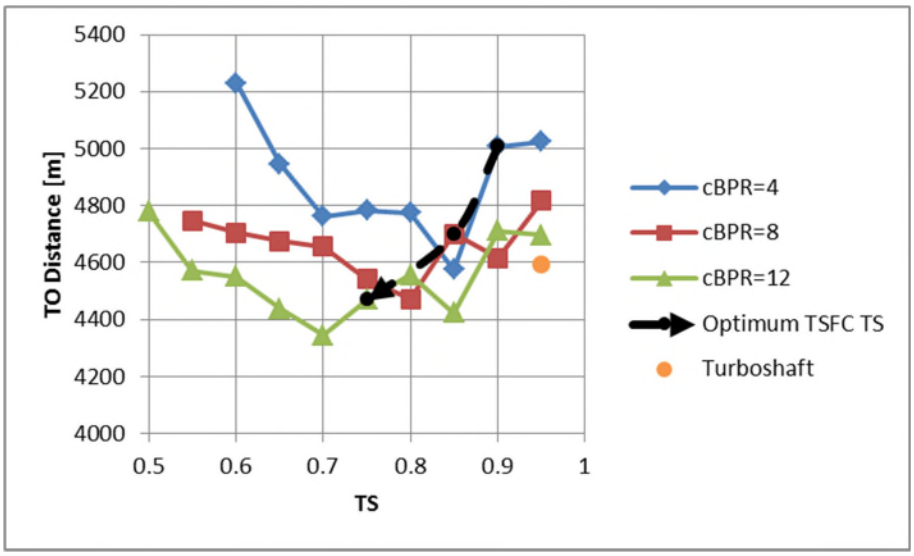

Figure 97: Take-off distance comparison for various turboshaft and different cBPR turbofan turbogenerators with different TS

Table 26: Comparison of take-off parameters for different cBPR configurations

	cBPR=4	cBPR=8	cBPR=12
ADP TS	0.9	0.85	0.75
Rotational Velocity [m/s]	92.6	92.6	93.6
C_u at V_{ROT}	0.4909	0.4801	0.4753
Ground run + Rotational distance [m]	4681	4373	4139
Transition distance [m]	327	327	331
Total take-off distance [m]	5008	4700	4469
Total SLS Thrust [kN]	487.94	521.14	549.58

A few observations can be made from the diagram. Firstly, the take-off distance in general seems to decrease as the cBPR is increased and when the thrust split level decreases although there are irregularities in some instances. Comparing the optimum TSFC cases for each cBPR, the reduction in take-off distance with increasing cBPR can be attributed to the increase in overall thrust available during take-off with increasing cBPR. The blowing coefficient decreases with increasing cBPR in the optimal TSFC trends as the thrust split level decreases and less thrust is provided by the fan array, thereby lowering the blowing coefficient. The increase in the thrust available however, reduces the distance to achieve the rotational velocity and offsets the increase in distance during the rotation phase.

In each selected cBPR, there also seems to be an optimal thrust split ratio that allows for a minimal take-off distance. In general, the overall SLS thrust available for take-off increases as the TSR decreases and the core engines provide a higher proportion of the thrust, thereby reducing the distance required to achieve the rotational velocity. However, the blowing coefficient decreases with decreasing thrust split ratio as less thrust is produced by the fan propulsors, resulting in an increase in the rotational distance. These two counteracting effects in terms of take-off distance results in an optimal TSR whereby lowest take-off distance is achieved. It should be noted that these configurations correspond to the optimal cFPR whereby lowest TSFC is achieved at the ADP.

In comparison to the take-off distance achieved by the turboshaft system, the turboshaft system achieves a lower take-off distance compared to the turbofan thrust split system with cBPR=4 and cBPR=8. However, a further increase in the cBPR of the turbofan system would further lower the optimal take-off distance to make it more beneficial as compared to the turboshaft system. This higher cBPR configuration would also correspond to a lower thrust split setting. As can be recalled previously, it has been mentioned that for a system with high intake pressure losses, a low thrust split level turbofan system might be beneficial in terms of reducing the fuel consumption at the ADP. Such a system would also seemingly be beneficial in terms of reducing the overall take-off distance.

9.6 Conclusion

The take-off performance of the N3-X has been simulated using both turboshaft system as well as a turbofan thrust split system. The modelling of the propulsion system at off design for both systems has been explained. Flap blowing significantly reduces the take-off distance of the N3-X by approximately 26% using the turboshaft system. The turbofan thrust-split system would be beneficial in terms of shorter take-off distance when the thrust split level is lower and also when the cBPR of the core turbofans increase.

Chapter 10

FURTHER POTENTIAL OF FLAP BLOWING

10.1 Introduction

This chapter would look at a potential modification of a TeDP aircraft utilizing flap blowing. In any aircraft, the take-off distance can be managed to a specified distance either by increasing the amount of thrust available at take-off or by increasing the wing area. Increasing the thrust available would allow the aircraft to achieve the required velocities at a faster rate while a bigger wing area would allow the aircraft to gain more lift at the velocity compared. Consequently, a reduction in wing area would thus increase the take-off distance of the aircraft.

It is opined that the aircraft can be modified in terms of re-sizing the wing area to enable the aircraft to achieve the same pre-determined take-off distance with the aid of flap blowing since a major design specification for the wing area is based around the take-off distance requirements. The wing area is generally calculated from the largest of three requirements; landing distance, take-off distance and fuel volume. In the case of the TeDP and the assumptions made, the fuel volume is primarily stored within the inner wing and would not be impacted by the resizing of the outer wing. A study by Mair [80] on take-off and landing distances for high-lift aircraft showed that take-off distance for such an aircraft utilizing high-lift devices would usually be at least or greater than the landing distance. Thus, the take-off distance becomes a primary design constrain for the sizing of the wing area. By utilizing flap blowing, the wing area can possibly be reduced to still achieve the original designed take-off distance. The reduction in wing area and

hence overall weight of the aircraft would then necessitate a re-design of the propulsion system and this might result in further overall fuel savings.

10.2 Potential Wing Area Re-size

As previously described in earlier chapters, the TeDP BWB aircraft is divided into 7 main components. When describing the re-size of wing area, this area will be limited to the outer wing as shown in Figure 98. There are a few justifications to this assumption. Firstly, the fan propulsor array and the flaps are either integrated or forms part of the inner wing. A change in the inner wing area would inevitably affect the propulsion system design parameters drastically. Second, the payload or the passengers in the case of a passenger transport aircraft would be located within the inner wing area. Any re-size of the wing area would impact upon the ability of the aircraft to transport the design payload. It is for this reason that in the weight module previously described, the outer wing weight estimation is based on a more detailed method that takes into account forces and loading at various flight conditions. To cater to the change in the structural support of the inner wing due to the change in loading from the re-size of the outer wing, the inner wing weight is estimated based on a fixed percentage of the overall aircraft weight.

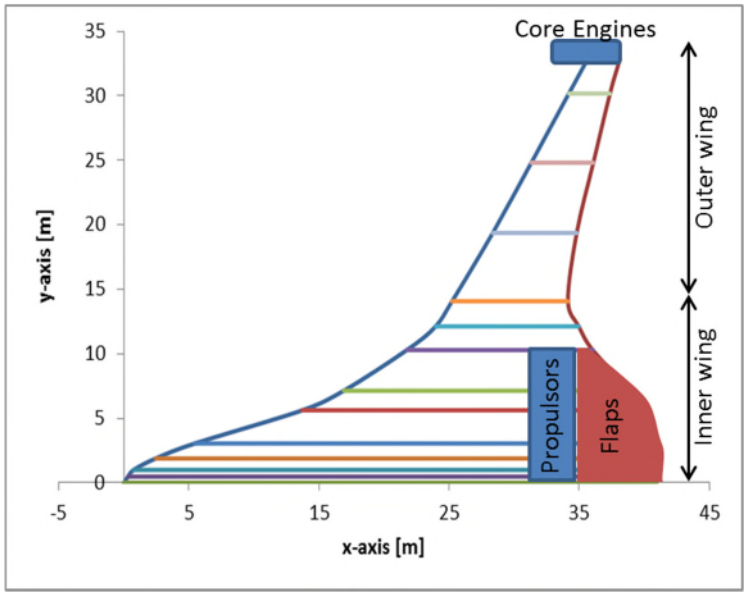

Figure 98: Outer wing of TeDP BWB

In terms of changing the outer wing area, this change is limited to +-30% of the original wing area. This value was assumed to ensure there are not too much significant changes in the shape of the aircraft especially in terms of blending of the leading and trailing edge between the inner and outer wing. Too big a change might lead to unexpected losses and shockwaves associated with sharp corners in flows. It should be brought up here that this wing area change is a first level analysis and consists of many assumptions and unknowns but would give an idea into the possibly benefits of such a design incorporating flap blowing.

In changing the area of the outer wing, the chord length for each aerofoil strip in the initial geometry is changed by the same percentage with equal increase or decrease in the physical location of the leading and trailing edge. The new outer wing area is then computed after all the aerofoils strips are blended together using OpenVSP. With the change in the outer wing strip chord, the individual strip aerodynamic property changes. Coupled with the change in the overall average chord of the aircraft, the overall aerodynamic properties as well as the impact on aerodynamic properties due to flap blowing have to be recalculated in the aerodynamics module. Lastly, in changing the outer wing area, the outer wing area weight has to be recalculated in the weight module. The impact on other parameters and other modules would then follow on from the overall design methodology that synergizes and integrates all aspects as previously shown and explained.

10.2.1 Case Study on N3-X

The explained methodology on changing the outer wing area is applied to the N3-X.

Firstly, the wing area of the N3-X is reduced by 10% to observe the impact on the total fuel consumption of the N3-X. The overall methodology is applied to this reduced outer wing N3-X to obtain the design and output parameters based on a turbofan thrust split system. Figure 99 shows the total fuel consumption for the designed systems for various cBPR at varying thrust split levels. The 10% wing reduction results in a propulsion system that is designed that consumes approximately 1.5-2% less fuel overall at various TSR and cBPR. This trend

underlines the possible potential of fuel savings by utilizing flap blowing to aid in reducing take-of distance and hence reducing the outer wing area.

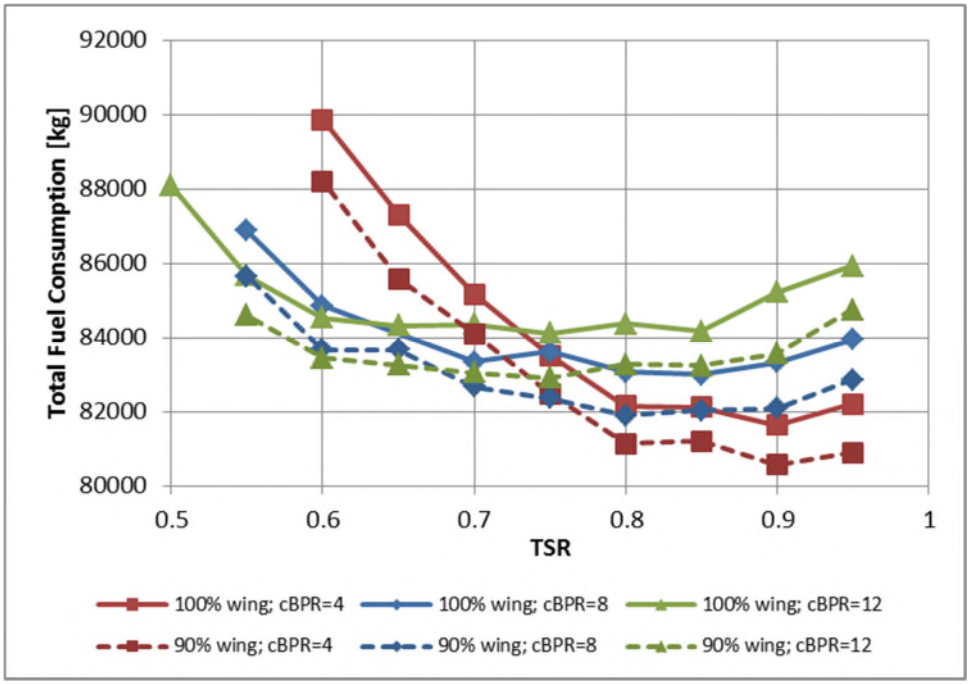

Figure 99: Comparison of total fuel consumption with 10% outer wing area reduction for different cBPR

Table 27 shows the corresponding take-off distances of the lowest total fuel consumption configuration for each cBPR. For comparison, the take-off distance of a non-flap blown turboshaft system is listed. Flap blowing can possibly aid in reducing the take-off distance by 26.3% when utilizing a turbofan system. With a 10% wing area reduction in the turbofan thrust split system, the take-off distance of N3-X increases by approximately 2-3% depending on the configuration. This thus underlines the potential in reducing the outer wing area of the N3-X while still maintaining a short take-off distance.

Table 27: Take-off distance of various outer wing area and core engine configurations

Configuration	Wing area re-size	Take-off Distance [m]
Turboshaft Non-Flap blown	0%	6204
Turbofan cBPR=4 Flap blown	0%	4576
Turbofan cBPR=4 Flap blown	-10%	4732
Turbofan cBPR=8 Flap blown	0%	4471
Turbofan cBPR=8 Flap blown	-10%	4566
Turbofan cBPR=12 Flap blown	0%	4343
Turbofan cBPR=12 Flap blown	-10%	4500

It is difficult to ascertain and define a required take-off distance for re-sizing the outer wing with the aid of flap blowing. Changing the take-off distance by too large an extent would involve substantial re-size of the wing and beyond the reasonable range of flap blowing provided by the propulsor fans. While it might make better comparisons when compared with similar design payload aircrafts such as the B777, it might prove beyond reasonable assumptions for the reasons above. For this reason and to demonstrate the potential effectiveness of re-sizing the wing, the pre-determined required take-off distance is defined using the take-off distance of the N3-X using a turboshaft system at 95% thrust split. It has been previously demonstrated that using a turbofan thrust split system could possibly aid in reducing the take-off distance of the N3-X as compared to the turboshaft system. This study here will concentrate on reducing the wing area of the turbofan system to achieve the longer take-off distance of a turboshaft system which is approximately 4600m. Figure 100 shows the total fuel consumption of each of the configurations described as well as the corresponding wing area to achieve the defined take-off distance. It can be observed that the wing area reduction is more for a higher cBPR turbofan system. It has been previously shown that a higher cBPR turbofan system would reduce the take-off distance more due to the higher thrust available at take-off. The total fuel consumption however, shows a minimal at cBPR=8. This is dependent on the overall design of the aircraft systems. An indicative of this can be reflected in the overall weight of the aircraft. The overall weight of the aircraft for a turbofan system of cBPR=4,

8 and 12 are 271 kN, 268 kN and 284 kN respectively. The lightest aircraft among the three is the one with a cBPR=8 and this consequently results in a lower trim intrinsic net thrust requirement and lower overall fuel consumption. The potential of fuel savings compared to the turboshaft system is in the region of 1% for such a pre-defined take-off distance, whereby the take-off distance has been increased by 2%, and thus highlights the potential of fuel savings when the wing area is reduced with the aid of flap blowing. The values while not entirely indicative, still allows an example of the usage of designed overall methodology to aid in optimization of the aircraft design at a preliminary design stage as well as synergizing various disciplines in the overall methodology and optimization.

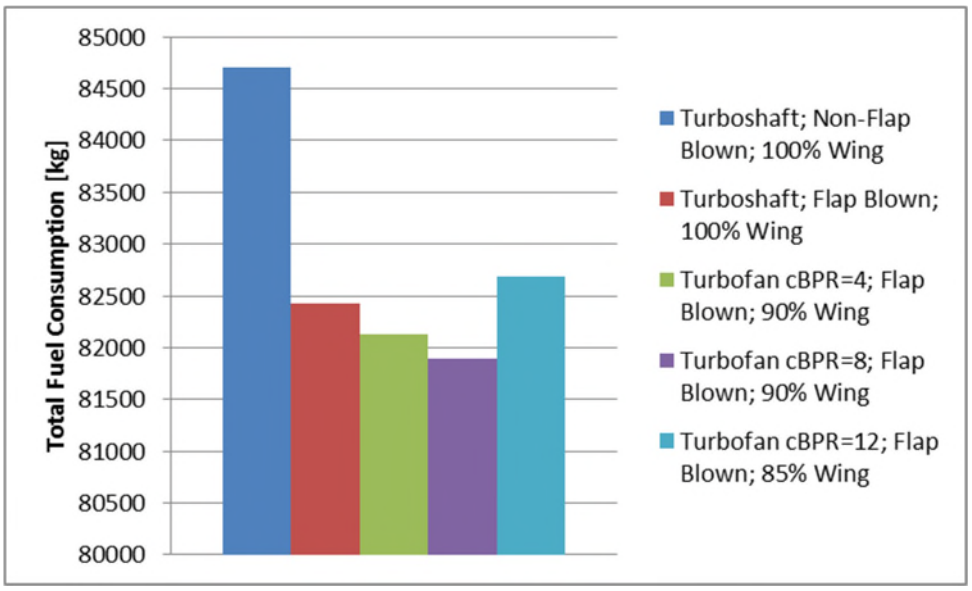

Figure 100: Total fuel consumption for outer wing reduced area due to pre-defined take-off distance

10.3 Conclusion

Overall, this chapter has demonstrated the potential of flap blowing to aid in re-sizing of the TeDP aircraft outer wing. Re-sizing the wing of a pre-designed aircraft to meet a design take-off distance with the aid of flap blowing might be possible in the hope of further reducing the total fuel consumption of the aircraft. Flap blowing significantly aids in reducing the take-off distance and increments in this reduced take-off distance can possibly result in reduced outer wing area and consequent reduced overall fuel consumption.

Chapter 11

CONCLUSIONS AND FUTURE WORK

11.1 Conclusions

A multi-disciplinary and multi-fidelity methodology has been developed for preliminary design and analysis of a Turboelectric Distributed Propulsion (TeDP) flap blown and/or thrust vectored aircraft. The developed strip methodology makes use of ESDU relations as well as theoretically and experimentally verified blowing equations. It addresses the impact of flap blowing on the aircraft aerodynamic properties in a flexible and easily adaptable way. The weight module estimates the weight of various defined components of the aircraft to obtain an overall weight for the aircraft. The flight dynamics module is centered on the open-sourced software, JSBSim to calculate the trim thrust requirements with various inputs from the other modules. The propulsion module caters to the design of the fan propulsor array and core engines. The core engines are modelled using Cranfield University's in-house engine design software, Turbomatch while the fan propulsor array follows basic fan design guidelines while incorporating the electric motor constrains and requirements. Off-design core engine and fan performance are also modelled and obtained from the propulsion module. The boundary layer ingestion (BLI) module accounts for the intake pressure losses as well as the deficiency in fan efficiency due to the ingestion of distorted flow from the boundary layer. The Discretised Miller (DM) method is adapted into the BLI module to account for the deficiency described. A methodology is also developed to determine the take-off distance of the TeDP flap blown aircraft that is easily adaptable and used in the early design phase. The overall methodology allows for varying different parameters and obtaining a converged solution that accounts for all the impact on the different disciplines of such a high integrated and synergized aircraft. The developed methodology

approach is a contribution to the community as it allow for the preliminary design and analysis of such an aircraft in all the various disciplines and allows for observation of various trends on the different disciplines that arises due to specific parameter changes.

The developed methodology is applied onto the N3-X for various case studies. The various trends observed are summarized below.

- Aerodynamics: The developed strip method code is verified with data from Tornado using the N3-X as a baseline aircraft. For the N3-X, the flaps are positioned at the trailing edge of the aircraft and forms part of the wing area. Flap blowing amplifies the lift and pitching moment coefficients. A positive or downwards flap deflection coupled with flap blowing will result in a bigger positive lift coefficient and a more negative or nose down pitching moment. The reverse is also true. In take-off conditions, the flaps are deflected upwards to generate nose up pitching moment and with flap blowing, the lift coefficient is reduced further while pitch up moment is increased.
- Flight Dynamics: The parametric impact of flap blowing on the aerodynamic properties and calculated N3-X weight are used as inputs into the flight dynamics module to determine the impact of flap blowing on the trim aerodynamic intrinsic net thrust. Flap blowing reduces the trim intrinsic net thrust requirements of the N3-X at the ADP and shows potential in reducing the overall fuel consumption. A pure thrust-vectored N3-X on the other hand, would require substantial increase in the thrust produced to achieve trim conditions in the ADP and is deemed unfeasible in the conditions. Parametric studies varying constant blowing coefficient coupled with fixed thrust vectoring angles during take-off also shows potential of reducing the N3-X take-off distance by up to 35%.
- Propulsion module: The method to model the fan propulsor array as well as the core engines has been introduced. Thrust split on such a TeDP aircraft is also defined and explained. The superconducting electrical systems that is present in a TeDP architecture has also been introduced

along with the constrains and estimated efficiencies of these electrical systems including the motor, generator, inverters, cryocoolers and transmission lines. The fan design outputs the overall blowing coefficient at both design and off-design point from the propulsor array.

- Boundary Layer Ingestion: A methodology to determine the boundary layer profile that references a baseline profile is explained allowing the profiles to be determined for varying longitudinal location as well as different flight conditions. The intake pressure losses are varied parametrically in the study to determine its impact on the overall power requirements on the system as well as the fuel consumption. It has been shown that reducing intake pressure losses is of paramount importance to make BLI effective in reducing fuel consumption. A 2% intake pressure loss would totally negate the positive impact derived from BLI. The Discretised Miller method is adapted to determine to the impact on the fan efficiency due to the distorted flow and has shown that less distortion from higher intake height would result in less deficiency in the fan efficiency and vice versa. Overall, there is an optimum intake capture sheet height or design fan pressure ratio whereby the power requirements are kept to a minimal and this optimum varies with different intake pressure losses assumed. The optimum is present due to the counteracting effects of lower inlet ram drag resulting in lower energy requirements from the fan stage and higher energy requirements from the fan stage when the intake pressure losses are present.
- Weight module: Increasing the number of fans in a fixed array width and fixed intake height results in smaller fans to fulfil the same thrust requirements. The smaller fans lead to a lighter overall fan array weight. However, the overall electrical systems weight increase with the number of fans and the overall propulsion system weight actually increases, possibly leading to higher trim intrinsic net thrust requirements and higher total fuel consumption as a consequent. However, it is reasonable to assume that bigger and less number of fans in a fixed intake height integrated system would lead to a more complex S-duct design and higher

intake pressure losses. The impact of intake pressure losses on the overall fuel consumption far outweighs the impact of increased weight and having more fans with smaller diameters is still favourable.

- Overall synergy of all modules: The overall complete methodology is applied on the N3-X aircraft. Similar trends for boundary layer ingestion impact are observed as per previously described and intake pressure losses plays a significant role in the overall fuel consumption, making reducing intake pressure losses a priority in such systems design. Assuming a 0.5% intake pressure loss, BLI reduces the overall fuel consumption of the N3-X by about 5.5% while the addition of flap blowing further reduces the overall fuel consumption to about 8.5% on a turboshaft core engine system. A turbofan core engine thrust split system is then introduced, designed and optimized as per general turbofan design guidelines. The thrust split system allows for less emphasis in reducing the intake pressure losses as a portion of the thrust is now produced by the core engines and less mass flow passes through the fan propulsor intake. It helps reduce the total fuel consumption for and the reduction in total fuel consumption is expected to be amplified when comparing higher intake pressure losses system for the reasons explained above. Flap blowing significantly reduces the take-off distance of the N3-X by about 26%. The take-off distance for a turbofan thrust split system is reduced when comparing to the turboshaft system and also allows for the motors and generators to be sized at the ADP instead of the take-off condition.
- Potential resizing of outer wing: The outer wing of the N3-X is resized to attain a specified design take-off distance. With flap blowing, the take-off distance reduces significantly as compared to the original design take-off distance. Thus, the possibility of reducing the wing area arises if the reduced take-off distance can be increased. The case study on the N3-X has shown that this is a possibility and the overall weight and total fuel consumption of the aircraft can be reduced with this consideration. A 2% increase in the take-off distance of the N3-X resulted in a 1% decrease in the overall fuel consumption.

11.2 Future Work

The developed methodology focuses on the preliminary design and analysis of a flap blown TeDP architecture BWB aircraft and various assumptions has been made to allow the implementation of the methodology. While off-design take-off analysis has been described, further refinements to the methodology needs to be considered to increase the fidelity and accuracy of the method. These include:

1. The developed strip method is a 2D methodology applied onto a 3D structure through summation and derived parameters from Tornado. However, while catering to the 3D effects on the original planform, the 3D effects of flap blowing are not considered. The flow across the flap from each fan propulsor nozzle could possibly overlap with each other, resulting in either losses as well as increased performance. Future work can and should possibly consider this and involve either CFD studies or empirical relations to account for this.
2. The drag coefficient prediction when incorporating flap blowing makes use of the original drag polar as the variations between a thin jet and thick jet has been shown to have huge variation in impact on the drag. For TeDP, the expected jet height region should be sufficiently small to not result in a huge increment in the drag coefficient. Further studies and methodology should be developed to capture this detail as the drag changes would impact upon the thrust requirements and hence, fuel consumptions.
3. Two methods have been used to define the sizing of the propulsion system as well as the electrical components. One assumes a turboshaft system designed for maximum output during the take-off condition and the system operates at a reduced load at the ADP while the other assumes a turbofan system that is designed for maximum output during the ADP condition and the motors and generators sized for it. The power produced by the power turbine in both cases have been checked in Turbomatch to ensure it produced at least or more than the required power for the propulsor fans in each scenario. The excess power produced by the power turbine has not been accounted for. This can be accounted for by either determining the power turbine operating line to determine if the power can be kept

constant or to the exact requirements at all design and off design conditions or to model the extra power available to be stored in possibly batteries. The first method would be useful to be implemented in Turbomatch to allow a fixed power output at the off design conditions while the second method would entail more complexities in battery modelling and its additional requirements such as weight, size and response time.

4. At the moment, the boundary layer profile for each fan propulsor is determined by a modified power law referenced to the centreline boundary layer profile. While is allows flexibility in varying the longitudinal and lateral location of the intake as well as differing flight conditions, there exists discrepancies with the actual boundary layer profile as the aerofoil shape changes across the aircraft span. As the name suggests, boundary layer ingestion focuses on the impact of ingesting the boundary layer; a more accurate method in determining the boundary layer would provide a much improved fidelity methodology. Further work can the N3-X aircraft can also be incorporated by obtaining boundary layer profiles through the use of CFD at various regimes to be used in the methodology.
5. The intake pressure losses in the methodology is assumed and parametrically altered. A more detailed method in determining the losses such as [81] would pay dividends in determining the possibility of such a system. By incorporating empirical relations or CFD results into the overall methodology would allow for an even more holistic and realistic determination on the effectiveness of BLI in such a system.
6. Much emphasis has been placed on the aerodynamic impact of flap blowing. However, another aspect to consider is the aerodynamic impact upstream of the propulsor intake such as that seen in [82]. In off-design conditions whereby the fan propulsors accelerate or decelerate the flow upstream of the intake due to the fan propulsor operation, the increased or decreased velocity across the airframe would impact upon the aerodynamic properties. A methodology to incorporate this into the overall method would provide a more accurate assessment of the aircraft performance especially at off-design conditions.

7. Most if not all of the related studies including this one have neglected the impact of additional drag due to the fan propulsors array setup as the additional wetted area is minimal compared to the aircraft without the fan propulsor array. However, with varying intake heights studied ranging from 0.4m to 1.5m, the possibility of the additional wetted area in drag assessment could be considered and implemented. Other losses such as drag installation losses should also be considered to account for the overall drag changes. Some approaches to be considered can be found in [83] [84].
8. Noise. Another discipline that can be considered in the methodology is the incorporation of noise prediction. One of the aims of the N+3 timeframe is the reduction of noise levels. This is especially pertinent to take-off scenarios and it would be helpful to incorporate this into the take-off simulations.
9. The weight prediction methodology employed here makes use of various existing relations as well as scaling factors to account for the weight of the components. Further work can be done especially for the electrical systems which are relatively new in the propulsion environment to obtain better empirical relations to be utilized.
10. Cooling aspects of electrical systems embedded in core engines. The presence of the generator in the core engine experiences high temperature from the flow. More study can be done on the performance of the generator under such conditions as well as cooling methodologies to be incorporated.

REFERENCES

[1] Joint Planning and Development Office, Next Generation Air Transportation System (NextGen), “Making the NextGen Vision a Reality. 2006 Progress Report to the Next Generation Air Transportation System Integrated Plan,” NextGen, Washington, US, 2006.

[2] R. Singh, “IMechE Prestige Lecture - Post Nubes Lux: Aerospace Propulsion,” Cranfield University, Cranfield, UK, 2011.

[3] A. A. Griffith, “Bibliographic data: GB720394 (A) — 1954-12-22,” 22 12 1954. [Online]. Available: https://worldwide.espacenet.com/publicationDetails/biblio?CC=GB&NR=720394. [Accessed 11 12 2013].

[4] W. Reyle, “Aircraft”. United Kingdom Patent 1,066,360, 1967.

[5] Lewis Research Center, “Aircraft Propulsion,” in *Proceedings of conference on aircraft propulsion*, Cleveland, 1970.

[6] J. A. Schetz, D. Hosder, V. Dippold and J. Walker, “Propulsion and Aerodynamic Performance Evaluation of Jet-Wing Distributed Propulsion,” *Aerospace Science and Technology,* vol. 14, no. 1, pp. 1-10, 2010.

[7] M. Buquet, “Distributed Propulsion: An Overview of Possible Transmission Technologies,” MSc Thesis, Cranfield University, Cranfield, UK, 2007.

[8] J. J. Berton, E. Envia and C. L. Burley, “An Analytical Assessment of NASA's N+1 Subsonic Fixed Wing Project Noise Goals,” Miami, 2009.

[9] H. D. Kim, “Distributed Propulsion Vehicles,” Cleveland, Ohio, USA, 2010.

[10] F. Lodesani, “Performance, Design and Numerical Optimisation of a Novel Distributed Propulsion System,” MSc Thesis, Cranfield, UK, 2012.

[11] F. Lodesani, “Performance, Desgin and Numerical Optimisation of a Novel Distributed Propulsion System,” MSc Thesis, Cranfield University, Cranfield, UK, 2012.

[12] C. A. Luongo, P. J. Masson, T. Nam, D. Mavris, H. D. Kim, G. V. Brown, M. Waters and D. Hall, “Next generation more-electric aircraft: A potential application for HTS superconductors,” *Applied Superconductivity, IEEE,* vol. 19, no. 3, pp. 1055-1068, June 2009.

[13] E. Ailam, D. Netter and J. Leveque, “Design and testing of a superconducting machine,” *Applied Superconductivity, IEEE,* vol. 17, no. 1, pp. 27-33, 2007.

[14] G. Brown, “Weights and efficiences of electric components of a turboelectric aircraft propulsion system,” in *49th AIAA Aerospace Sciences Meeting including the New Horizons Forum and Aerospace Exposition*, Orlando, FLorida, 2011.

[15] “Superconductivity,” [Online]. Available: http://en.wikipedia.org/wiki/Superconductivity.

[16] J. L. Felder, H. D. Kim and G. V. Brown, “Turboelectric Distributed Propulsion Engine Cycle Analysis for Hybrid-Wing-Body Aircraft,” in *47th AIAA Aerospace Sciences Meeting Including the New Horizons Forum and Aerospace Exposition*, Orlando, Florida, 2009.

[17] H. Smith, “Airframe integration for distributed propulsion systems,” in *21st ISABE Conference*, Busan, Korea, 2013.

[18] C. Snyder, J. Berton, G. Brown and J. Dolce, “Propulsion investigation for zero and near-zero emissions aircraft NASA/TM2009-215487,” NASA Glenn Research Center, Cleveland, Ohio, 2009.

[19] D. Thisdell, “Biomethane-lng fuel 'nearly elimibats co2',” *Flight International,* p. 183(5394):40, 2013.

[20] D. Verstraete, “The Potential of Liquid Hydrogen for Long Range Aircraft Propulsion,” PhD Thesis, Cranfield University, Cranfield, UK, 2009.

[21] E. M. Greitzer, “N+3 Aircraft Concept Designs and Trade Studies,” Massachusetts Institute of Technology, Cambridge, USA, 2010.

[22] S. Sato, P. C. Mody, D. K. Hall, E. D. l. R. Blanco and J. I. Hileman, “Assessment of Propulsion System Configuration and Fuel Composition on Hybrid Wing Body Fuel Efficiency,” Orlando, Florida, USA, 2011.

[23] J. L. Felder, G. V. Brown, H. D. Kim and J. Chu, “Turboelectric Distributed Propulsion in a Hybrid Wing Body Aircraft,” Gothenburg, Sweden, 2011.

[24] J. L. Felder, H. D. Kim and G. V. Brown, “An Examination of the Effect of Boundary Layer Ingestion on Turboelectric Distributed Propulsion Systems,” *49th AIAA Aerospace Sciences Meeting including the New Horizons Forum and Aerospace Exposition, Orlando, Florida,* p. 300, 4-7 Jan. 2011.

[25] H. D. Kim, G. V. Brown and J. L. Felder, “Distributed turboelectric propulsion for hybrid wing body aircraft. Prepared for the presentation at the 2008 International Powered Lift Conference sponsored by the Royal Aeronautical Society in London, England,” 2011.

[26] V. M. Lugo, “Effects of Boundary Layer Ingestion and Thrust Vectoring in Distributed Propulsion,” MSc thesis, Cranfield University, Cranfield, UK, 2010.

[27] B. Gal-Or, Vectored Propulsion, Supermaneuverability and Robot Aircraft, 1st ed., New York: Springer, 1991.

[28] K. A. Deere, “Summary of Fluidic Thrust Vectoring Research at NASA Langley Research Center,” 2003.

[29] D. A. Spence, “The Life Coefficient of a Thin Jet-Flapped Wing,” *Proceedings of the Royal Society of London,* vol. 251, pp. 407-425, 1959.

[30] J. Williams, S. F. J. Butler and M. N. Wood, “The aerodynamics of jet flaps,” Ministry of Aviation, London, 1963.

[31] R. U. Naveed and J. F. Whidborne, “Propulsion and Flight Controls Integration for a Blended-Wing-Body Transport Aircraft,” *Journal of Aircraft,* vol. 47, p. 3, 2010.

[32] B. W. McCormick, Aerodynamics, Aeronautics and Flight Mechanics, 2nd ed., New York: John Wiley, 1995.

[33] R. u. Naveed, “Propulsion and Flight Controls Integration for the Blended Wing Body Aircraft,” PhD Thesis, Cranfield University, Cranfield UK, 2009.

[34] H. V. Castro, “Flying and Handling Qualities of a Fly by Wire Blended Wing,” PhD thesis, Cranfield University, Cranfield UK, 2003.

[35] A. P. Plas, M. A. Sargeant, V. Madani, D. Crichton, E. M. Greitzer, T. P. Hynes and C. A. Hall, “Performance of a Boundary Layer Ingesting (BLI) Propulsion system,” *AIAA,* p. 450, 8-11 Jan. 2007.

[36] A. M. O. Smith and H. E. Roberts, “The Jet Airplane Utilizing Boundary Layer Air for Propulsion,” *Journal of the Aeronautical Sciences,* vol. 14, no. 2, pp. 97-109, 1947.

[37] A. Plas, “Performance of a Boundary Layer Ingesting Propulsion System,” MSc Thesis, Massachusetts Institute of Technology, 2006.

[38] H. D. Kim and F. James, “Control volume analysis of boundary layer ingesting propulsion systems with or without shock wave ahead of the inlet,” Orlando, Florida, 2011.

[39] J. P. Longley and E. M. Greitzer, “Inlet Distortion Effects in Aircraft Propulsion,” *AGARD,* pp. 6-1-6-18.

[40] C. Liu, D. Ihiabe, P. Laskaridis and R. Singh, “A Preliminary Method to Estimate Impacts of Inlet Flow Distortion on Boundary Layer Ingesting Propulsion System Design Point Performance,” *Journal of Aerospace Engineering,* 2013.

[41] E. Valencia, “PhD Thesis: Investigation of Propulsion Architectures for Advanced Distributed Propulsion Systems,” Cranfield University, Cranfield, UK, 2014.

[42] M. Hepperle, “Javafoil,” 2014. [Online]. Available: http://www.mh-aerotools.de/airfoils/javafoil.htm. [Accessed 2014].

[43] T. Melin, Tornado User Manual, 2000.

[44] ESDU, “ESDU 94028 - Increments in aerofoil lift coefficient at zero angle of attack and in maximum lift coefficient due to deployment of a plain trailing-edge flap, with or without a leading-edge high-lift device, at low speeds,” IHS ESDU, 1994.

[45] C. E. Lan and J. F. Campbell, “NASA Technical Note TN D-7936 THEORETICAL AERODYNAMICS OF UPPER-SURFACE-BLOWING JET-WING INTERACTION,” NASA, Washington D.C, 1975.

[46] ESDU, “ESDU 87024 - Low-speed drag coefficient increment at constant lift due to full-span plain flaps,” IHS ESDU, 2006.

[47] ESDU, “ESDU Aero F.02.01.07 - Conversion factor for profile drag increment for part-span flaps,” IHS ESDU, 2000.

[48] D. Kuchemann and J. Weber, Aerodynamics of Propulsion, McGraw-Hill Book Co., Inc., 1953.

[49] G. S. Jones and R. J. Englar, “AIAA 2003-3411 - Advances in Pneumatic-controlled high-lift systems through pulsed blowing,” in *21st Applied Aerodynamics Conference*, Orlando, Florida, 2003.

[50] K. -C. Pfingsten, R. Radespiel and M. Kamruzzaman, “Use of Upper Surface Blowing and Circulation Control for Gapless High-Lift Configurations,” in

CEAS/KATnet Conference on Key Aerodynamics Technologies, Bremen, Germany, 2005.

[51] ESDU, “ESDU 98017 - Aerofoil and wing pitching moment coefficient at zero angle of attack due to deployment of trailing-edge plain flaps at low speeds,” IHS ESDU, 2004.

[52] NASA, “OpenVSP,” [Online]. Available: http://www.openvsp.org. [Accessed 2014].

[53] T. A. Wick, J. R. Hooker, C. J. Hardin and H. C. Zeune, “Integrated Aerodynamic Benefits of Distributed Propulsion,” in *53rd AIAA Aerospace Sciences Meeting*, Kissimmee, Florida, 2015.

[54] Berndt, Jon S; JSBSim Development Team, “JSBSim Reference Manual,” 2011.

[55] D. L. Rodriguez, “A multidisciplinary optimization method for designing boundary layer ingesting inlets,” Department of Aeronautics and Astronautics Stanford University, Stanford University, 2001.

[56] R. F. Stengel, Flight Dynamics, Princeton: Princeton University Press, 2004.

[57] J. D. Anderson, Jr, Aircraft Performance & Design, International ed., WCB/McGraw-Hill, 1999.

[58] M. W. Osborn, D. R. Moore and J. R. Steinke, “Aerodynamic Performance of a 1.35-Pressure-Ratio Axial-Flow Fan Stage,” NASA Scientific & Technical Information Office, Cleveland, Ohio, 1978.

[59] V. J. Fidalgo, C. A. Hall and Y. Colin, “A Study of Fan-Distortion Interaction Within the NASA Rotor 67 Transonic Stage,” *ASME Journal of Turbomachinery,* vol. 134, 2012.

[60] H. Saravanamuttoo, C. Rogers, H. Cohen and P. V. Straznicky, Gas Turbine Theory, 6th ed., Harlow, England: Prentice Hall, 2009.

[61] P. Pilidis and J. R. Palmer, Gas Turbine Theory and Performance, Cranfield University MSc. Notes, 2013.

[62] Cranfield University, The Turbomatch Scheme, Cranfield, 2010.

[63] P. J. Masson, D. S. Soban, E. Upton, J. E. Pienkos and C. A. Luongo, “HTS motors in aircraft propulsion: design considerations,” *Applied Superconductivity, IEEE,* vol. 15, no. 2, p. 2218/2221, 2005.

[64] D. Friedman, “Aerodynamic prediction methodology and test validation for an efficient low-noise hybrid wing body subsonic transport, NASA Contract NNL07AA54C, 2nd Annual Review,” NASA Ames Research Center, 2010.

[65] C. B. Johnson and D. M. Bushnell, “Power-law velocity-profile-exponent variations with reynolds number, wall cooling, and mach number in a turbulent boundary layer, NASA Technical Note NASA TN D-5753,” NASA, Washington D.C, April 1970.

[66] Y. Cengel and J. M. Cimbala, Fluid mechanics fundamentals and applications, McGraw-Hill, 2013.

[67] R. V. Florea, C. Matalanis, L. W. Hardin, M. Stucky and A. Shabbir, “Parametric Analysis and Design for Embedded Engine Inlets,” in *48th AIAA/ASME/SAE/ASEE Joint Propulsion Conference & Exhibit*, Atlanta, Georgia, 2012.

[68] A. D. S. Carter, “The low speed performance of related airfoils in cascade,” NGTE 1949, NGTE R55, 1949.

[69] A. R. Howell, “Fluid dynamics of axial compressors,” *Proceedings of the Institution of Mechanical Engineers Development of the internal combustion turbine,* pp. 441-452, June 1945.

[70] D. C. Miller and D. L. Wasdell, “Off-design prediction of compressor blade losses,” *IMECHE,* pp. C279/87, 1987, 1987.

[71] N. White, A. Tourlidakis and R. L. Elder, “Axial compressor performance modelling with a quasi-one-dimensional approach,” *Proceedings of the Institution of Mechanical Engineers, Part A: Journal of Power and Energy,* vol. 216, no. 2, pp. 181-193, 2002.

[72] P. I. Wright and D. C. Miller, “An improved compressor performance prediction model,” London, 1991.

[73] F. Schwenk, G. Lewis and M. Hartmann, “A preliminary analysis of the magnitude of shock losses in transonic compressors,” NACA-RM-E57A30, 1957.

[74] C. Y. Liu, “PhD Thesis: Turboelectric Distributed Propulsion System Modelling,” Cranfield University, Cranfield, UK, 2013.

[75] R. Kirner, “PhD Thesis: An Investigation into the Benefits of Distributed Propulsion on Advanced Aircraft Configurations,” Cranfield University, Cranfield, UK, 2014.

[76] J. Roskam, Airplane Design, Part 5, Lawrence, Kansas: DARcorporation, 2003.

[77] P. Lolis, “PhD Thesis: Development of a Preliminary Weight Estimation Method for Advanced Turbofan Engines,” Cranfield University, Cranfield, UK, 2014.

[78] E. Torenbeek, “Development and Application of a Comprehensive, Design-sensitive Weight Prediction Method for Wing Structures of Transport Category Aircraft,” Delft University of Technology, Delft, Netherlands, 1992.

[79] C. A. Nicholas, Jet Propulsion: a simple guide to the aerodynamic and thermodynamic design and performance of jet engines, 2 ed., Cambridge: Cambridge University Press, 2003.

[80] W. A. Mair and B. J. Edwards, “A Parametric Study of Take-Off and Landing Distances for High-Lift Aircraft,” Ministry of Aviation Aeronaturical Research Council, Cambridge, 1965.

[81] J. Bijewitz, A. Seitz and M. Hornung, “Extended Design Studies for a Mechanically Driven Propulsive Fuselage Aircraft Concept,” in *2018 AIAA Aerospace Sciences Meeting*, Kissimmee, Florida, 2018.

[82] A. T. Perry and P. Ansell, “Aero-Propulsive and Propulsor Cross-Coupling Effects on a Distributed Propulsion System,” in *2018 AIAA Aerospace Sciences Meeting*, Kissimmee, Florida, 2018.

[83] L. Leifsson, A. Ko, W. H. Mason, J. A. Schetz, B. Grossman and R. T. Haftka, “Multidisciplinary design optimization of a blended-wing-body transport aircraft with distributed propulsion,” *Aerospace Science and Technology,* no. 25, pp. 16 - 28, 2013.

[84] W. A. Mair and D. L. Birdsall, Aircraft Performance, Cambridge: Cambridge University Press, 1992.

Appendix A

N3-X Aerodynamic Properties

A.1 N3-X Aerodynamic Properties

The N3-X aerodynamic properties derived from Tornado and used in the calculations for the N3-X aerodynamic code and flight dynamic modelling are shown here in the various figures with the polynomial equation. They are computed across a range of CG locations and input into the flight dynamics code to allow a variable CG during the simulations.

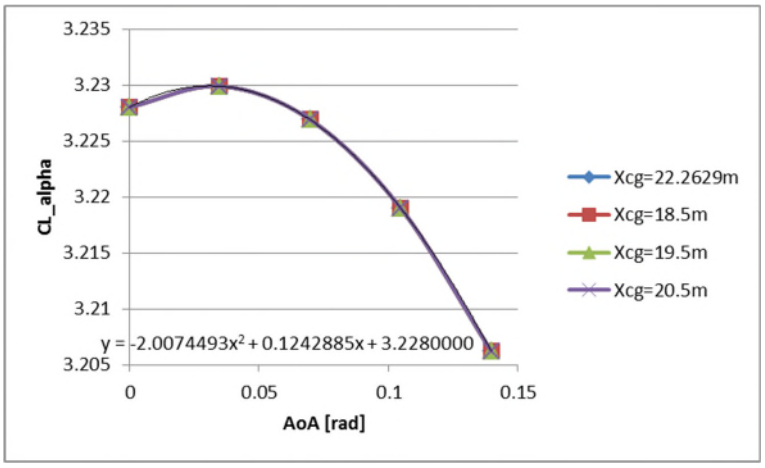

Figure A-1: CL_alpha vs AoA

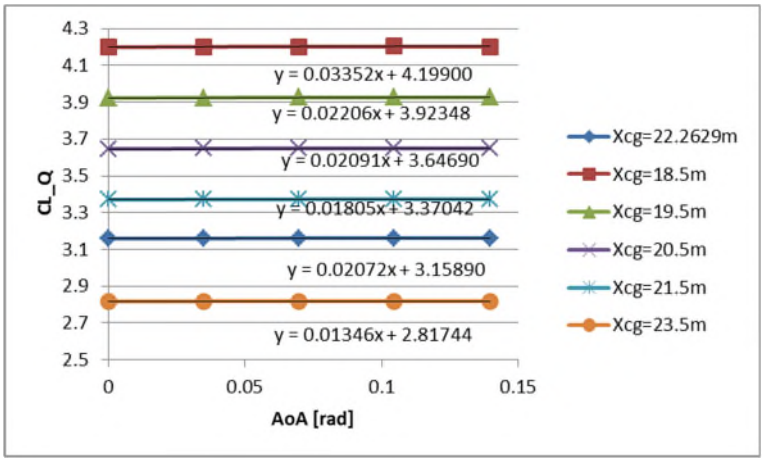

Figure A-2: CL_Q vs AoA

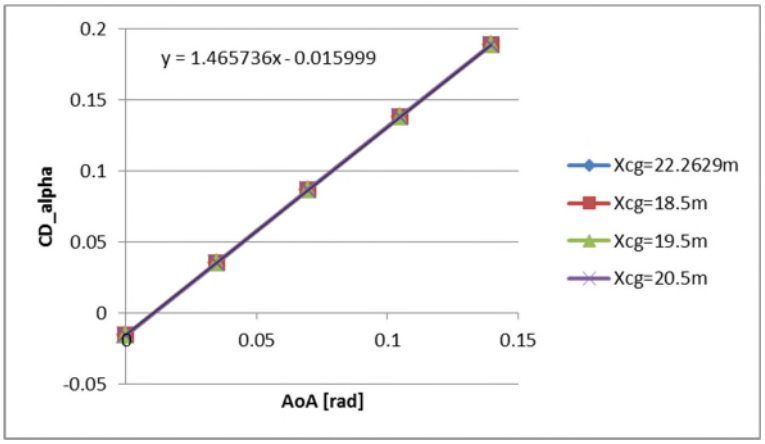

Figure A-3: CD_alpha vs AoA

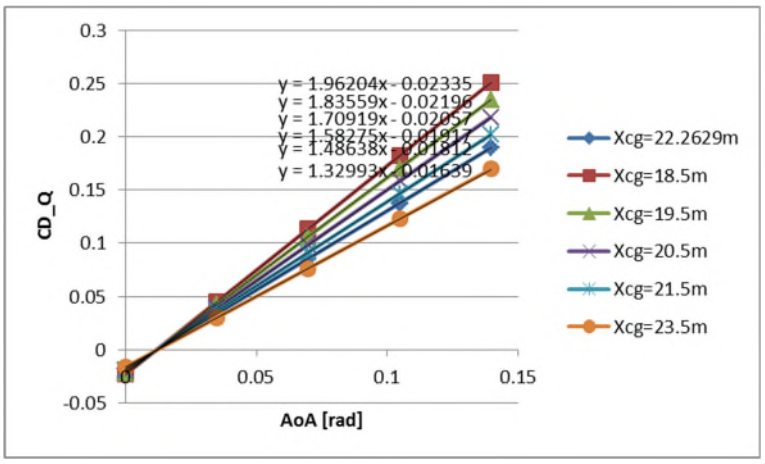

Figure A-4: CD_Q vs AoA

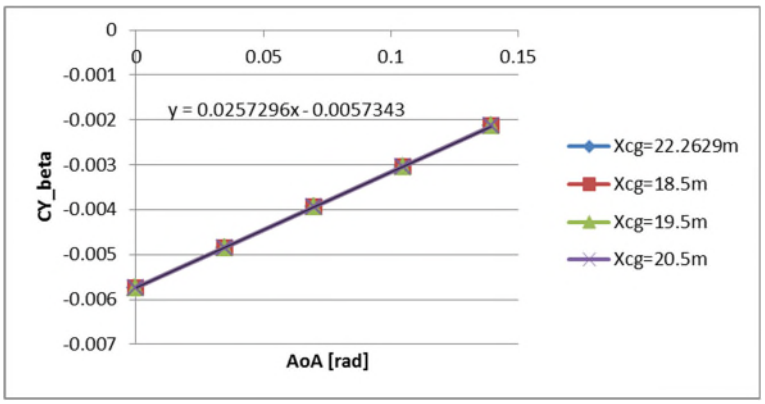

Figure A-5: CY_beta vs AoA

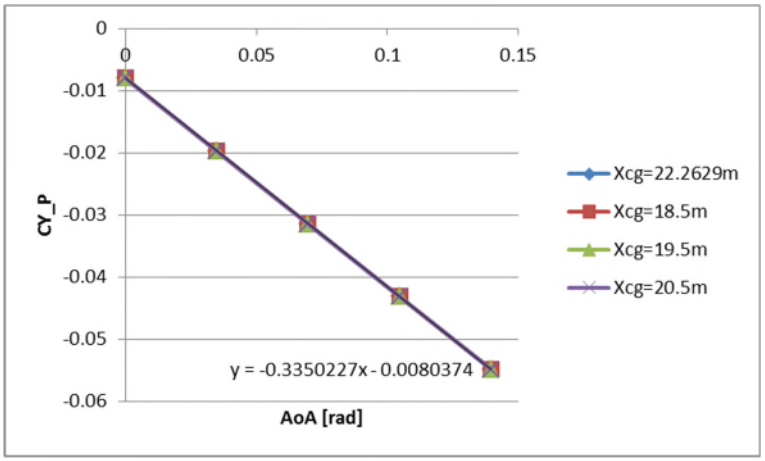

Figure A-6: CY_P vs AoA

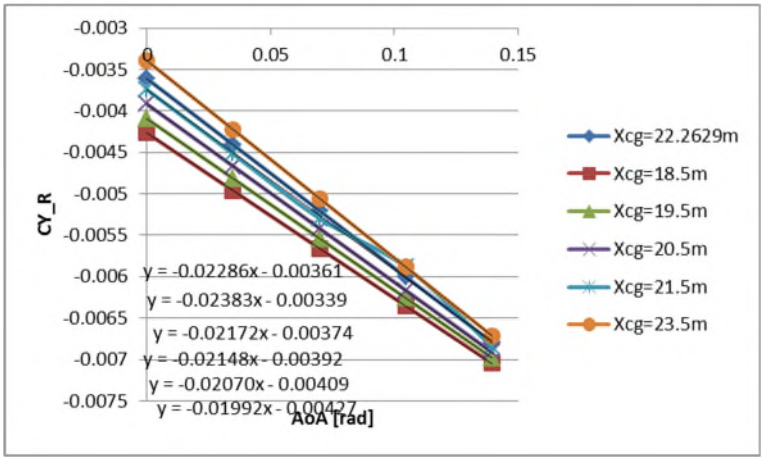

Figure A-7: CY_R vs AoA

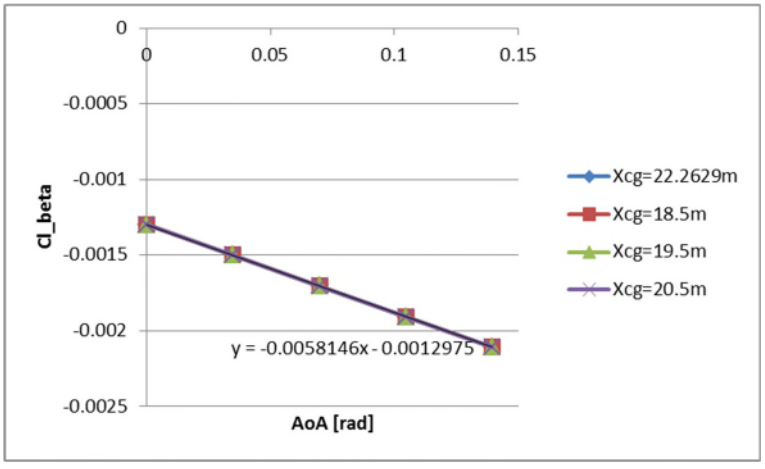

Figure A-8: Cl_beta vs AoA

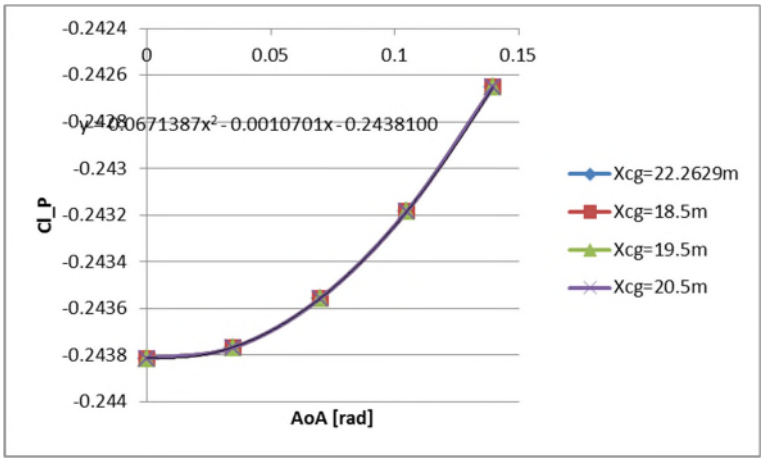

Figure A-9: Cl_P vs AoA

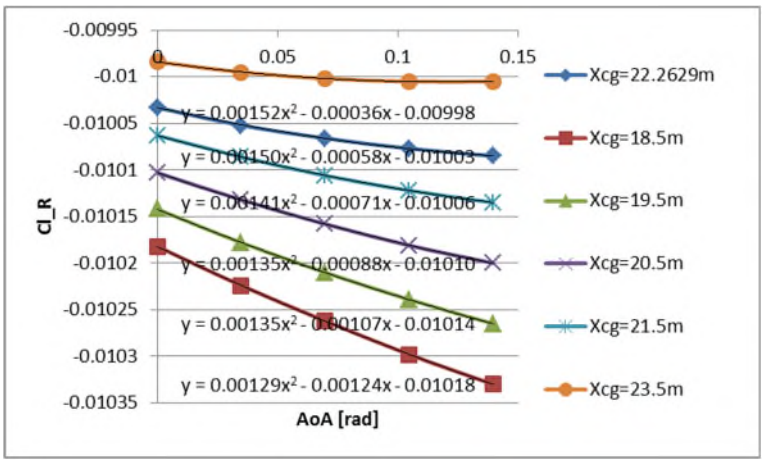

Figure A-10: Cl_R vs AoA

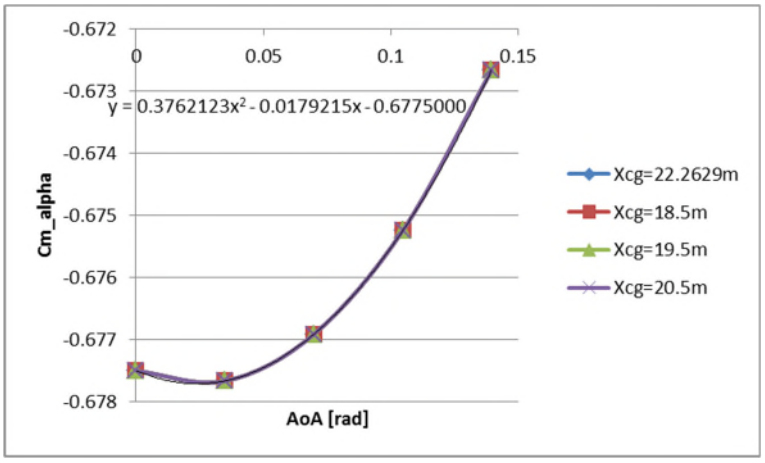

Figure A-11: Am_alpha vs AoA

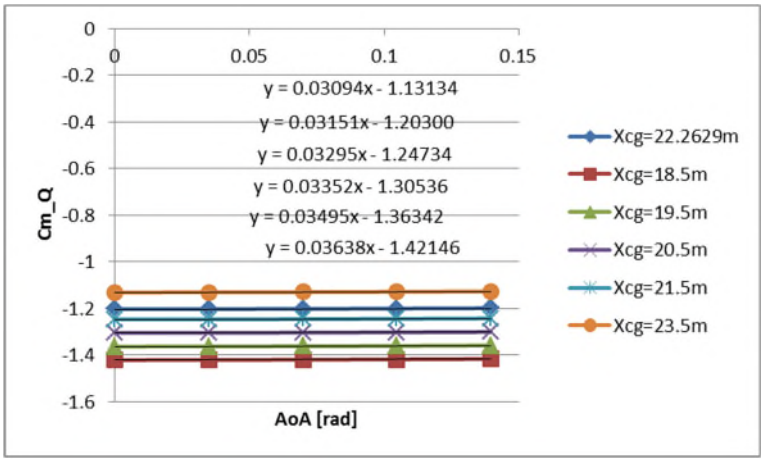

Figure A-12: Cm_Q vs AoA

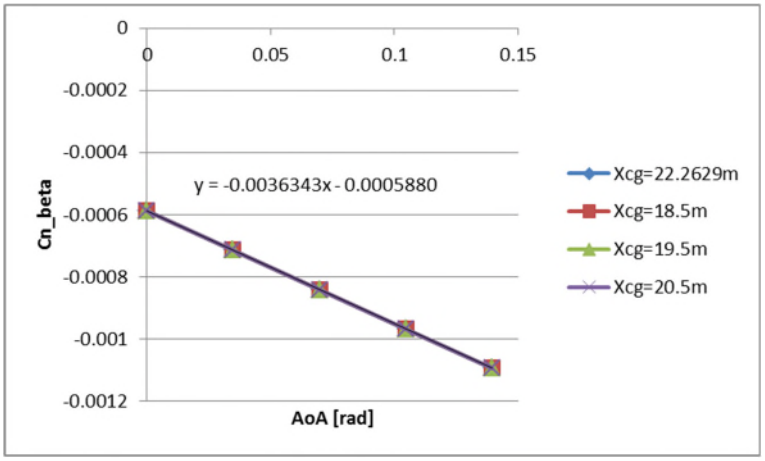

Figure A-13: Cn_beta vs AoA

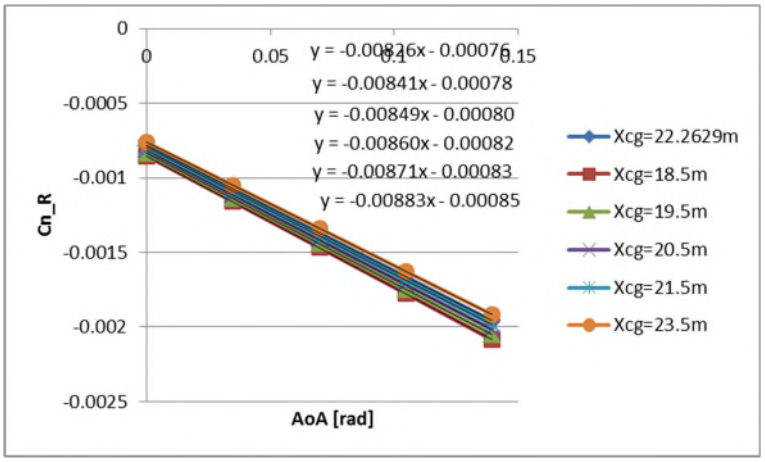

Figure A-14: Cn_R vs AoA

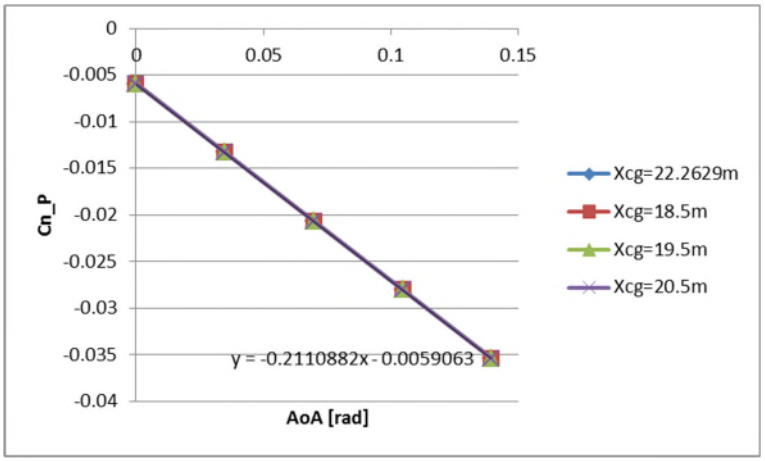

Figure A-15: Cn_P vs AoA

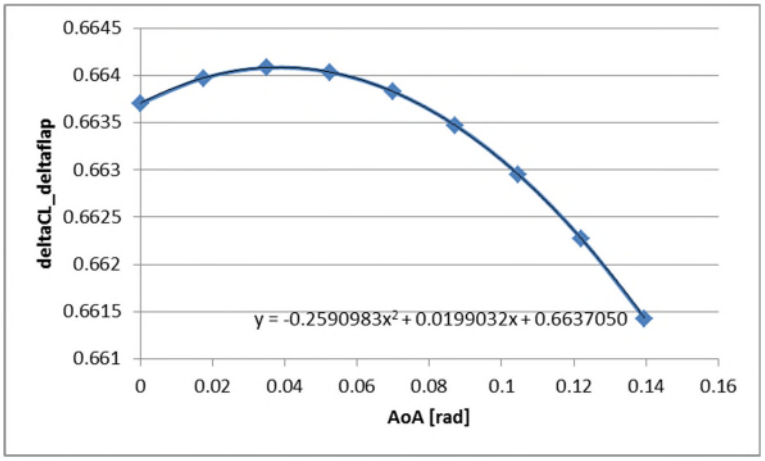

Figure A-16: deltaCL_deltaflap vs AoA

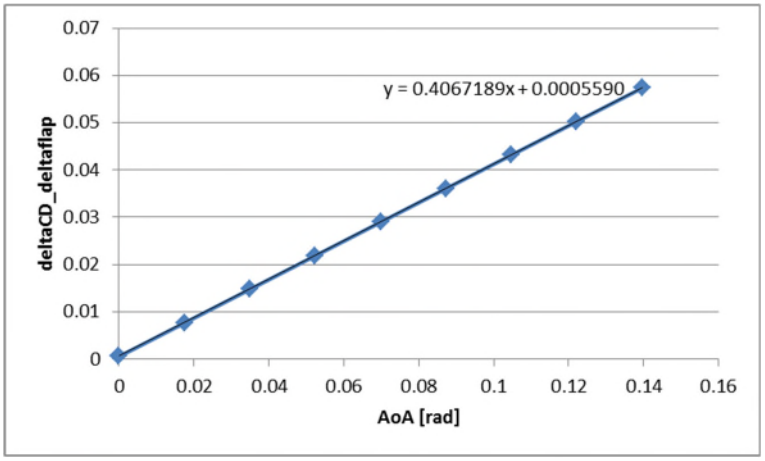

Figure A-17: deltaCD_deltaflap vs AoA

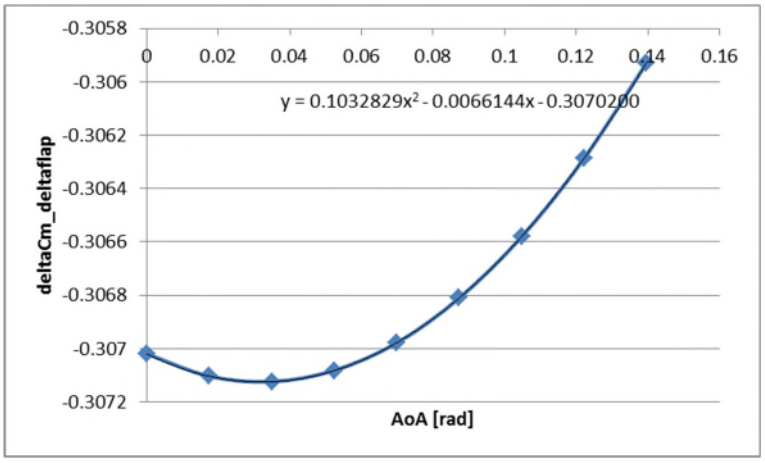

Figure A-18: deltaCm_deltaflap vs AoA

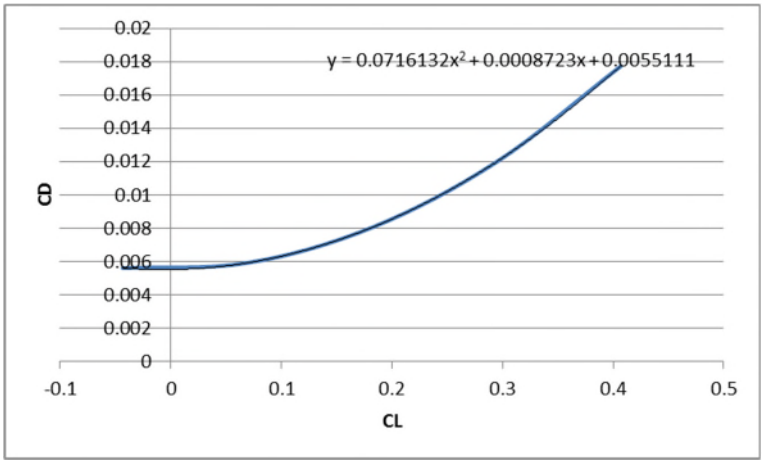

Figure A-19: Drag polar